Chapter 1.

Introduction and motivation

1.1 Background and motivation

Hard materials find extensive use as wear parts and cutting tools. Aluminum oxide exhibits a hardness of 16 - 18 GPa. This hardness has been reported to reach 24 GPa when submicron sized alumina is used [1]. A number of patents exist which disclose the use of alumina as a coating on PcBN, either as a PVD-generated thin coating [2,3,4] or as a polycrystalline coating sintered on top of the PcBN layer at high pressures and high temperatures[5].

Two principal factors have limited the widespread use of alumina tools [6]. These are low fracture toughness and low thermal conductivity , which increases the susceptibility of the tool to damage by thermal shock. Fracture toughness of aluminum oxide based ceramics has been increased through introduction of partially stabilized tetragonal zirconium oxide into the aluminum oxide matrix resulting in a sacrifice in hardness. The addition of transition metal carbide (particulary TiC) has resulted in improved thermal conductivity, hardness and fracture toughness compared to monolithic aluminum oxide[6]. Applications of these two aluminum oxide composites in metal cutting range from cast iron machining at higher cutting speeds to steel at moderate speeds.

A number of researchers have also explored the possibility of improving the properties of alumina , either by doping [7] or the addition of strengthening phases [8]. In particular, Nihara [9] has shown that addition

of nanosized silicon carbide in alumina modifies the mode of fracture from intergranular to transgranular, with a resulting 30% increase in fracture strength and an increase in slurry erosive wear resistance by a factor of 3.

Cubic boron nitride is the second hardest material known to man after diamond. It owes its hardness to the high degree of covalence which is isoelectronic to that of diamond. The incorporation of cubic boron nitride as a second phase in an alumina matrix has not yet been reported. It is envisaged that the incorporation of cubic boron nitride can result in improved properties of alumina. In particular fracture toughness and hardness are most likely to improve by incorporation of a harder phase. From the rule of mixture the predicted hardness of the resulting composite can be approximated by the equation

$$H_{Comp} = (100 - x)H_{Al_2O} + xH_{cBN}$$

Where H_{comp} is the predicted hardness of the composite, H_{Al2O3} and H_{cBN} are the hardness values of Al_2O_3 and cBN respectively and x is the volume fraction of cBN in the composite. The presence of cBN grains in an alumina matrix is also expected to deflect cracks resulting in improved fracture toughness due to internal stresses.

The main problem in sintering alumina with some cubic boron nitride arises from the fact that

1. Cubic boron nitride riverts to the soft hexagonal allotrope if heat treated to temperatures around 1400 ^{o}C and

2. If firing is done in an oxidizing atmosphere, cubic boron nitride gets oxidized into B_2O_3 at temperatures around 1000 ^{o} C.

Thus the first problem to be addressed in this research project was to develop a way of co-sintering the composite at temperatures lower than the hexagonalisation temperature of cubic boron nitride. This was achieved by using the reaction bonded aluminum oxide technique. This technique involves attrition milling mixtures of Al and Al_2O_3 in a ratio of say, 50:50 by volume followed by firing slowly in an oxidizing atmosphere so as to oxidize all the aluminum particles into new alumina. One main advantage of this technique is that the newly formed Al_2O_3 bonds with the original Al_2O_3 to form a coherent alumina monolith which sinters at temperatures much lower than the conventional sintering of alumina.

The issue of cubic boron nitride oxidation was addressed by separating the heat treatment cycle into two regimes. The first heat treatment cycle meant for oxidizing aluminum into alumina (RBAO) was done in air at temperatures not exceeding 1000 ^{o} C. This was then followed by sintering in an inert atmosphere (Argon or vacuum) at 1300 ^{o} C.

Thus the main aim of this project was to develop a process of co-sintering cubic boron nitride and alumina to full density without oxidizing and/or hexagonalising the cubic boron nitride.

1.2 Project Overview

This thesis is divided into five chapters as follows.

The first chapter is an introduction on alumina and cubic boron nitride as ceramic materials their properties and existing products made from them.

This is followed by chapter 3 which gives details of all chemicals used, equipment and analytical techniques employed to characterize materials.

Chapter 4 deals with the experimental results obtained at various stages from milling of the raw materials through compaction into green bodies and initial heat treatment up to final sintering. This chapter also includes an in depth investigation of the oxidation kinetics of aluminum into alumina in the reaction bonded aluminum oxide process. In particular the effects of compaction pressure , temperature and chemical composition and their effects on the oxidation behaviour of aluminum are discussed. The interaction of Al_2O_3 and cubic boron nitride taking into account the relevant phase diagrams and thermodynamic considerations are also discussed in this chapter.

The final chapter is conclusion and suggested future work.

Chapter 2: Literature review

2.1 Introduction

- Working definition of ceramic materials includes all inorganic and non-metallic materials which can be ionic or covalently bonded and can be crystalline or amorphous and are produced by the action of heat[10] . This definition includes materials not normally called ceramics, but which have ceramic –type properties, notably brittleness. Typical examples of advanced ceramics of practical importance include borides, carbides nitrides, silicides, carbon and oxides. Most ceramics are characterized by having high hardness and low fracture toughness. Inorganic compounds of groups III, IVa, and VIa in the periodic table have high hardness, low thermal expansion and high thermal conductivity and excellent oxidation and corrosion resistance, hence are candidates for speed cutting tool materials. Among these compounds alumina Al_2O_3, silicon nitride Si_3N_4, titanium carbide TiC, titanium carbonitride Ti(CN), diamond and cubic boron nitride cBN are actually being used as cutting tools [11] .

The ideal properties which any cutting material should possess in order to carry out its function are:

a. Hardness. The cutting tool needs to have a hardness value greater than that of the work piece in order to with stand the wear action taking place.
b. Toughness. The cutting tool needs to be sufficiently tough so that it can withstand any interruptions or vibrations occurring during the machining process.

c. Hot strength. This is necessary in order to overcome the heat generated at the cutting tool-work piece interface.
d. Thermal conductivity. This is necessary so that the heat generated at the cutting tool – work piece interface should be conducted way.

Hardness and fracture toughness

Hardness is the resistance of a material to indention by another material and is directly related to the elastic moduli of the material which in turn is dependent on the nature of the chemical bonding and crystal structure of the material [12].The rigidity of the crystal lattice and the inherent strength of the chemical bonds contribute to the hardness of the material. The hardest known materials diamond and cubic boron nitride have cubic crystal systems and strong covalent bonds. Typical hardness values for most commonly used materials are shown in the table 2.1..

Fracture toughness can be viewed as a measure of the degree of brittleness of a material[13]. In general increasing hardness brings with it a reduction in toughness implying that those materials in the higher hardness region (Ceramics) are brittle.

Table 2.1 Typical hardness values of common materials.

Material	Hardness (GPa)
Diamond	75
Cubic Boron nitride	45
Boron carbide	30
Silicon Carbide	26
Alumina	21
Tungsten Carbide	19
Zirconium Oxide	15
Hardened steel (65 HRC)	8
Soft Steel (85 HRB)	1.9

Toughening mechanisms in ceramics

Since ceramics are generally brittle approaches for producing strong ceramics have been directed at enhancing fracture toughness. Much work has been done in investigating ways of improving fracture toughness of ceramics. Much improvements in enhancing toughness of ceramics has been through the control of microstructural characteristics. Some of the approaches to enhance the toughness of ceramics include the following.

a. Microcracking.

If microcracks are formed ahead of a propagating crack, they result in crack branching, which in turn will distribute the strain energy over a large area resulting in a decrease in stress intensity factor at the principal crack tip. Crack branching can also lead to enhanced toughness because the stress required to drive a number of cracks is more than that for driving one crack[14]. One good example of microcrack toughening is Al_2O_3 toughened with monoclinic ZrO_2. Here microcracks

occur within regions of local residual tension, caused by thermal expansion mismatch or by transformation.

b. Particle toughening.

Interaction between particles that do not undergo phase transformation and a crack front can result in toughening due one of the following: crack bowing between particles, crack deflection at the particles or crack bridging by ductile particles. Brittle materials containing a second phase have been found to have higher fracture toughness than those of homogenous materials and the toughness increases with increase in volume fraction of dispersed phase and decreases with dispersed particle size[15]. The most effective morphology for deflecting crack propagation has been found to be rod-shaped grains and whiskers[16].

Another crack deflection mechanism for toughening ceramics is as result of the existence of local residual stress in the vicinity of the dispersed secondary phase. Composites with 25% vol TiC particles in a matrix of SiC have been found to have a 60% higher fracture toughness and 40% higher strength than the matrix material alone. The improved flexural strength and fracture toughness in this system is thought to result from crack deflection due to residual stress[17].

c. Transformation toughening

This involves a phase transformation of second phase particles at the crack tip with a shear and dilational component, thus reducing the tensile stress concentration at the crack tip [14]. In composites such as alumina containing partially stabilized zirconia, the volume change associated with the phase transformation in zirconia ($ZrO_{2\,(t)} \rightarrow ZrO_{2(m)}$) particles is exploited to obtain enhanced toughness. This transformation

is accompanied with a volume expansion which result in stresses that tend to closes the crack leading to an increased toughness [18] . Thus the fracture toughness of Al_2O_3 based ceramics can considerably be enhanced by incorporating fine monoclinic ZrO_2 particles. A hot pressed composite containing 15% vol% ZrO_2 has a fracture toughness of 10 MPa m ^{½} [19 19].

d. Whisker or fiber reinforcement

The toughening of ceramics by brittle fibers and/or whiskers occurs subject to debonding at the interface[20]. In the absence of debonding, because the fiber and matrix typically have comparable toughness, the composite is brittle and satisfies a rule of mixtures (figure 2.1). Debonding reduces the amplitude of the stress concentration at the fiber along the matrix crack front and, when sufficiently extensive, allows the crack to circumvent the fiber, leaving the fiber intact in the crack wake. The intact fiber inhibits crack opening and allows a composite toughness exceeding that of either constituent (figure 2.1).

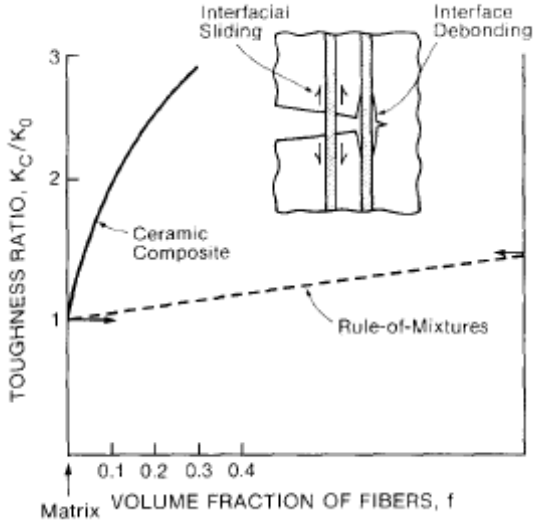

Figure 2.1 The role of debonding in whisker toughening [20]

Other factors affecting hardness and toughness of ceramic materials.

The actual hardness of a material depends on several factors, some of which are grain size, density and purity just to mention a few. Z. Misirli et al [21] did some work to demonstrate the effect of additives on the microstructure hardness and fracture toughness of alumina ceramics. In their work they evaluated hardness and fracture toughness for alumina samples with various Silica contents. They found out that both hardness and toughness increase as SiO_2 content of alumina decrease. They attributed this degradation in properties to the increasing amount of glassy phase at the grain boundaries.

In yet another development A. Krell [22] did some work which showed that significant increase in hardness can be obtained by reducing the grain size of sintered alumina down to the submicron range. An explanation offered for this improvement was the reduction in grain pull out frequency which is directly related to wear and hardness.

A. Muchtar *et al*[23] have also shown that decreasing grain size can result in enhancement of fracture toughness of alumina based ceramics. In this case fracture toughness enhancement was attributed to shift of fracture mode from trans-granular in coarse grained samples to inter-granular in submicron grained samples.

A milestone in improving fracture toughness of alumina by decreasing grain size was reported by R.S. Mishra and A. K. Mukherjee [24] who proved that the toughness of alumina can be increased to 8MPa $m^{1/2}$ by using nanosized grains.

2.2 Alumina

Aluminum oxide (Al_2O_3) commonly known as alumina is one of the most widely used, technical ceramic material. Alumina as a raw material occurs abundantly in nature, most often as impure hydroxides which are the essential constituents of bauxite ores. Bauxite is an impure mixture of gibbsite $Al(OH)_3$ = α $Al_2O_3.3H_2O$, boehmite and diaspore which are polymorphs of AlO(OH)= $Al_2O_3.H_2O$ respectively [25]. The usefulness of alumina hinges on its properties namely, high melting temperature, chemical resistance, electrical resistance and hardness [25] .A diverse range of types of alumina exists with a wide range of properties as shown in table 2.2.. The major markets for alumina-based ceramics on a weight basis are refractories (50%), abrasives (20%), whitewares and spark plugs (15%) and engineering ceramics (10%) [26].

Table 2.2 Properties of Alumina ceramics [27]

Property	Symbol	Units	C610 Mullite ceramic 50-65% Al_2O_3	C620 Mullite ceramic 65-80% Al_2O_3	C780 Aluminum-oxide 80-86% Al_2O_3	C786 Aluminum-oxide 86-95% Al_2O_3	C795 Aluminum-oxide 95-99% Al_2O_3	C799 Aluminum-oxide >99% Al_2O_3
Density	ρ	g/cm^3	2.6	2.8	3.2	3.4	3.5	3.9-3.98
Strength	σ	MPa	120	150	200	250	280	300
Hardness	Hv	-	-	-	-	-	1600-1700	1800-2200
Fracture Toughness	K_{IC}	$MPam^{1/2}$	-	-	-	-	4	4
Specific resistivity @ 20 °C	ρv>20	Ωm	10^{11}	10^{11}	10^{12}	10^{12}	10^{12}	10^{12}
Specific resistivity @ 600 °C	ρv>600	Ωm	10^{4}	10^{4}	10^{5}	10^{8}	10^{6}	10^{8}
Thermal expansion @30-600 °C	$\alpha_{30\text{-}600}$	$10^{-6}K^{-1}$	5-7	5-7	6-8	6-8	6-8	7-8
Specific heat capacity @ 30-600 °C	$C_{p30\text{-}600}$	$JKg^{-1}K^{-1}$	850-1050	850-1050	850-1050	850-1050	850-1050	850-1050
Thermal conductivity	$\lambda_{30\text{-}100}$	$Wm^{-1}K^{-1}$	2-6	6-15	10-16	14-24	16-28	19-30

Crystal structure of Alumina and transition aluminas

Aluminum oxide, commonly referred to as alumina possesses strong ionic inter-atomic bonding giving rise to its desirable material characteristics. It exists in several crystalline phases which all rivert to the most stable hexagonal α phase (corundum) at elevated temperatures. This is the phase of particular interest for structural/ engineering applications.

Many processes such as the oxidation of Aluminum metal and heating of gibbsite ores result in the formation of intermediate metastable alumina phases before the stable α phase is formed[25]. These transitional phases are denoted as γ(Gamma), χ(Chi) , η(Eta), ε, δ(Delta) , θ(Theta)and Ќ(Kappa) and are of importance because of their use as catalysts or catalyst supports, adsorbents coatings and soft abrasives. The sequence of transition aluminas that forms is strongly dependent on the starting material its coarseness and crystallinity, heating rate, the amount of water vapor in the atmosphere and by impurities present. The sequences of transition aluminas are given in figure 2.2.1 [28] [29] . These sequences are generally accepted, although there is no clarity on the X-ray identification of some phases and the existence of others. Transition aluminas have partially disordered crystal structures all based on a close –packed oxygen sublattice with varying interstitial aluminum configurations. Transition aluminas can not be considered true polymorphs of α-alumina. The low temperature ones in particular may contain some residual OH anions. Moreover, the sequence of transformation is not reversible, that is, neither α-alumina nor any of the high temperature aluminas can be converted to one of the transition aluminas that occur at a lower temperature and therefore may be classified as thermodynamically unstable. Crystallographic properties of transition aluminas are given in table 2.3

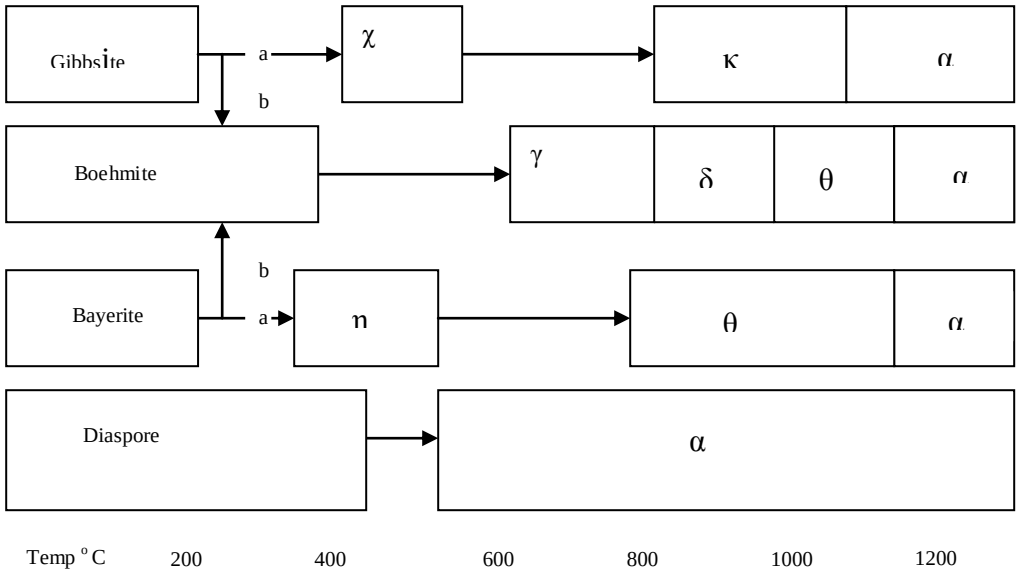

Figure 2.2. Phase transformation sequences of aluminum hydroxides [25]

Enclosed area indicates range of stability. Open area indicates range of transition. Path b is favored by moisture, alkalinity and coarse particle size (100μm): path a by fine crystal size (below 10 μm). As equilibrium is approached the structures become more ordered forming a hexagonal oxygen sublattice until stable α- alumina is formed. Unlike the transition aluminas the crystal structure of α-alumina is well known. The crystal structure is often described as having O^{2-} anions in an approximately hexagonal close packed arrangement with Al^{3+} cations occupying two-thirds of the octahedral interstices as shown in figure 2.3 crystallographic properties of transitional aluminas are shown in table 2.2.

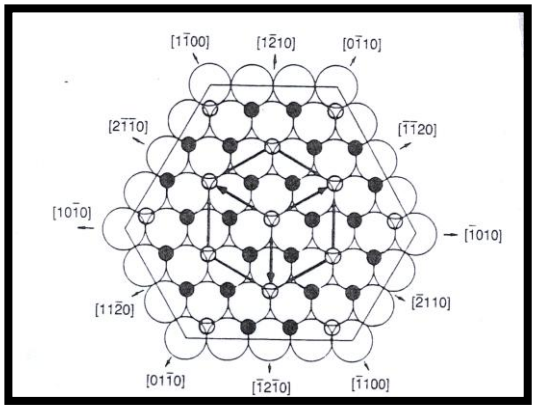

Figure 2.3 Crystal structure of α-alumina [26]

Table 2.2 Crystallographic Parameters of transition aluminas

Phase	Crystal system	Unit Cell Parameters(Angstrons)		
		a	b	c
Alpha	Cubic	4.98		
Chi	Cubic	7.95		
Eta	Cubic	7.90		
Gamma	Tetragonal	7.95	7.95	7.79
Delta	Tetragonal	7.96	7.96	23.47
Iota	Orthorhombic	7.73	7.78	2.92
Theta	Monoclinic	5.63	2.95	11.68
Kappa	Orthorhombic	8.49	12.73	13.39

Sintering of alumina

Sintering is a process whereby a material , usually in the form of a powder is subjected to heat treatment resulting in particles bonding together to form a coherent body with reduced porosity , increased density and improved hardness, toughness and strength.

From a processing point of view it is important to note that there are several processing variables that affect densification/ sintering of a material hence properties of the final product. These include initial green density of compact, temperature, time, heating rate, particle size and particle size distribution, purity of starting material and chemical additives.

Effect of heating rate on the sintering of alumina.

The actual effect of heating rate on densification and grain growth is not clear, and different research groups have reported conflicting experimental results. For example Stanciu et al [30] reported that the final grain size scaled inversely with the heating rate. This is contrary to Murayama and Shin [31] who reported that the grain growth was enhanced by faster heating rate. Y. Zhou et al [33] tried to explain this disparity by using two Al_2O_3 powders with different particle sizes and sintering them to different temperatures at different heating rates. They found out that in general rapid heating rate resulted in reduced grain growth and the level of reduction depended on the initial powder size and sintering temperature.

However the effect of heating rate on densification was not monotonic. In the early stages of sintering, where densification is just starting faster heating rate resulted in higher densities and at later stages where densification had proceeded to rather high degrees faster heating rate led to lower densities.

Effect of grain size and grain size distribution on the sintering of alumina

It is well known in classical sintering theory that during sintering densification and grain growth are two competing processes, and both of them are driven by the capillary force that is proportional to the reciprocal of grain size. Thus the smaller the initial powder size, the larger the densification and grain growth rates during sintering [32]. Work done by Y. Zhou et al [33] has shown that under identical sintering conditions powders with finer initial particles always attain higher densities and larger grain growth compared to powder with coarser particles. In addition powders with finer particles also start to densify at lower temperatures and densify at greater rates compared to powders with coarser particles [33] .

The main obstacles in obtaining ceramics with theoretical density have been attributed to non uniformities in the green bodies and particle size distribution and degree of agglomeration of the starting powder are the main origins of the non uniformities [34].

While it is well known that packing of a powder with a bimodal particle size distribution results in higher green density than a mono sized powder due to the effective interspace filling between coarse particles by fine particles [35] enhanced densification in compacts prepared from powders with bimodal or wide size distribution has not been observed. On the other hand powders with narrow size distribution have been reported to result in sintering to high final densities mainly because of their uniform pore size distribution [36 37] .

In a separate development Tsung-Shou and Michael D. Sacks [38] investigated the effect of grain size distribution on the densification and sintered microstructure of Al_2O_3. In their work agglomerate-free

powders having the same median particle size, but different widths of distribution , were prepared by sedimentation of high purity commercial aluminas. Compacts prepared with broad particle size distribution powder had a higher green density and smaller median pore channel radius compared to compacts prepared with narrow particle size distribution powder, indicating that fine particle were efficiently filling the interstices formed by larger particles. Both narrow and broad size powders reached final density at the same time/temperature schedule and had essentially the same average grain size and grain size distribution. It should be noted however that some experimental observations [39] suggest that the problem of exaggerated grain growth may arise if the particle size distribution of the starting powder becomes too broad.

Effect of impurities on the sintering of alumina.

Research has been done to investigate the influence of minor chemical constituents on the sintering of alumina[40]. Previous studies have already shown that MgO is a beneficial sintering aid while CaO and SiO_2 have deleterious influence on the sintering of alumina[41],[42].Previous experimental studies have shown that abnormal grain growth is strongly related to the presence of impurities, most notably CaO and SiO_2 which form an intergranular liquid phase (anorthite) which induces grain faceting leading to a more tabular grain morphology which eventually leads to abnormal grain growth. In their work S. Bae and S. Baik [40] demonstrated that abnormal grain growth is not an intrinsic property of commercial alumina but rather is an extrinsic property controlled by minor constituents that can be present in the original powder or introduced during powder processing and

subsequent sintering. In conventional sintering practice the furnace wall , heating elements are also possible sources of contamination.

Influence of atmosphere on the sintering of alumina

The influence of atmosphere on the sintering behavior of alumina has been studied extensively. Early studies revealed that the gases in the sintering atmosphere must be soluble in alumina in order for the near-theoretical density to be achieved [43] , [44]. Insoluble gases generate a back pressure which opposes the shrinkage of pores and thereby reduces the driving force for densification. In general solid state sintering of alumina in reducing atmosphere (hydrogen) results in fully densified products while products fired in air have residual porosity. This porosity remains because in the last stages of sintering all of the pores are isolated within the oxide grains and further shrinkage would require the pore gas to dissolve in the oxide and diffuse to the external surface via grain boundaries. Nitrogen is not soluble in alumina at the sintering temperature and therefore the pores only shrink until the increased internal gas pressure balances the reduction in surface energy during the process. Hydrogen on the other hand is soluble and diffuses rapidly out of the system 26. More recently it has also been shown [45] that a fully dense hot-pressed alumina will swell if annealed in an atmosphere containing sufficient quantity of oxygen. In this case the oxygen reacts with the impurities to produce gases which will then generate pressures high enough to nucleate voids within the structure. It has also been demonstrated that the sintering atmosphere affects the morphological development of the final microstructure. Mocellin et al [46] ,[47]. observed that when alumina was sintered in hydrogen, the pore

phase was predominantly confined to the grain boundaries , whereas in nitrogen or oxygen the pores became entrapped within the grains. Thompson and Harmer [48] investigated the effect of atmosphere on the final stage sintering kinetics of ultra –pure alumina. In particular they investigated the effect of oxygen partial pressure on densification rate and grain growth rate. They concluded that sintering in low oxygen partial pressure enhances densification rate and increases grain growth rate. Additionally it was also observed that sintering in low oxygen partial pressure enhances relative pore mobility and reduces the susceptibility to pore/ boundary separation.

Pressure assisted sintering.

Sintering with the aid of mechanical pressure is called hot pressing. The sample is heated to high temperatures and mechanical pressure is applied to increase the driving force for densification by acting against the internal pore pressure without increasing the driving force for grain growth. Practical advantage of hot pressing is that dense samples with minimal grain growth can be obtained at much lower temperatures[49] .

The material to be hot pressed is first precompacted before being placed in a hot press die to get a reasonable green density. One major disadvantage of this technique is that sample shapes are limited.

Another pressure assisted sintering technique was described by Hardtl[50] . This technique is called hot isostatic pressing. In this technique no die is used and an inert gas is employed as an isostatic pressure medium. Because the working fluid is a gas it is necessary that the ceramic to be hot pressed be sintered first. This first sintering must yield a material having no open or interconnected porosity otherwise no force will be transmitted to the component. One advantages of this technique over hot pressing are that the sample

shape is not critical since pressure is applied isostatically. Another additional benefit is the elimination of unwanted reactions between sample and die walls which can be a problem in uniaxial hot pressing.

Alumina based composites

Although alumina is one of the widely used technical ceramics because of its low density, high strength, high hardness and high temperature capability it however has some draw backs. For an example its fracture toughness makes it difficult to withstand severe conditions applied for example, in the field of high-speed cutting tools. Significant advancement has been made in understanding toughening mechanisms and some of these have been applied to improve the toughness in the range 8-15 $MPam^{1/2}$ From the view point of multiphase ceramics, the flexural strength and fracture toughness of the matrix materials can be enhanced by incorporating second phases [51],[52]. The addition of hard secondary phases such as TiC, Ti(CN), WC and SiC to alumina matrix provides great improvement in mechanical properties [54, 55, 61, 62, 63, 64]. The most important Al_2O_3 based composites are those which contain TiC and ZrO_2. Their properties compared to pure alumina are shown in table 2.3.

Alumina-TiC composites

The hardness of alumina has also been shown to increase by adding between 30 % and 40 % of TiC[53]. Such additions improve both hot hardness and room temperature hardness but reduces the fracture toughness. The increased hardness makes it more suitable for finishing operations and for machining harder steels. The colour of this type of Ceramic is black and is known on the market as *Black Ceramic* [53] .

K.F. Cai et al [54] investigated the effect of TiC additions on the properties of alumina. Both the hardness and fracture toughness

increased with increase in TiC content up to 30% vol and could certainly, be extrapolated to still higher values. The increase in hardness with increase in TiC could be explained by the fact that TiC is relatively harder than Al_2O_3 and increase in fracture toughness was attributed to effects of crack deflection and grain bridging by TiC grains. X.Q You et al [55] investigated the effect of grain size on mechanical properties and thermal shock resistance of Al_2O_3-TiC composites. In addition to the remarkable improvement in mechanical properties imparted by adding TiC into alumina composites they also found out that decreasing grain size of Al_2O_3 and TiC results in improved thermal shock resistance.

Alumina –ZrO_2 composites(ZTA)

Zirconia toughened alumina (ZTA) is a well known two-phase binary ceramic formed by adding ZrO_2 powder to Al_2O_3 powder and sintering to form a dense product with improved toughness over conventional alumina ceramics [26]. Thus the development of Zirconia-toughened-alumina (ZTA) composites was aimed to substitute alumina ceramics in applications where a higher fracture resistance is required [2]. The presence of second phase zirconia results in an enhancement of flexural strength, and fracture toughness mainly attributed to the stress-induced phase transformation. Work done previously has shown that volumetric fraction of added zirconia is directly related to fracture resistance of ZTA composites[56, 57 ,58 59,]. However it has also been shown that addition of ZrO_2 to an alumina matrix results in a hardness decrease[60]. Such effect is associated with the lower hardness of zirconia compared to that of alumina.

Table 2.3 Al_2O_3 composites of commercial importance

	Al_2O_3 30% TiC	Al_2O_3 40% TiC	Al_2O_3/ZrO_2	Al_2O_3
Density ($g/cm^{3)}$	4.22	4.36	4.01	3.9
Hardness(HV)	1810	1820	1700	2000
Bending strength (MPa)	600-800	600-800	450	300-600
K_{IC}(MPa $m^{1/2}$)	5.4	5.2	4.5	3-4
Λ, W/mk	30	35	15	20-30
α, 10^{-6} K^{-1}	7	7	7	7-8
R_{spec} 10^3 Ωcm	4	2	10^{11}	10^9
Application	Cutting tool	Cutting tool	Cutting tool & wear parts	Cutting tool & wear parts

Alumina-WC composites

Lin Wang et al [61] investigated the influence of adding WC particles on the Mechanical properties of alumina-matrix composites. In their work they found out that dispersing tungsten carbide particles as a second phase in an alumina matrix results in a composite with improved mechanical properties. Flexural strength and fracture toughness of the Al_2O_3 -WC composite (6 vol% WC) sintered at 1450 ^{o} C reached 581 MPa and 5.13MPam$^{1/2}$ respectively [61]. They concluded that a decrease of the matrix grain size (due to pinning effect of WC grains) contributed to increase in strength and presence of WC grains resulted in a more tortuous crack-path which delays crack propagation leading to increase in fracture toughness. Wilson et al [62] obtained fracture toughness of 7.1 MPam$^{1/2}$ by hot pressing alumina and WC (20 vol%) at 1450 ^{o} C in flowing argon. The hardness obtained in this work was (19MPa) which is adequate for cutting tool applications, and is comparable to those of

other hot –pressed materials. Microstructural investigations showed that toughening was also due to crack deflection around the homogenously distributed WC in the alumina matrix.

Alumina –(TiW)C composites

Wilson et al [63] also investigated the effect of mixed carbides as Ti and W carbides on the mechanical properties of alumina matrix. Both Titanium carbide and Tungsten carbide have been extensively studied as reinforcing components in alumina ceramic matrix. Titanium carbide and Tungsten carbide have room temperature hardness values in the range of 18-23 and 17-22.5 GPa respectively [55, 63] .

Alumina-SiC composites

Young et al [64] fabricated Al_2O_3-SiC composites containing variable amounts of SiC particles (5 to 30vol %) dispersed in an alumina matrix and tested its potential as a cutting tool. The Al_2O_3 composites exhibited higher hardness compared to the unreinforced matrix whereas the fracture toughness remained practically constant up to 10% loading of SiC. Cutting tests done revealed that introduction of SiC results in increased hardness and decreased grain size of the material, thereby greatly improving its cutting performance, compared to the commercial tools made of monolithic Al_2O_3 and Al_2O_3-TiC composites.

Reaction bonded aluminum oxide (RBAO)

Most aluminas sinter to full density at temperatures not lower than 1500 ^{o} C unless there are some additives. In addition there is some shrinkage associated with high temperature sintering of alumina. Reaction bonded aluminum oxide (RBAO) is a technique pioneered at

Technische Universitat Hamburg-Harburg [65] to produce dense alumina matrices at much lower temperatures with minimal shrinkage.

In this technique attrition milled Al/Al_2O_3 powder compacts are heat treated in air such that all the Al gets oxidized into Al_2O_3 which then sinters and bonds with the original Al_2O_3 to form a dense monolithic alumina at temperatures much lower than that needed to conventionally sinter alumina on its own. Another advantage is that oxidation of Al into Al_2O_3 is accompanied by a volume increase which can compensate firing shrinkage, thus enabling near net shaping. Other advantages of this technique over conventional sintering of alumina include high green strength, glass-phase-free grain boundaries and easy adaptability to incorporation of second phase without causing the harmful residual stresses normally encountered with shrinking matrix materials [65,67,68].

Work done by Claussen *et al* [66]has shown that strength of reaction bonded aluminum oxide bodies is comparable to that of conventionally sintered dense alumina fired at higher temperatures.

Processing parameters affecting properties of RBAO bodies.

In an ideal reaction bonded aluminum oxide process all or most of the Al should be converted into Al_2O_3 resulting in a homogenous matrix. However in practice many problems are encountered e.g cracking, bloating and incomplete reaction. Some of these problems can be avoided if proper processing parameters are used. D. Holz et al [67] investigated the effect of processing parameters on phase and microstructural evolution in RBAO ceramics. They observed that important parameters controlling the reaction bonding of Al_2O_3 are Al content, particle size and morphology of starting powders and green density. In principle high Al content is necessary in order to exploit the outstanding properties of RBAO (i.e the volume increase hence near-net-shaping) Suvaci and Messing[68] concluded that the maximum

aluminum content of the precursor powder is limited to 60 vol % and for aluminum contents above 60%, samples could not be completely oxidized and would exhibit a dense oxide crust and an aluminum rich core at the end of the reaction-bonding stage.

In general size of the Al particles affects strongly the microstructural and compositional homogeneity of the sintered components [68, 69]. Large Al particles make fast and complete oxidation difficult and this can lead to microstructural failures and heterogeneous particle distribution. The critical aluminum particle size (i.e the largest aluminum particle size that can be used to obtain dense ceramic materials via the RBAO process) was determined to be approx 1.5μm [68].

E Suvaci and G. L. Messing [70] investigated the effect of initial α-Al_2O_3 particle size in RBAO process on the phase transformation of aluminum- derived γ-Al_2O_3 to α-Al_2O_3. They concluded that γ-Al_2O_3 to α-Al_2O_3 transformation have significant effect on subsequent sintering kinetics, temperature and microstructure[71], [72], . They demonstrated that coarse α-Al_2O_3 used in normal RBAO process does not result in a sufficiently high nucleation to affect the γ-Al_2O_3 to α-Al_2O_3 phase transformation and seeding with fine α-Al_2O_3 results in high nucleation frequency which have the resultant effect of reducing the transformation temperature to as low as 963 ^{o} C. This smaller particle size of the seeded RBAO Al_2O_3 decreases the sintering temperature to 1135 ^{o} C. Thus demonstrating that seeding is a viable method to tailor the phase transformation and subsequently improve densification in RBAO process.

The green strength of RBAO compacts can be attributed to the presence of aluminum. On milling the Al particles are plastically deformed, resulting in strong Al/Al contacts bridging the Al_2O_3 particles. This results in high green density and green strength compared to that of conventional ceramic green bodies[73] . The pore system in RBAO

compacts controls the oxygen flux and thus the oxidation reaction. This means that although high green density of compacts favors low shrinkage and near-net-shape forming it makes oxidation reaction difficult and would result in incompletely reacted pellets.

Milling of RBAO powders

Since properties of reaction bonded aluminum oxide ceramics is dependent on the size, morphology and homogeneity of the precursor powder it means milling is the central processing step which determines the properties of the powder and eventually the fired component. It would be extremely harmful for the reaction bonding process if only a fraction of the Al particles are effectively milled while the rest survive because of undesired parameters or equipment setting. Important parameters determining the quality of RBAO precursor powders are (a) the volume ratio of the powder mixture to milling balls. (b) the rotation speed (c) the milling time and (d) type of milling solvent [67].

F. Essl et al [69] investigated the effects on the milling efficiency of milling medium and crystal size of the abrasive component. In their work they compared organic solvents of different polarities namely, ethanol, acetone and cyclohexane. They concluded that cyclohexane (which is non polar) is more efficient than the two polar solvents ethanol and acetone. They explained their finding in terms of stability. In the non-polar cyclohexane there is no stabilization and so the slurry tends to form powder agglomerates which are assumed to enhance the milling efficiency.

They also assessed the effect of particle and crystal size on milling efficiency. It was established that altering particle and crystal size does not have an effect if milling is being done in non polar cyclohexane. However in polar solvents milling efficiency is significantly lower with fine alumina (median particle size: 0.5µm, crystallite size < 0.1µm) than

when using coarser alumina (median particle size 18μm, size of crystallites 1-2μm).

II-Soo Kim and Sang[74] investigated the effect of different ball size and alumina type on the processing of RBAO ceramics. The two types of aluminas compared were fussed alumina and calcined alumina and with all other parameters being constant they found out that fused alumina is ground more effectively compared to calcined alumina and this was attributed to the morphology of the former being sharp edged. The investigation of different ball size distribution involved comparing 3mm balls with 50% 3mm balls + 50% 5mm balls. They observed that small single size balls were more efficient compared to mixed size balls. This was explained by considering the fact that probability of contact between ball and powder is higher using small single size balls than mixed size.

Mechanism of oxidation of Al in RBAO

In order to tailor the final properties of a RBAO body it is necessary to understand the mechanism with which Al is being oxidized into Al_2O_3. The RBAO process has been intensively characterized by dilatometry and thermogravimetry [75]. Typical TGA/DTA and dimensional changes for the reaction bonded aluminum oxide process are shown in figure 2.4. The oxidation of Al starts at low temperatures (>350 ^{o} C). Before oxidation of Al heating of RBAO compacts is associated with mass loss due to evaporation of organic phases and decomposition of hydrolysis products, boehmite and diaspore. At temperatures below 450 ^{o} C the reaction products are mainly amorphous Al_2O_3 and some traces of crystalline γ-Al_2O_3 and above 450 ^{o} C Al oxidizes directly to crystalline γ-Al_2O_3 and the preexisting amorphous phase also crystallizes to γ-Al_2O_3. Maximum oxidation occurs at around 520 ^{o} C when there is rapture of Al particles caused by decomposition of boehmite and

diaspore. After this stage oxidation rate slows down again (between 520-660 ^{o} C). Above 660 ^{o} C (melting point of Al) the rate increases again. This can be explained by poor wetting of Al_2O_3 by liquid Al resulting in liquid Al spilling into the void spaces where it gets readily oxidized. This process continues until all Al is oxidized.

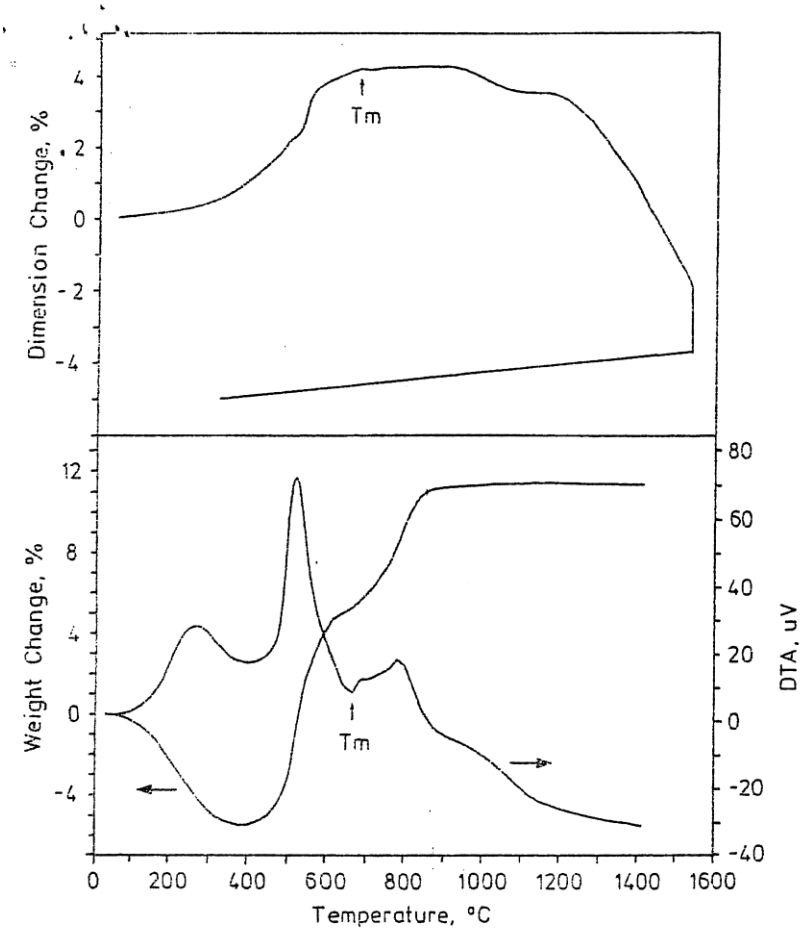

Figure 2.4 Typical TDA/TGA and dimensional changes for reaction bonded aluminum oxide process[75]

The suggested reaction and mechanisms by Nils Claussen et al [73] have been strongly supported by kinetic and thermodynamic studies[75]. Based on isothermal reaction data, it was demonstrated that the reaction kinetics in RBAO process follow a parabolic rate law and

reaction rate depends strongly on the particle size of Al and is controlled by oxygen diffusion. The activation energy of the process before the melting point of Al (660 ^{o} C) was 112KJ/mol compared to 26kJ/mol above the melting temperature. This fact is evidence that the reaction changes from gas-solid to gas –liquid after the melting of Al Before melting of Al the gas is diffusing through along the porous grain boundaries and after the melting point the molten Al spills into the void space . In this situation there would be direct contact between oxygen and Al resulting in overall reduction in activation energy of the process.

Solid State Chemistry for oxidation of Al in RBAO

In many gas-solid reactions the solid is porous, allowing diffusion and reaction to take place simultaneously through out the solid. Thus the reaction can be considered to take place at a diffuse zone rather than at a sharp boundary as is the case in non-porous solids. Most of the work done on solid state reactions has been based on the shrinking unreacted core model [76] [77].

Since many solid reactants have some initial porosity and the simple shrinking unreacted core model is often inapplicable to such systems, there have been efforts to find valid models for these reaction systems.

In general heterogeneous reactions involving a porous solid and a gas generally include the following steps[78].

1. Diffusion of the reactant gas within the pores of the solid.
2. Chemical reaction of the solid with the gas.
3. Diffusion of the gaseous product (if any) from the solid.

Thus as in any other chemical reaction system it is very important to understand the relative significance of these steps in order to understand the overall kinetics of the reaction system.

Unlike in nonporous solids where there is a sharp boundary between the unreacted core and the completely reacted layer in the case of porous solids there is a gradual change in the degree of conversion through out the particle. The external layer will be completely reacted after a certain time and the thickness of this completely reacted layer will increase toward the interior of the particle. Under these conditions in contrast to non-porous solids, the reaction within the partially reacted zone occurs simultaneously with diffusion of fluid reactants in this zone. Thus the problem reduces to determine which of the processes diffusion or reaction is rate determining.

If diffusion is rate determining, the reaction will occur in a narrow boundary between the unreacted and completely reacted zones. If on the other hand reaction is the rate determining step then the concentration of the gas will be constant through out the solid and the reaction will take place uniformly through out the solid [78], [79].

S. P. Gaus et al [80] developed a model for the reaction bonded aluminum oxide process which indicates that the process is controlled by a combination of reaction and diffusion. In their model they plotted the conversion profile of Al as a function of position within a pellet for various reaction rates. In the case where the reaction rate was too low it was seen that the concentration profile of Al was constant through out the pellet. This is explained by the fact that at low reaction rates there is enough gas through out the pellet and so the reaction proceeds uniformly through out. Plot of aluminum with distance in this case was as shown in figure 2.5a.

In the other extreme where the reaction rate was too high the reaction occurred on the external layer leaving an unreacted core that shrinks as the reaction proceeds. In this case concentration gradient of aluminum was as shown in figure 2.5 b.

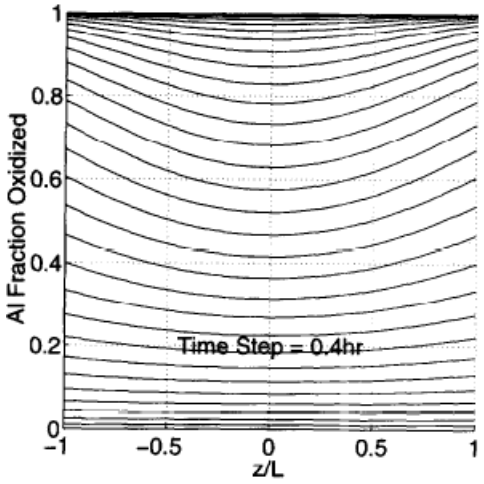

Figure 2.5 a. Concentration profile of Al oxidized as a function of distance when reaction is rate determining[80].

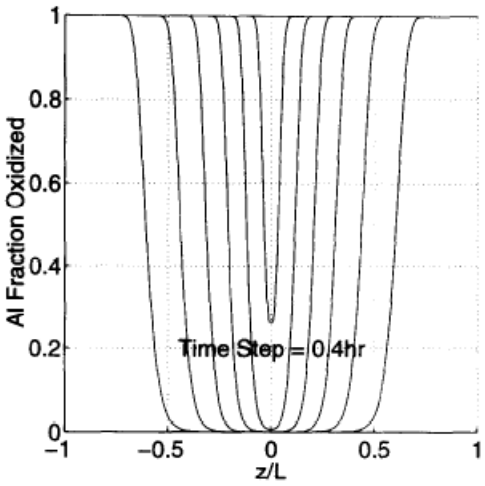

Figure 2.5 b. concentration profile of Al oxidized as a function of distance when diffusion is rate determining[80].

Modification of the RBAO process.

In order to reduce the shrinkage and even to achieve net-shaping the RBAO process can be modified in various ways by incorporating other metal or ceramic additives that exhibit a larger volume expansion on oxidation. For instance Zr is associated with a volume expansion on oxidation of 49%, Ti 76%, Cr 102%, and Nb 174% [73].

Claussen et al [73] showed that the microstructure and mechanical properties of RBAO can be improved by incorporating 5-20% vol ZrO_2. The grain size of the matrix was shown to decrease with increase in ZrO_2 This is due to the fine distribution of ZrO_2 particles at grain boundaries. This hinders grain growth in the sintering stage.

Garcia et al [81] processed RBAO powders consisting of Al (40%), Nb_2O_5-stabilised ZrO_2 (Nb-OZP, 20%), Al_2O_3 (30 vol %) and Nb (10 vol %) by the standard RBAO route. In spite of the high compression pressures used (900 MPa) all the al and Nb oxidized below 900 ^{o}C. Nb

assisted in reducing the sintering shrinkage by a larger volume expansion on oxidation. An interesting feature of this material was the formation of needle-like grains consisting of Zr and Nb oxides. These needle-like grains act as reinforcement particles by mechanism of crack deflection and bridging resulting in improvement in fracture toughness.

S. Scheppokat et al [82] tested TiC and TiN as candidate materials for particle reinforcement for RBAO. Since both TiC and TiN are not sufficiently oxidation- resistant to withstand the heating cycle needed to completely oxidize Al in RBAO process some modifications were done so as to retain TiC and TiN after sintering.

In the case of TiC containing composite a precursor powder was prepared which contained TiO_2 to act as an oxygen donor for Al. The presence of TiO_2 eliminated the need for an oxidation step in air and allowed the TiC pre-added to the composition to remain unoxidised**.** The composites were fired in argon without a prior oxidation step. The amount of TiO_2 added was calculated so as to be enough to completely oxidize the available Al.

For TiN containing composites advantage of an exchange reaction between TiO_2 and AlN to form Tin and Al_2O_3 was utilized. Thus in this case powders containing TiN and AlN were heat treated in air up to 700 ^{o}C At this stage all the TiN was converted to TiO_2. From this stage the atmosphere was then changed to argon so that the formed TiO_2 reacts with the pre-added AlN to form Al_2O_3 and TiN. These samples achieved a 96% density flexural strength of 280MPa and fracture toughness of 3.3 MPa $m^{1/2}$

2.3 Boron nitride

Boron nitride is a synthetic material which although discovered in the early 19th century was not developed as a commercial material until the latter half of the 20th century. Boron and nitrogen are neighbours of carbon in the periodic table and their atomic radii are also similar to that of carbon. It is not surprising therefore that boron nitride and carbon exhibit similarity in their crystal structure.

In the same way as carbon exists as graphite and diamond, boron nitride can also be synthesized in hexagonal and cubic forms.

Cubic boron nitride is the second known hardest material after diamond. The compound crystallizes with a zinc blende structure which closely resembles that of diamond with boron in 000 and nitrogen in ¼ ¼ ¼ in a fcc lattice [95]. Thus each atom is tetragonally linked to four neighbouring boron or nitrogen atoms by strong covalent bonds as shown in figure 2.6. It is this strong covalent bonding which is responsible for the extreme hardness in both diamond and cBN, and it also gives a reasonable explanation for the somewhat lower hardness of cBN in comparison with diamond[83].

Properties of cubic boron nitride.

Most of the properties of cubic boron nitride are similar to those of diamond because of their electronic and structural properties which are similar. Cubic boron nitride is the second hardest known material after diamond. Compared to diamond cBN has several other advantages, in particular higher thermal stability, stronger chemical stability with respect to ferrous alloys, the possibility of n or p doping and the emission of blue light at the p-n junction [84]. The table below summarizes the most important properties of c-BN and diamond.

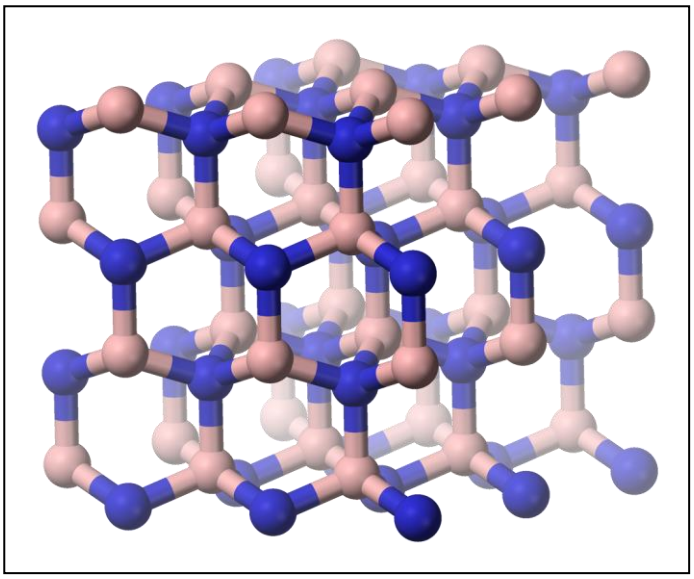

Figure 2.6 Crystal structure of cubic boron nitride[85]

Table 2.4 Physiochemical properties of cBN and diamond [84].

	cBN	Diamond
Structure	Cubic *F*43*m*	Cubic *Fd*3*m*
Unit cell parameter (Å)	a=3.165	a=3.567
Interatomic distance (Å)	d=1.57	d=1.54
Density (g cm $^{-3}$)	3.48	3.52
Hardness(Kg mm $^{-2}$)	4500	9000
Conductivity (W cm K)	13	20
Expansion ($^{o}C^{-1}$)	4.8	3.5
Stability against oxidation (^{o}C)	1200	600
Graphitization (^{o}C)	>1500	1400
Resistivity (Ω cm)	10^{10}	10^{16}
Refractive index (5893 Å)	2.117	2.417

Synthesis of cubic boron nitride

Cubic boron nitride is normally synthesized from the hexagonal polymorph, hBN by applying high pressures and high temperatures. In principle it is possible to synthesize cBN from hBN by solid state phase transformation at high pressure and high temperature without using any catalysts[86]. However for practical purposes solvent catalysts are used to reduce the high pressure high temperature conditions. The first successful synthesis of cBN by high pressure and high temperature, similar to that of diamond using Li_3N as catalyst was first reported by Went orf in 1957 [87] . Since then various kinds of catalysts, which reduce the temperature and pressure needed to synthesize cBN, have been examined by various authors[88] [89].

Approximately fifty different kinds of catalysts such as alkali and alkaline earth metal nitrides, fluoronitrides and ammonium borates have been found to have catalytic effect on the formation of cBN. Most of these materials form a eutectic with boron nitride and formation of cBN proceeds via the dissolution of hBN in the eutectic liquid followed by precipitation of cBN in its thermo dynamical stable region[90] .Some of the materials known as effective catalysts for cBN synthesis are Lithium, magnesium, calcium, and their nitrides or boron nitrides (e.g Li_3BN_2, Mg_3BN_3 and $Ca_3B_2N_4$) [91] [89] .

Boron nitride Phase transformations.

Since boron nitride exists in two major crystalline forms, hexagonal Boron Nitride and Cubic Boron nitride, intensive research has been done to elucidate the temperature – pressure conditions under which such transformations take place.

A phase diagram of boron nitride was first reported by Bundy and Wentorf in 1963[92] , with cBN being the stable phase at ambient conditions. This was changed however, in an ensuing publication by Corrigan and Bundy in 1975[93], who considered a phase transition line parallel to that of graphite/diamond, thereby intersecting at room temperature at 1.3 GPa and thus implying now cBN at low pressure a meta stable phase. This picture was adopted for many years until calculations by Solozhenko [94] demonstrated cBN as the stable phase. In order to further clarify the discrepancies on the cBN phase diagram G. Will et al [95] also did some investigative *in situ* diffraction experiments at high temperature and pressure to see the transformation from hBN to cBN and the back transformation from cBN to hBN. In their work they concluded that the phase diagram of boron nitride is not comparable to that of carbon as was assumed in the past. They also concluded that the cubic phase is definitely the stable phase at low pressures and that the transformation depends strongly on parameters like grain size, defect concentration and purity of the starting material.

Factors affecting transformation boron nitride.

H. Lorenz *et al* [96] investigated the influence of initial crystallinity on high pressure –high temperature transformation of boron nitride by using boron nitride powders with different initial crystallinity. They observed that for the most disordered material (amorphous BN) the direct transformation to cBN starts at relatively low pressures and temperatures (1200 ^{o}C and 7.2 GPa). This meant that decreasing BN crystallinity of the initial material leads to a considerable reduction of the thermodynamic conditions needed to produce cBN.. HRTEM investigations showed that an amorphous layer forms around the growing cBN grain and this enhances the diffusion of the growth units to the interface of the new phase.

H. Sachdev *et al* [97] investigated the effects of grain size and impurities on the cBN to hBN transition. They found out that powders with smaller grain size transform into hBN at much lower temperatures compared to powders with bigger grains. Three different powders with grain sizes of 0.75 -1.5μm, 40-80μm and 600μm had conversion temperatures of 900, 1300 and 1500 ^{o}C respectively. This can be explained by the fact that powders with smaller grain size have a higher surface to- bulk ratio therefore would react much quicker than larger crystals [97] . They also found out that presence of impurity (boron oxide) on the surface of cBN also influences the conversion mechanism. Conversion of cBN to hBN proceeds by forming an intermediate rhombohedral phase and it is considered that boron oxide acts as a catalyst for the formation of rhombohedral boron nitride [97] .

Oxidation of boron nitride

One advantage of cBN over diamond is its resistance to high temperature oxidation. However at elevated temperatures boron nitride would also start to oxidize. Thus in order to predict high temperature properties of Boron nitride based composites it is necessary to have an understanding of its behavior at elevated temperatures. V.A. Lavrenko and A.F. Alexeev [98] did some work to investigate the high temperature oxidation of various Boron nitride samples in the temperature region of 600- 1200 ^{o}C. They found out that in the temperature range 600 - 800 ^{o}C boron nitride does not react with oxygen. Boron nitride oxidation was observed to start at 900 ^{o} C and oxidation kinetics behaved in a parabolic manner until 1200 ^{o} C then it behaved in a linear manner. Oxidation product was mainly B_2O_3 observed as thin film covering the original material and NO_2 gas. N. Jacobson and S. Farmer [99] also studied high temperature oxidation of boron nitride in the temperature range 900- 1200 ^{o} C. They found out that the main oxidation product was $B_2O_{3(l)}$ and that the oxidation kinetics are sensitive to crystallographic orientation , porosity and impurity levels.

Boron nitride cutting tools

Cubic boron nitride has high hardness and thermal conductivity second only to diamond and a low affinity to ferrous materials hence it is widely used in grinding and cutting applications for ferrous materials. CBN is normally used as a cutting material when hard metals become limited in the cutting speeds that can be employed. This applies to hard work piece materials such as high speed steel, tool steels, case hardened steels, chilled cast iron, satellite etc. It offers no advantages and does

not perform well on soft steels, inconel and nimonics and austenitic stainless steel [53] .

PCBN works by self-induced hot cutting, a process which causes local softening in the shear zone of the work piece material. The heat generated is discharged through the chips as well as through the PcBN insert, leaving the hardness of the work piece unaffected. In achieving effective self-induced softening of the work piece, PcBN's high hot hardness and chemical stability are fully exploited. Good toughness and cutting edge stability are also important under these machining conditions [100].

Typical cBN Cutting tools

Conventional cBN based composites available commercially as cutting materials contain a ceramic or metallic binder which facilitates sintering and optimize cutting performance. Usually metals of group 4, 5 and 6 of the periodic table and/or other metallic elements, such as aluminum, cobalt and nickel are used to activate sintering[101], [102] . Table 2.5 shows properties of typical cBN cutting tools with different binders.

CBN cutting tools can also be available as solid indexable inserts or as inserts consisting of an upper face of cBN laid onto a hard metal base. It can also be available as a piece of cBN brazed onto a corner of a hard metal indexable insert. Solid indexable inserts are particularly suitable for heavier roughing work, especially for machining tools [53].

Table 2.5 Typical properties of cBN cutting tools[103]

Wt % cBN	Binder phase	Elastic modulus(GPa)	Poisson's ratio	cBN grain size (μm)
90	AlN and AlB2	648	0.145	15
80	TiC and Al compounds	981	0.160	10
50	TiC and Al compounds	595	0.170	1-2
45	TiC and Al compounds	582	0.177	1-2

PCBN Physical and Mechanical properties.

The physical properties of PCBN cutting tool materials is determined by a number factors. The cBN grain size and content can affect the abrasion resistance, edge quality and thermal conductivity of the PCBN product. For machining conditions where the mode of wear is predominantly abrasion , for example in the machining of cast iron coarse grain, high cBN content material will give optimum performance and for finish machining where good edge quality is required, fine grained lower cBN content material would be appropriate [100]. Type of binder phase used also has a considerable effect on the performance of PcBN materials, particularly in the case of low cBN content products where the PCBN binder content can be less than 50% by volume. Figure 2.6 shows the relationship between cBN content and grain size on PCBN properties of some commercial PCBN cutting tools.

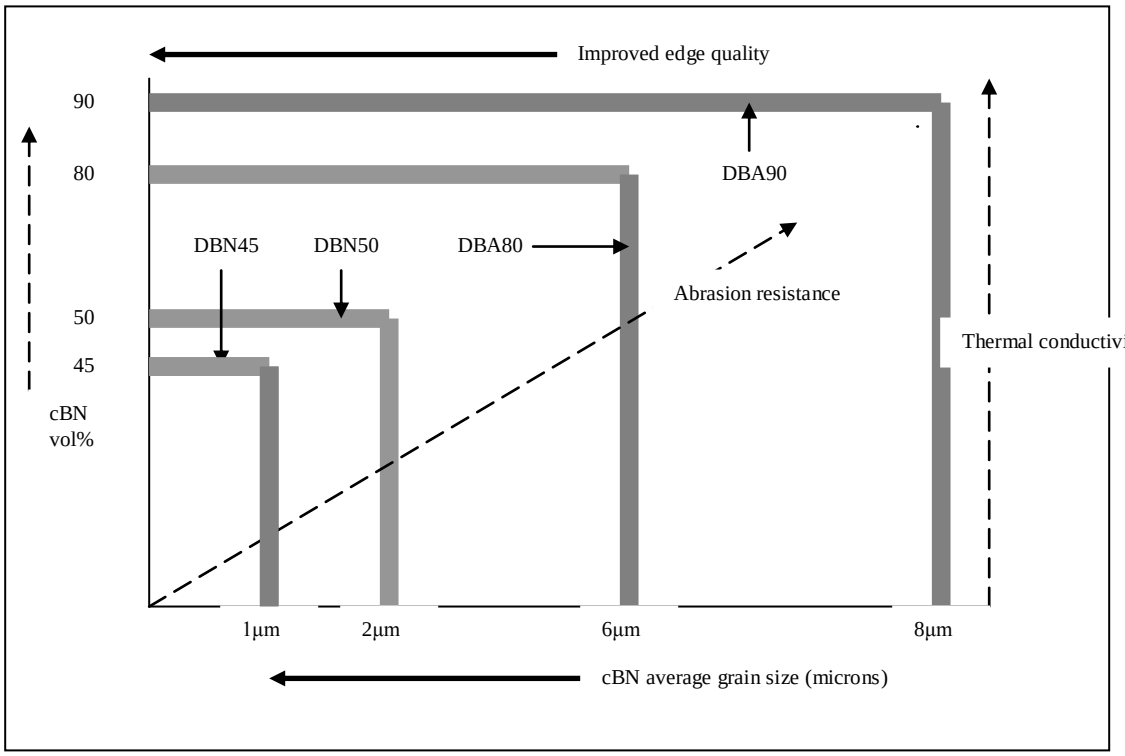

Figure 2.7 Effect of cBN content and grain size on PCBN properties[104]

Recent developments in cBN cutting tools

Benko *et al* [101] studied the phases and microstructures developed in cBN composite synthesized by hot pressing with Al as the binding phase in the molar ratio BN;Al of 9;1. They observed that BN and Al reacted to form AlN and that in the area between AlN and BN phases polycrystalline AlB_{10} and AlB_{12} phases could be seen. Hardness of the samples increased after annealing and thermal treatment also resulted in increase in mechanical strength of the sintered BN-Al system.

In another investigation Benko *et al* [105] also looked at the phases and properties of composites cBN-TiN and cBN-TiC. Experimental cBN-TiC/TiN composites were prepared by high pressure hot pressing and samples were subsequently heat treated It was shown that in the

temperature range 1000 to 1400 ^{o}C TiN reacts with cBN to form one new phase , TiB_2 and that TiC reacts with cBN forming two new phases TiB_2 and $TiC_{0.8}N_{0.2.}$

On the other hand, a polycrystalline cBN compact with no additives (PCBN) can also be synthesized by direct transformation from a low pressure phase of BN under ultra high pressure and high temperature[106] ,[107] T. Ohashi *et al* [102] studied the influences of synthesizing conditions on properties of PCBN such as microstructure, hardness, cutting performance and thermal conductivity. In their work hBN was used as starting material and was converted to cBN by treating it at 6.8 GPa and at temperatures from 1800 ^{o} C to 2500 ^{o} C. Samples treated at 1800 ^{o} C consisted of hBN and cBN started to form at 2100 ^{o} C. At 2100 ^{o} C the microstructure consisted of fine (<1μm) homogenous cBN grains and became heterogenous with some coarse grains at 2300 ^{o} C and at 2500 ^{o} C there was remarkable grain growth with twinning. It was observed that hardness decreased with increase in processing temperature, probably due to grain growth. Thermal conductivity increased with increase in processing temperature, probably due to the fact surface area decreases with increase in processing temperature. For cutting tests results it was found out that sample processed at 2100 ^{o} C had excellent wear resistance while sample processed at 2500 ^{o}C had similar wear resistance to conventional cBN-Co composites.

Chapter 3: Experimental Details

This chapter give details of the raw materials used, equipment and analytical techniques employed for characterizing materials in this thesis.

3.1 Chemicals

Chemicals used in this study and their respective specifications are shown in table 3.1.

Table 3.1 Chemicals used.

Chemical	Supplier	Grade and properties
Aluminum	Saarchem (R.S.A)	99.8% purity with particle size of 2-5microns
Alumina	Sumitomo (Japan)	A-Alumina (AKP50) with a purity of 99.99% and particle size of 0.1 -0.3 microns
Cubic Boron nitride	Element Six (RSA)	Particle size 2 -5 microns
Cyclohexane	Associated Chemicals (RSA)	Assay purity of 98.5%
Stearic acid	Hopkin and Williams (UK)	Iodine value < 4% and an acid value of 200 to 100. Sulphated ash <0.1%
Zinc stearite	Riedel-de-Haen (Germany)	Assay of Zinc 10-12% and ash content of 12-15%

3.2 Equipment

Attrition mill

A Szegvari attritor system type B from Union Process was used for milling powder raw materials. The attritor was water cooled fitted with a 750cc alumina vessel and an alumina agitator. In this work 2mm alumina balls were used as milling media and cyclohehane was used as milling solvent.

Rot vapor

A Heidoiph Laborota 4000 rot vapor fitted with a hot water bath was used to dry off the solvent (cyclohexane) from the milled slurry to form powder.

Uniaxial press

A custom made uniaxial hydraullic press with a 30mm radius plunger capable of delivering a pressure of 40MPa was used to make the pellets. Although the press plunger is capable of delivering a maximum pressure of 40MPa higher pressures were achieved by using dies with smaller cross sectional area. For this work a stainless die with an internal diameter of 18mm was used .

Box furnace

A Eurotherm 2416 box furnace manufactured by Elite Thermal systems capable of heating up to 1600 ^{o} C was used to heat treat the pellets so as to convert aluminum into alumina. To avoid any possible reaction or cross contamination all samples to be fired were placed in alumina boats.

Hot press

A unaxial hot press system was used to densify the samples. This system is equipped with a carbon heated furnace with a maximum obtainable temperature of 2000 ^{o}C and a steel loading frame capable of delivering loads of up to 10 000 Kg. This force is applied unaxially through graphite punches. In addition the system is also equipped with a water cooling system and a vacuum pump capable of attaining vacuum levels of 10 mtorr. All samples were either heated in Argon atmosphere or under vacuum.

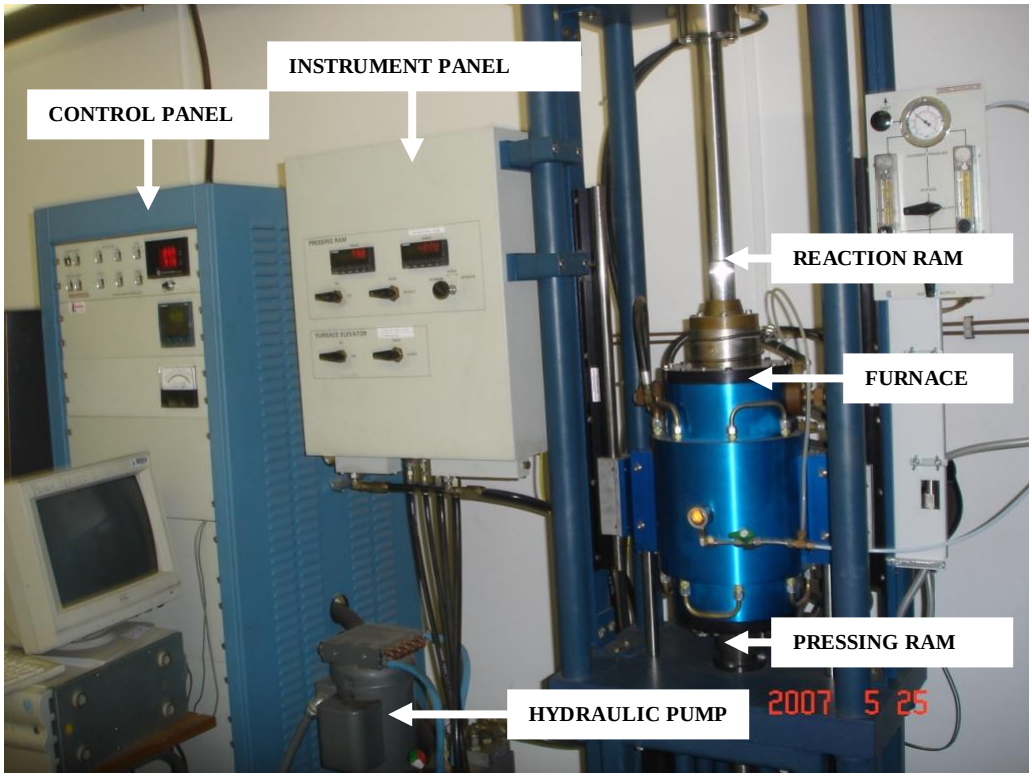

Figure 3.1 Hot press system.

3.3 Analytical techniques

Phase analysis (Qualitative and quantitative) X-ray diffraction

Qualitative and quantitative phase analysis of powders, reacted pellets and sintered samples was done using X-ray diffraction. For green and reacted samples (partially sintered) measurements were done on the surface and for sintered samples measurements were done on polished cross section. Diffraction patterns were collected using a Bruker AXS D8 machine equipped with a primary beam Göbel mirror, a radial soller slit, a V Åntec-1 detector and using Cu-K $_{\alpha}$ radiation (40kV, 40mA). Data were collected in the 2θ range 5 to 90 ^{o} in 0.021 steps, using a standard scan speed with an equivalent counting time of 14.7 s per step.

For qualitative analysis the resulting diffractograms were analysed using X'Pert high score software developed by Philips.

Quantitative phase analysis was done using the following equation

$$I_{(hkl)} = K_m K_p \quad \text{.....(1)}$$

Where $I_{(hkl)}$ is the peak intensity , K_m represents the physical constant and measurement factors (which is constant for all samples measured on the same machine under the same conditions) and *Kp* represent the phase related factors.

Kp for each phase was then calculated using the equation

$$Kp = \frac{p_{hkl}}{V^2} F^2_{hkl} \frac{1+\cos^2 2\theta_{hkl}}{2\sin 2\theta_{hkl} \sin \theta_{hkl}} \quad \text{.....(2)}$$

Where $p_{(hkl)}$ is the multiplicity, V is the cell volume and F is the structure factor. The intensity $I_{(hkl)}$ for each peak was determined by taking the peak area of the respective signal using a mathematical software.

Having evaluated the intensity and K_p the volume fraction of each respective phase was then calculated using the relationship

$$V\%_{(Al_2O_3)} = \left[\frac{\frac{I_{(hkl)}}{Kp_{Al_2O_3}}}{\left(\frac{I_{Al_2O_3}}{K_{p_{Al_2O_3}}}\right)+\left(\frac{I_{Al}}{Kp_{Al}}\right)+\left(\frac{I_{BN}}{Kp_{BN}}\right)+\left(\frac{I_{Al_4B_2O_9}}{Kp_{Al_4B_2O_9}}\right)} \right] * 100 \ldots\ldots\ldots\ldots\ldots (3)$$

Peaks and relevant parameters used for quantifying each phase are shown in table 3.2.

Table 3.2 Phase parameters used for quantification.

Phase	2θ	$h\ k\ l$	P	F^2	V	K_p	*Ref*
Al_2O_3	35.14	104	6	6496	255	2.874	1-071-1123
Al	38.47	111	8	1283	66.9	9.025	1-089-2769
cBN	43.26	111	12	267.5	47.4	4.326	1-079-062
$Al_{18}B_4O_{33}$	16.46	110	4	607.14	164	2.104	0-029-0009

Particle size determination -Malvern analyzer

A Malvern Mastersizer 2000 was used for particle size determination. A small quantity of powder was diluted in ethanol in a small beaker, then placed in an ultrasonic bath to break up any agglomerates. The analyzer was filled with ethanol and then the diluted powder was slowly added The accuracy of the equipment is ±4% (volume median

diameter). In all instances the pump speed was set at 40% of its maximum and the ultrasonics adjusted to 80% and a 45mm focal length lens was used.

Microstructural analysis-Scanning electron microscope

A Joel scanning electron microscope was used to assess the microstructure of the materials after reaction and hot pressing. The microscope was normally operated at an accelerating voltage of 20 kV. Before analysis samples were coated with gold to provide conductivity and were the mounted on graphite tape before analysis.

Pore size and distribution- Mercury Porosimeter

Median pore diameter of green and reacted samples were determined using mercury porosimetry (Poresizer 9320, Micrometrics, USA).

Density measurements.

Density of green and reacted samples was determined geometrically, by measuring the mass, diameter and height of the pellets.

Density of sintered samples was determined using the Archimedes method. Samples were weighed dry (M_d) before being boiled in water for three hours in order to drive air from the pores. After boiling the samples were left soaking in the water overnight. The mass of the samples suspended in water (M_s) was determined followed by the soaked mass (M_w). Please note that before determining the soaked mass the samples were first wiped with a light towel to remove excess water from the surface of the samples. The density and porosity of the samples was then calculated using the following equations.

$$Density = \left[\frac{M_d}{M_w - M_s} \right] \quad \text{.....(1)}$$

$$Porosity = \left[\frac{M_w - M_s}{M_w - M_d} \right] * 100 \text{ .....(2)}$$

Where ever possible density values were expressed as a percentage of the expected theoretical density. The expected theoretical densities were calculated from the percentage mass composition of the constituent phases and their respective theoretical densities using the formular.

$$\rho = \frac{100}{\sum \frac{\%M_x}{p_x} + \frac{\%M_y}{p_y} + \frac{\%M_z}{P_z}} \text{ .....(3)}$$

Where M_x, M_y and M_z are the percentage mass compositions of phases x, y and z and ρ_x, ρ_y and ρ_z are the respective theoretical densities.

Hardness and Fracture toughness measurements

Hardness measurements were done using a Leco V-100 hardness tester. All measurements were done using a load of 10 Kg for 10 Sec. Hardness was calculated using the formular

$$H_v = 1854.4 \frac{P}{(2a)^2}$$

Where

P = Applied load in newtons and $2a$ = Indentation diagonal in μm.

Fracture toughness determinations were done by measuring crack lengths from the indented sample according to the equation given below.

$$K_{IC} = 0.0889 * \sqrt{\frac{H_v * P}{4 * l}} \quad (103)$$

Hv = Vickers hardness

P = Load and

$l = c - a$ Where $2a$ is the indentation diagonal and $2c$ is the combined length of two opposite cracks including the indentation diagonal length.

3.4 Experimental procedure

Milling

Weighed quantities of alumina, aluminum and cubic boron nitride were slowly charged into a 750 ml alumina vessel containing cyclohexane, 1mm alumina balls and 0.5% stearic acid. The amount of stearic acid added was determined from the total mass of alumina, aluminum and cBN .The vessel was attached to a Szegvari attritor system fitted Al_2O_3 blades rotating at a speed of 50rpm. When all the powder has been added the rotation speed was increased to 700rpm and the powders were milled for eight hours.

In each instance the masses of alumina, aluminum and cubic boron nitride charged were determined in such away as to give respective volume percentages required for that particular batch. Densities of alumina, aluminum and cubic boron nitride used for this determination are 3.98, 2.7 and 3.48 g/cm^3 respectively. . In each instance the volume ratio of powder to balls was 1:5 and the vessel was filled up to two thirds of its volume capacity.

The starting compositions (volume) of powder mixtures used in this work are given in table 3.2 .

Please note that elsewhere in this work samples will be designated according to their initial Al:Al_2O_3:BN compositions (volume %) before milling. For an example **502030** refers to sample with the following initial compositions of Al (50 volume %), Al_2O_3 (20 volume %) and BN (30 volume %) and **505000** refers to sample with an initial composition of Al (50 volume %) and Al_2O_3 (50 volume %).

Table 3.3 Mass composition of starting materials

	Compositions (Mass %) and designations			
Material	**502030**	**504010**	**454510**	**505000**
Al	42.32	41.03	26.23	40.42
Al_2O_3	24.95	48.39	53.40	59.58
BN	32.73	10.58	10.38	0

Drying and sieving

After milling the slurry was transferred to a rotary evaporator with a water bath set at ± 60 ^{o} C. The alumina balls used for milling were thoroughly washed with cyclohexane and the resultant elutants was also transferred to the rotary evaporator to maximize on the recovery of milled powders . After drying the powders were passed through 38μm sieve to break soft agglomerates.

Cold pressing.

The powders were then weighed out into ± 2.00gram quantities for green compaction. Green compacts were produced using stainless steel dies with an internal diameter of 18 mm and a custom made uniaxial press described in section *2.2.3*. For each powder composition samples were pressed at three different pressures that is 45, 90 and 180 MPa.

Heat treatment.(Oxidation)

The green pellets were reacted in air in a box furnace (Lenton) described in section *2.2.4* in order to facilitate conversion of Aluminum metal into the oxide

$Al + 3/2\ O_2 \rightarrow Al_2O_3$.

In a typical heat treatment cycle the samples would be heated from ambient temperature up to 500 ^{o}C at a rate of 3 ^{o}C per minute followed by a soak at 500 ^{o} C for 300 minutes. From 500 ^{o} C the temperature would increase at a rate of 3 ^{o}C to the required reaction temperature ., Once the reaction temperature has been attained the furnace would start to cool down to ambient temperature at rate of 10 ^{o}C per minute. However for samples heat treated to 1000 ^{o}C a soaking time variable was also introduced into the study whereby instead of stopping the reaction after reaching 1000 ^{o}C samples were soaked for different times i.e 0 , 60, 180 and 300 minutes to assess the effect of soaking time on the reaction before cooling to ambient temperature.

After heat treatment samples were assessed for the following density , mass, dimensions (diameter and height), and phase analysis (both qualitative and quantitative) using X-ray diffraction as described in section *2.3.2*.

Hot pressing

A hot press equipment described in section 3.2.5 was used to densify the samples. Reacted pellets were placed in 18mm diameter graphite pots equipped with pistons of same diameter. Before sintering all graphite components, including punch and die were coated with an hBN suspension.

After placing the samples in the furnace the whole system was evacuated to pressures less than 100 mtorr using a vacuum pump. This

was followed by purging argon into the system at a rate of 40ml/min. Once there was a stable flow of argon in the system the furnace was switched on and rumped at a rate of 40 ^{o}C per minute to a temperature which is 100 ^{o}C less than the intended sintering temperature. At this point the hydraulic system was then activated and load was slowly applied until the desired load was attained. Once the desired load was attained the temperature was rumped to the desired value and soaked for the required time. During the soaking period pressure was maintained manually. After the soak period the load was removed and furnace rumped down to ambient temperature at a rate of 10^{o} C per minute. Below is a schematic representation of a typical temperature – pressure profile used.

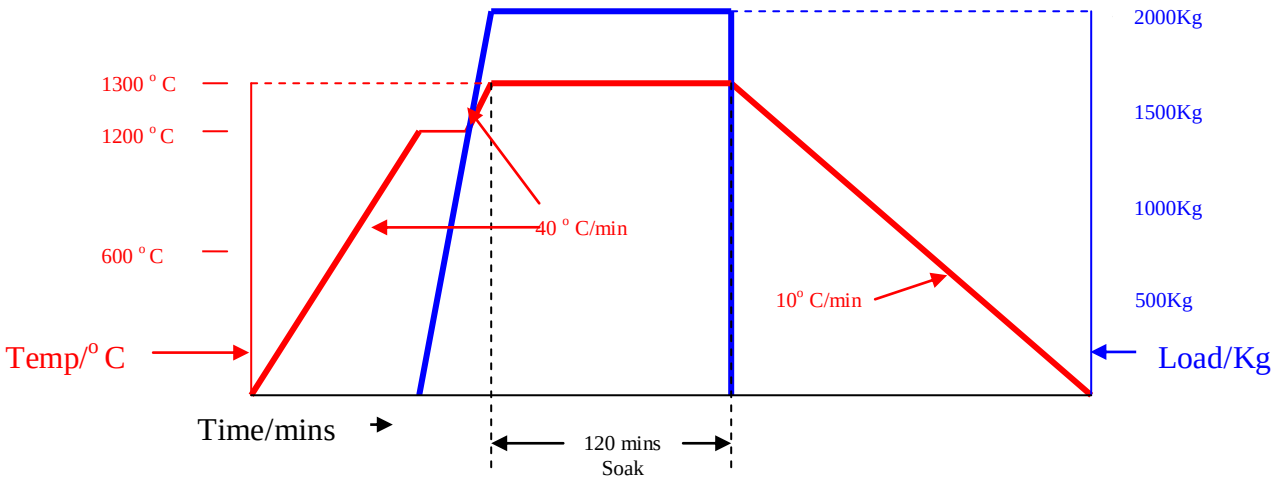

Figure 3.2 Schematic representation of the heat treatment - pressing cycle used to densify samples.

Chapter 4: Results and discussions.

Introduction

This chapter deals with the experimental results obtained at various stages from milling of the raw materials through compaction into green bodies and initial heat treatment up to final sintering. At each of these processing stages various techniques are used to characterize properties of the materials. These are discussed together with their effects on the properties of the final product. Also discussed in this chapter is the oxidation kinetics of Al into Al_2O_3 and the interaction of cBN with Al_2O_3 together with the relevant phase diagrams and thermodynamic considerations.

4.1 The milling Process

Wet milling of Al_2O_3 and Al raw materials is a very important step which predetermines the characteristics of the precursor powders hence properties of the final product. Success of the reaction bonded aluminum oxide process depends to a large extent on the particle size of the aluminum. Coarse aluminum particles result in incomplete oxidation leading to microstructural in homogeneities. Thus the primary objective of the milling process is to produce fine aluminum crystallites and to have them homogenously distributed with the alumina and cBN particles. Only Al and Al_2O_3 mixtures were attrition milled and after milling and drying the right amount of cBN was then added to the milled powder and sonicated in cyclohexane for ten minutes.

Predicting characteristics of the milled powders became a complicated issue because the chemistry of one of the components (aluminum) changed during milling i.e oxidation and hydroxylation.

Optimization of the milling process involved monitoring particle size distribution morphology and surface area of the milled powders as a function of milling time.

Particle size distribution.

Size distribution of the raw materials in the received state was measured using Malvern Analyzer (see section 3.3.2 for details). The powders were milled as described in section 3.2.1 with samples being withdrawn periodically to check size distribution as a function of time (see Figure 4.2).

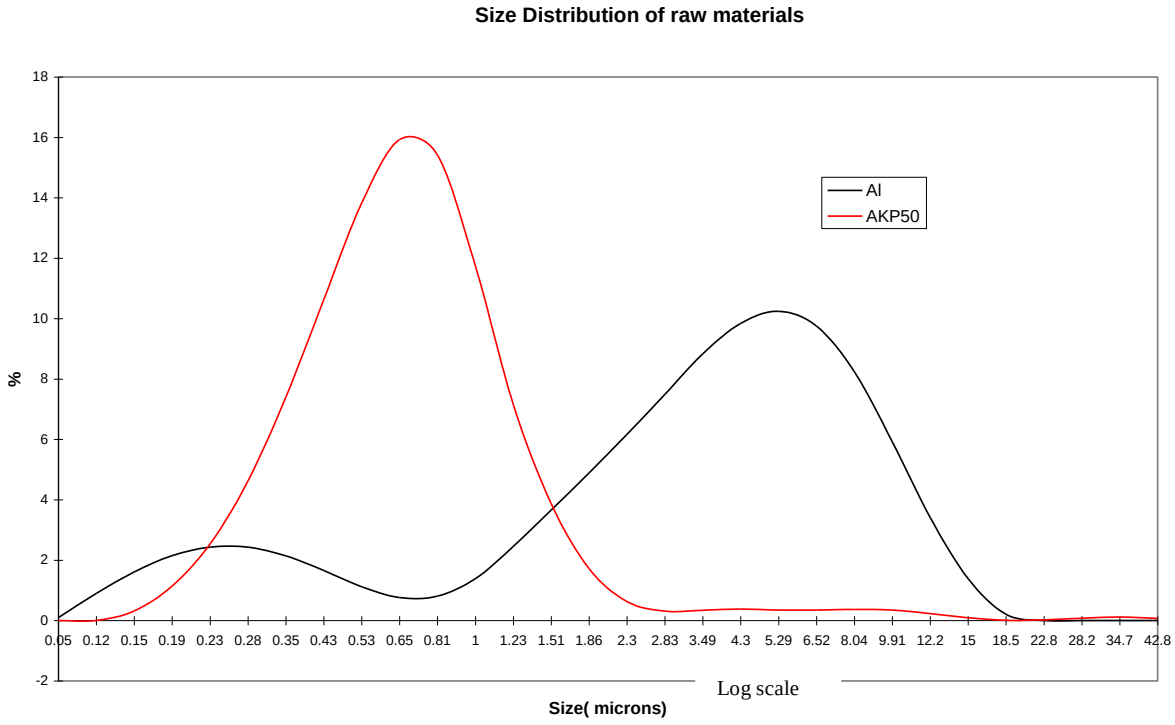

Figure 4.1 Particle size distribution of aluminum and alumina before milling.

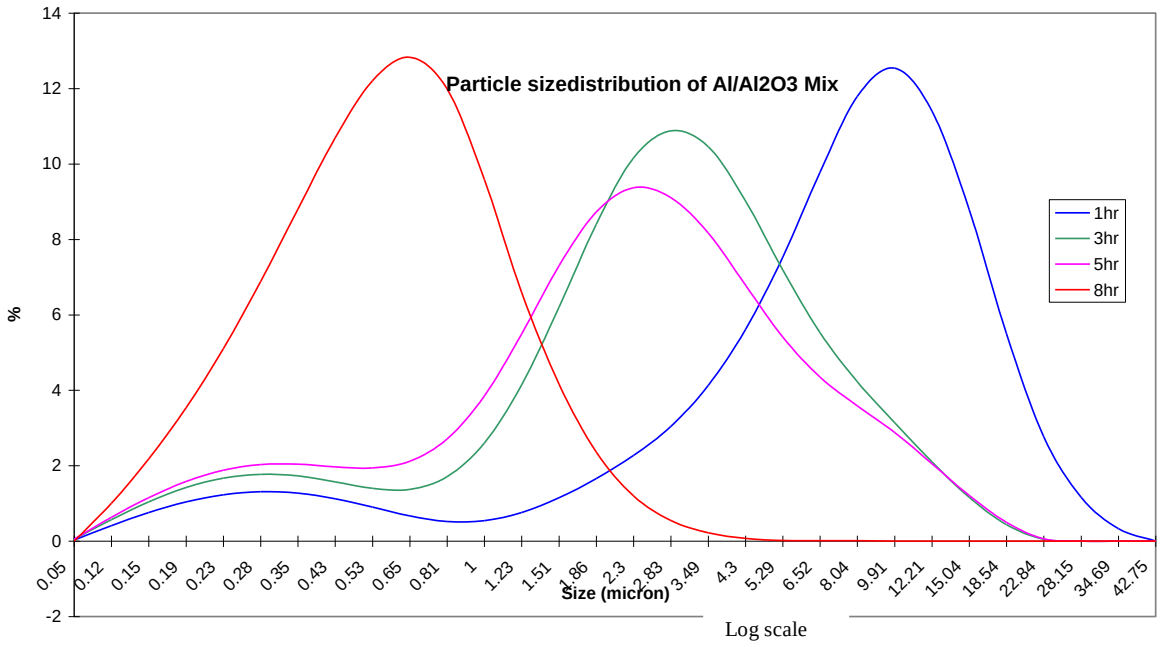

Figure 4.2 Particle size distribution of 505000 powder as a function of time.

The starting aluminum had a bimodal distribution of particles with a mean size of 4 microns and the particles are coarser than those of alumina. As a result the size distribution of the 505000 mixture before attrition milling also exhibits a bimodal distribution .However as milling proceeds the distribution shifts to finer size and after eight hours the mixture had a monomodal distribution with a mean particle size of 400 nanometers.

Morphology of the powders.

The morphology of the starting materials are shown in figures 4.3 and 4.4. As seen in the micrographs, Aluminum consists of spherical particles ranging in size from 2 to 5 microns. Alumina consists of very fine powder with most particles falling within the sub micron region.

During the initial stages of milling the aluminum particles get deformed and flattened into flakes by the milling forces. This is mainly due to their ductility and the resultant morphology is shown in figure 4.5 for powder mixture milled for one hour. As milling continues the flakes impinge on each other resulting in size reduction. Alumina, because of its abrasive nature also contributes in cutting the flakes resulting in size reduction such that after eight hours of milling the powder consists of very fine flakes of Al homogenously mixed with Al_2O_3. This is shown in figure 4.6.

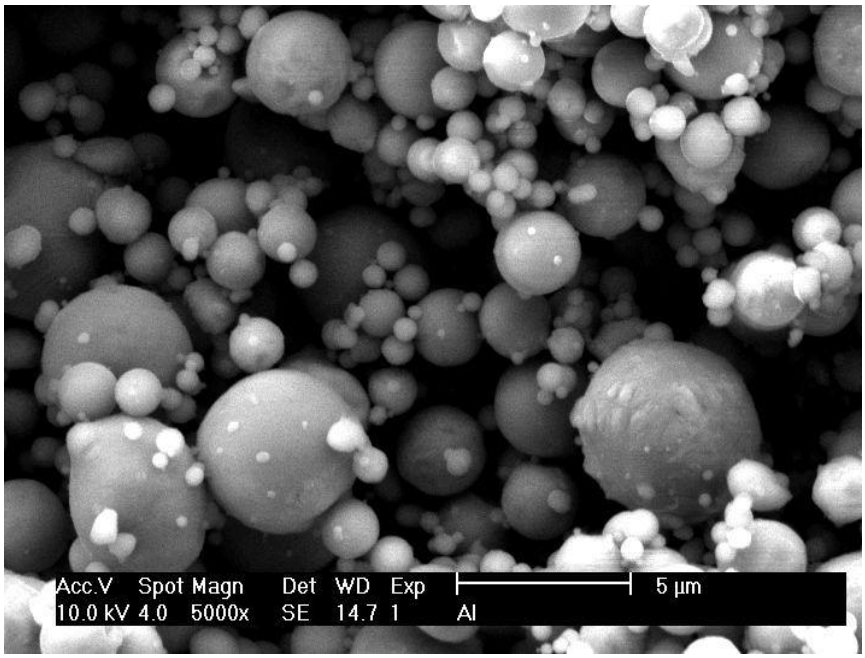

Figure 4.3 Morphology of the raw aluminum powder before milling.

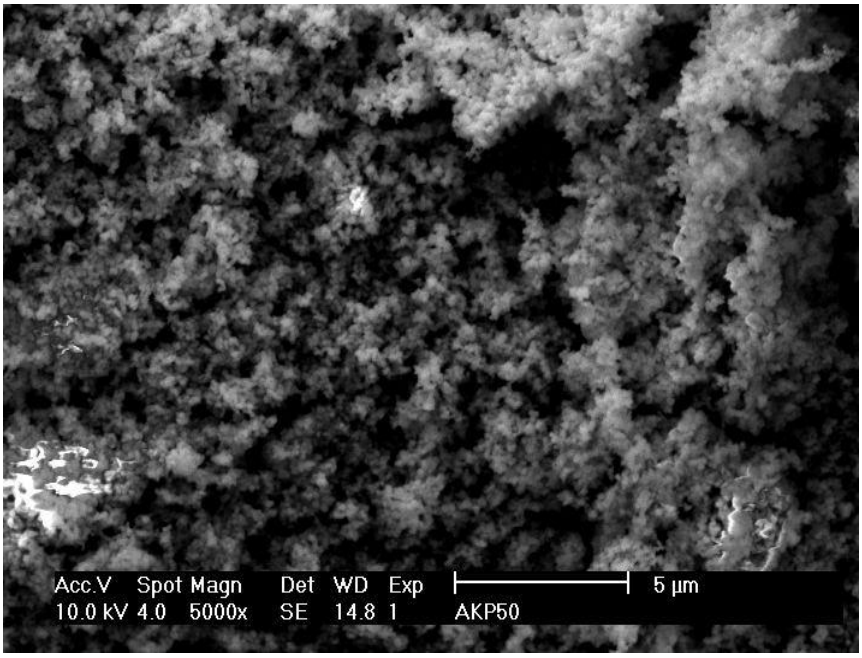

Figure 4.4 Morphology of the raw alumina powder before milling.

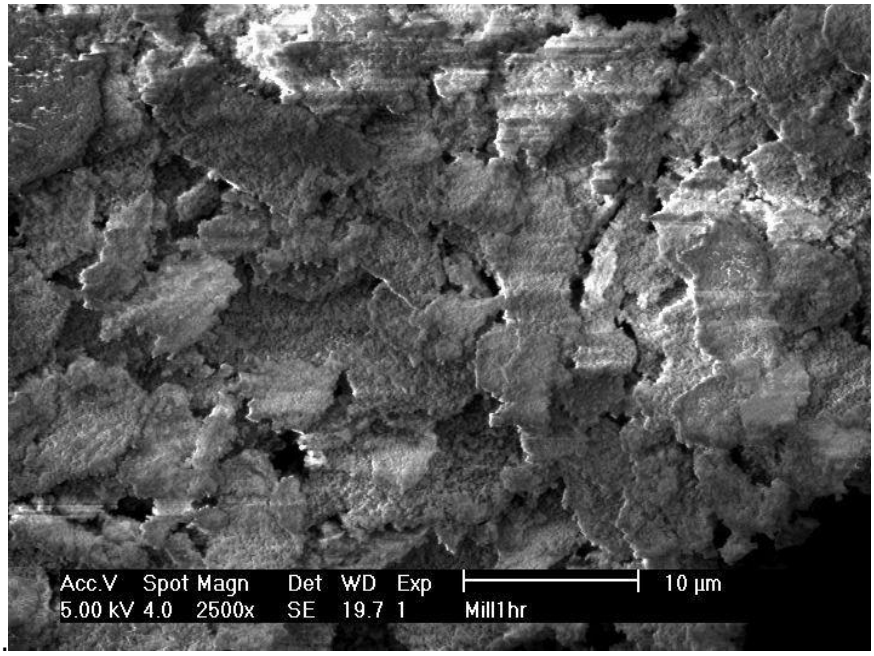

Figure 4.5 Alumina/Aluminum mixture (505000) after 1 hour of attrition milling.

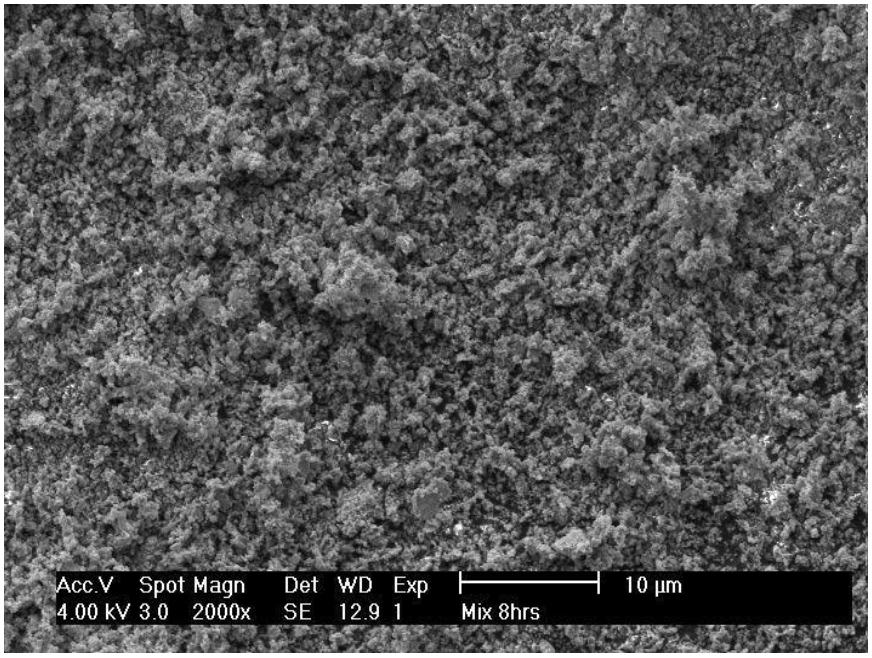

Figure 4.6 Alumina/Aluminum mixture (505000) after 8 hours of attrition milling.

Oxidation during milling

The milling process results in the formation of new Al surfaces which then react with air to form new oxide phases. Figure 4.7 shows X ray diffractograms of sample 505000 as a function of milling time. From the diffractograms it is evident that as milling proceeds the Al peak decreases in intensity and also becomes broader. The decrease in intensity is due to some of the aluminum being oxidised. However the fact that there is no corresponding increase in the alumina intensity can be attributed to the armophous nature of the oxidation products. The broadness of the Al peak with milling time is caused by the distortion of the Al crystal lattice and reduction in Al crystallite size with milling.

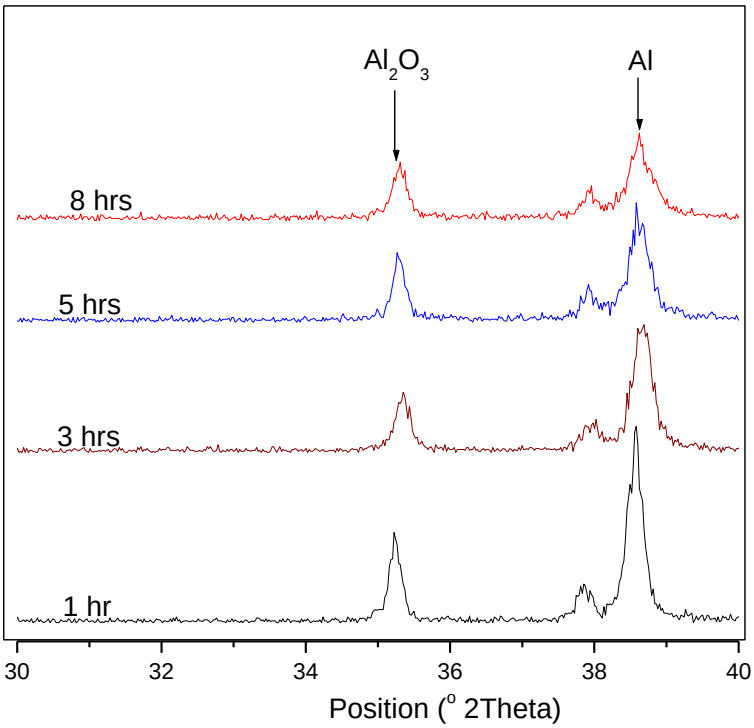

Figure 4.7 X ray Diffractogram for composition 505000 milled for 1, 3, 5 and 8hours.

Quantitative phase analysis described in section 3.3.1 was used to quantify the amount of aluminum oxidized during milling for all the precursor powders used in this study. The amount of aluminum oxidized during milling expressed as a percentage of the initial amount present before milling was determined for all the precursor powders used in this study and results are shown in the table 4.1.

The amount of aluminum oxidized during milling is almost constant for all precursor powders regardless of composition.

Table 4.1. Amount of Al oxidized during milling

Sample	502030	504010	454510	505000
% Al Oxidised during milling	24.0	22.0	24.3	23.4

4.2 Properties of green bodies.

Characteristics of reacted bodies in the reaction bonded aluminum oxide process (RBAO) depends to a large extent on properties of the green bodies. Of particular interest are the green densities and pore characteristics.

Green densities are important because they determine green strength hence easy with which samples can be safely handled in the green state. In addition higher green densities result in smaller shrinkage during firing. Excessive shrinkage is undesirable because it results in distortion and increased chances of failure.

Pore size and distribution of green bodies is important because it determines oxygen flux diffusing through the sample which in turn determines the easy with which aluminum is converted into alumina.

Green densities

Densities of green bodies of various compositions pressed at different pressures were determined just after cold pressing by measuring the height, diameter and mass of the pellets.

For all compositions green density increases with increase in compaction pressure. This is expected since with increasing pressure there is more effective packing of particles resulting in a more dense body. Green density increases with increase in cBN loading. This can be due to the presence of cBN particles which are larger than Al/Al_2O_3 . figure 4.8 shows variation of green density as a function of compaction pressure for samples of various compositions.

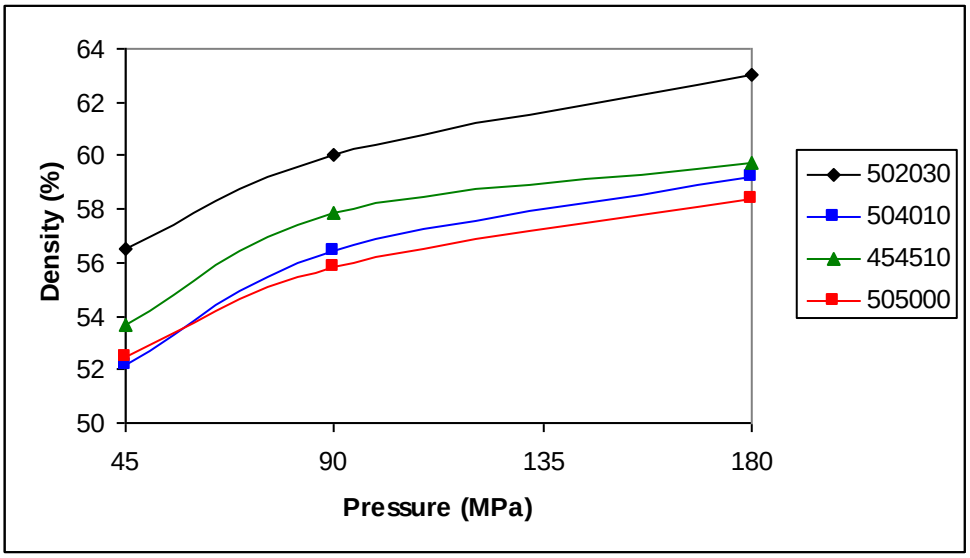

Figure 4.8 Green density as a function of compaction pressure.

Pore characteristics.

Porosity and mean pore diameters of bodies compacted under different pressures were measured using Poresizer 9320, Micrometrics, USA .

Table 4.2 Porosity and mean pore sizes for samples compacted under different pressures.

Sample	Pressure MPa	Total porosity (%)	Mean Pore diameter (μm)
502030	45	43.50	0.1208
502030	180	37.00	0.0931
504010	45	47.81	0.0816
504010	180	40.79	0.0596
454510	45	46.53	0.0798
454510	180	41.10	0.0486
505000	45	47.50	0.087
505000	180	41.62	0.0274

The results show, that materials with the highest cBN loading have the highest mean pore diameter. This is expected since cBN particles are much larger than aluminum and alumina resulting in much larger pores being left between two adjacent cBN particles. For each composition an increase in compaction pressure results in a decrease in total porosity and median pore diameter. This larger pore size of the cBN containing samples is also evident from the SEM micrograph of the fractured surfaces in figure 4.10.

Microstructural features

Microstructure of fractured surfaces for green bodies are shown in figures 4.9 and 4.10. From figure 4.9 it is evident that the green bodies consists of a uniform Al/Al_2O_3 submicron matrix. However it is difficult to distinguish Al and Al_2O_3 using SEM due to the emdebment of Al_2O_3 in Al. Figure 4.9 shows a fractured surface of sample containing cBN (502030). Here large cBN grains can be clearly seen evenly distributed within the submicron Al/Al_2O_3 matrix.

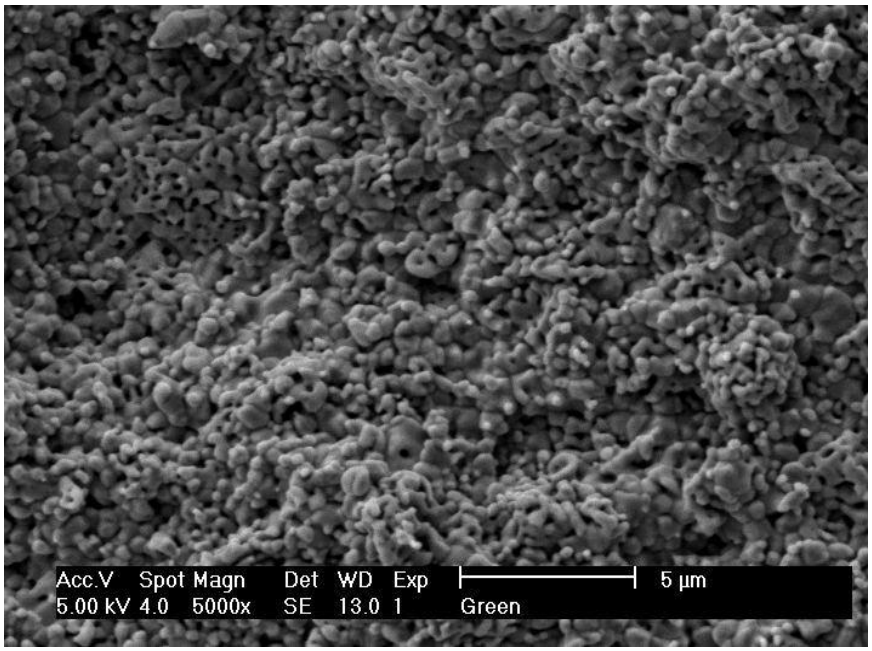

Figure 4.9 Micrograph of green fractured surface of sample 505000 compacted at 90 MPa.

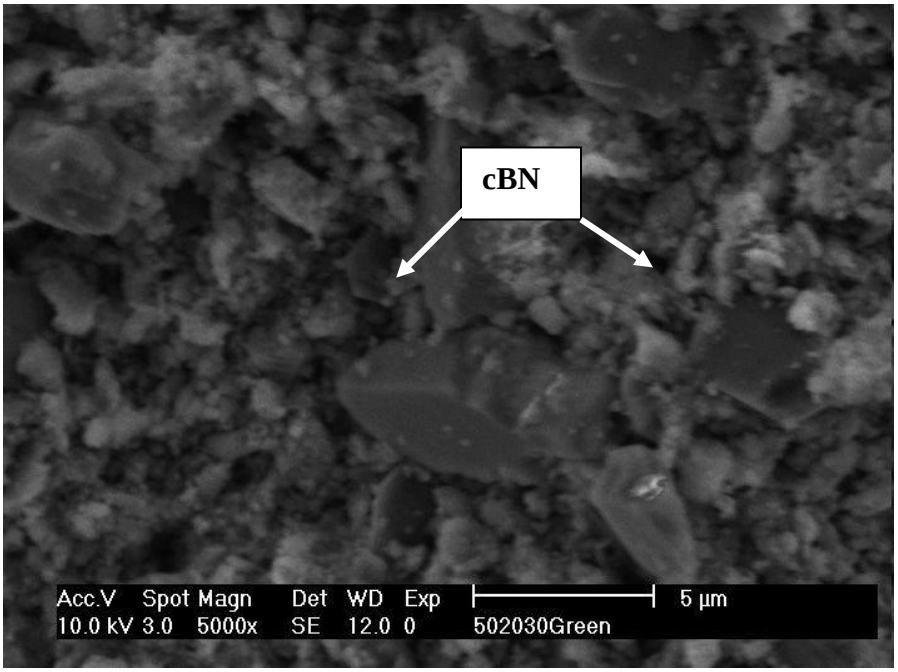

Figure 4.10 Micrograph of green fractured surface of sample 502030 compacted at 90 MPa .

4.3 Kinetic Studies.

Successful fabrication of reaction bonded aluminum oxide composites with cBN as second phase depends on the possibility to oxidize aluminum at temperatures at which cBN does not oxidize.

This section deals with assessing the combined effects of pressure, temperature, time and chemical composition on the oxidation of Al in the reaction bonded aluminum oxide process.

Quantification and interpretation of kinetic data relies on the definition of the degree of reaction. Degree of reaction must be defined such that it represents the reaction system accurately.

In this study two different parameters are employed to define the degree of reaction. The first one is mass change, (ΔW) incurred during oxidation of Al into Al_2O_3. This parameter assumes that $Al + 3/2\ O_2 \rightarrow Al_2O_3$ is the only reaction occurring during heat treatment of Al, Al_2O_3 and cBN mixtures in air hence any mass change incurred during heat treatment is attributed to the oxidation of aluminum. Raw data for this assessment was obtained by heat treating weighed pellets of various compositions compacted at different pressures (45 MPa and 180 MPa) to different temperatures ranging from 500 ^oC to 1000 ^oC at intervals of 100 ^oC. Soaking period at any particular temperature was zero minutes except for 500 ^oC and 1000 ^oC where additional soaking periods of 60, 120 180 and 300 minutes were also done. Degrees of reaction in each case was then calculated by comparing mass gain after heat treatment with initial mass before heat treatment.

The second parameter for measuring degree of reaction involved expressing amount of Al metal remaining after reaction as a percentage of the amount of Al initially available before heat treatment.

In this case quantitative x-ray diffraction was used to quantify the amount of aluminum remaining after heat treatment. This was then

expressed as a percentage of the initial amount present before heat treatment. The amount of aluminum present before heat treatment was corrected to take into account amount of aluminum oxidized during attrition milling.

Both methods are discussed in full in sections 4.3.1 and 4.3.2, respectively.

4.3.1 Mass change as a measure of degree of reaction.

Since the reaction $2Al + \frac{3}{2}O_2 \longrightarrow Al_2O_3$ ……ΔM = 88.88%

is accompanied by mass change one obvious way of quantifying degree of reaction would be by considering mass change incurred as a result of aluminum oxidation during heat treatment. If all initially available aluminum is oxidized then the theoretical mass gain incurred as a result of this oxidation is given by the equation

$$\Delta W_{Th} = \left[\left(\frac{M_{Al} * 1.88 + M_{Al_2O_3} + M_{BN}}{M_{Al} + M_{Al_2O_3} + M_{BN}} \right) - 1 \right] * 100 \text{ ……} \textbf{(4.3.1)}$$

Where M_{Al}, M_{Al2O3} and M_{BN} are the percentage of masses of Al, Al_2O_3 and cBN in the initial precursor powders.

The experimental mass change ΔW_{exp} incurred as a result of heat treatment was calculated by subtracting initial mass of pellets (before reaction) from the reacted mass i.e

$$\Delta W_{\exp} = \left(\frac{W_r - W_g}{W_g} \right) * 100 \quad \text{.....(4.3.2)}$$

Where W_g and W_r are the green and reacted masses, respectively.

Degree of reaction was then calculated by expressing, ΔW_{exp} *as* a percentage of ΔW_{Th}

$$\%RXN_w = \left(\frac{\Delta W_{Exp}}{\Delta W_{Th}} \right) * 100 \quad \text{.....(4.3.3)}$$

Results for mass change as a function of temperature and pressure for all sample compositions are presented in tables A.9 to A.12 in the Appendix section of this thesis.

Oxidation kinetics at 500 ^oC

Since the melting point of aluminum is around 660 ^oC two oxidation regimes are recognized in the Al/Al_2O_3 system. The first one is gas/ solid oxidation which occurs before the melting point of aluminum and the second one is gas liquid oxidation which occurs after the metal has melted. Previous studies have shown that the solid-gas oxidation reaction is extremely important because formation of too much liquid aluminum results in flaws and microcracks that can not be removed during sintering [65]. From this point of view it is therefore important to have as much aluminum being oxidized in the solid state as possible. It has also been reported that up to 60% of Al in RBAO can be oxidized between 450 and 660 ^{o} C [72].

In order to maximize oxidation in the solid state kinetic experiments were done at 500 ^oC to optimize time required to achieve maximum oxidation in the solid state. All sample compositions were heat treated at 500 ^oC for 0, 60, 120, 180 and 300 minutes and degrees of reaction as defined in equation 4.3.3 were determined and results are shown in figure 4.11 .

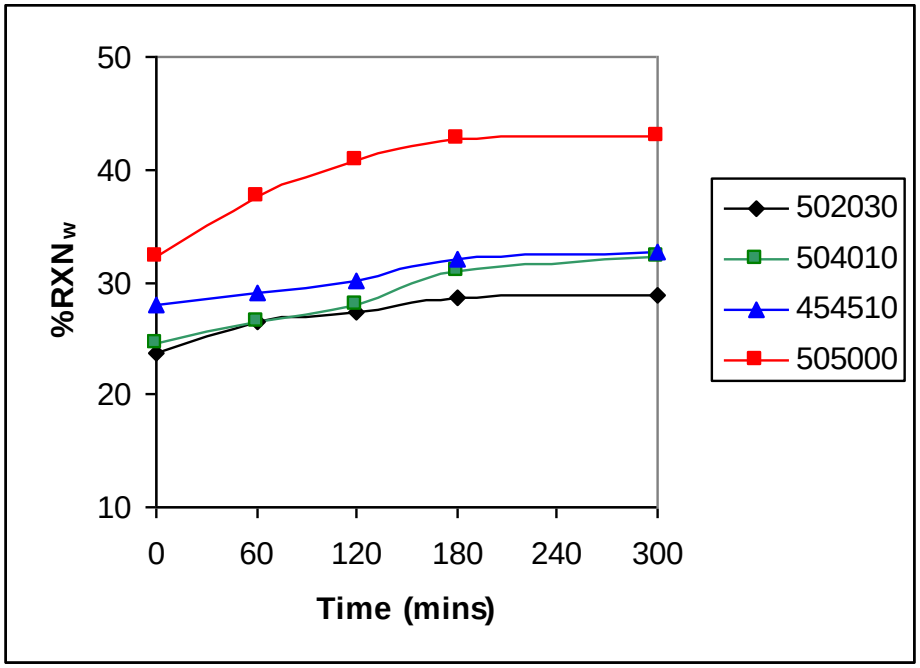

Figure 4.11 Mass change as a function of time at 500 ^{o}C for samples compacted at 45 MPa.

From the graphs in figure 4.11 it is clear that for all compositions there is a gradual increase in mass with increase in dwell time. For all sample compositions it can also be seen that after about three hours there is no significant change in mass implying that there is a limited amount of aluminum that can be oxidized in the solid state. This can be explained by considering that at this stage aluminum oxidation is proceeding by gas diffusion via microcracks developed in the oxide layer which also continuously increases in thickness resulting in retardation of the reaction.

Composition 505000 (without cBN) exhibits the highest mass change through out and sample 502030 with the highest cBN exhibits the lowest mass change. One plausible explanation to this could be the possibility of $B(OH)_3$ being formed on the surface of cBN. On heat treatment this $B(OH)_3$ would then decompose into B_2O_3 which then

forms a glassy phase around the aluminum particles thereby protecting them against reaction with oxygen.

Mass change as a function of temperature was evaluated from 500 to 1000 ^{o}C. In each case dwell time was 0 minutes. Figures 4.12 shows mass change as a function of temperature for all sample compositions compacted at 45 MPa.

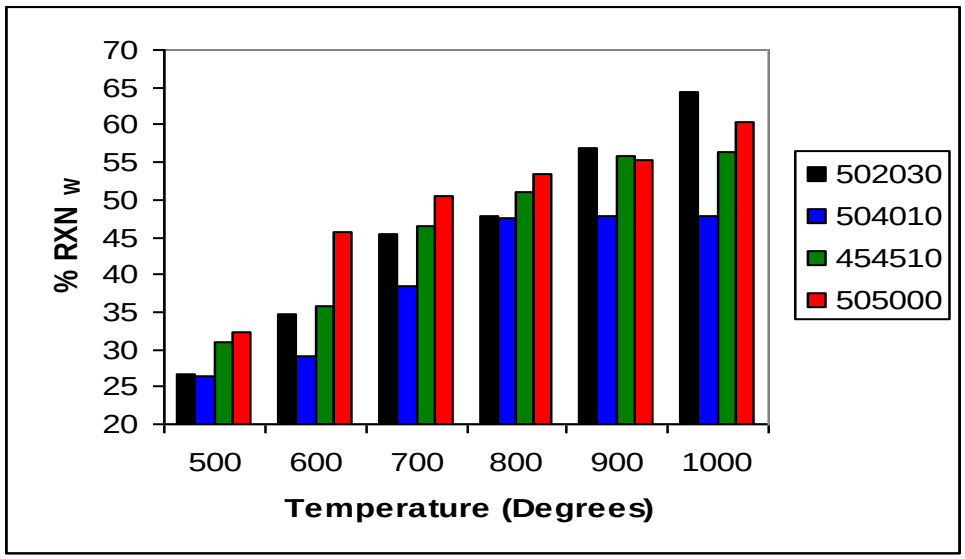

Figure 4.12 Mass change as a measure of degree of reaction for samples prepared at 45 MPa.

In general mass change increases with increasing temperature for all samples. Sample 505000 (without cBN content) has the highest mass change and sample 502030 (with highest cBN) has the lowest mass change. Samples 504010 and 454510 (with 10% cBN fall somewhere in between these two extremes. This trend is true up to 800 ^{o}C

At higher temperatures this trend gets reversed (502030 exhibits higher mass change than 505000). This could be due to the fact at higher temperatures for samples with cBN there is an additional mass gain due to oxidation of cBN and formation of alumino borate phases (discussed in section 4.4 of this thesis)

The effect of compaction pressure was investigated by using samples compacted at 45 MPa and 180 MPa (See graphs 4.13 to 4.16 below).

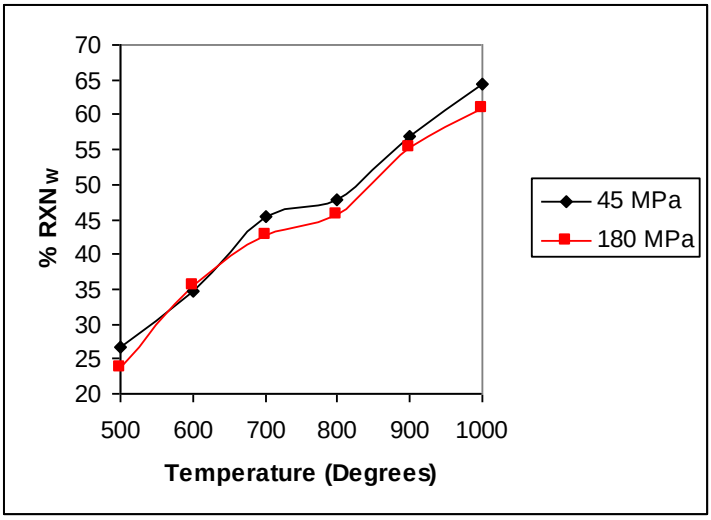

Figure 4.13 Effect of compaction pressure (45 and 180 MPa) on mass change for sample 502030 as a function of temperature.

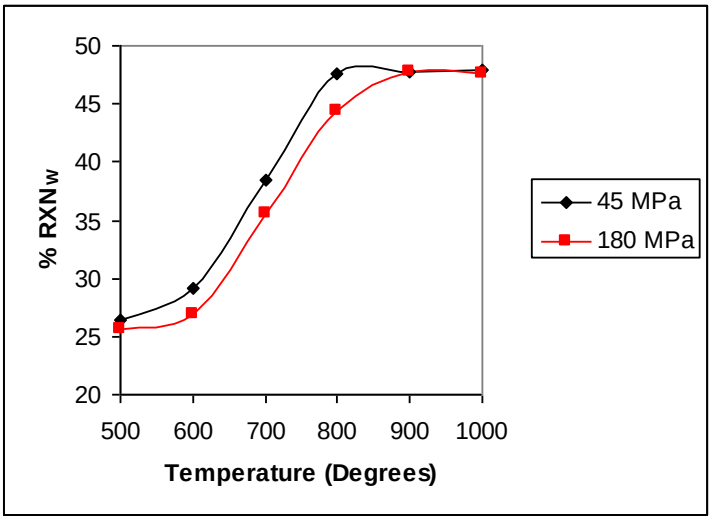

Figure 4.14 Effect of compaction pressure (45 and 180 MPa) on mass change for sample 504010 as a function of temperature.

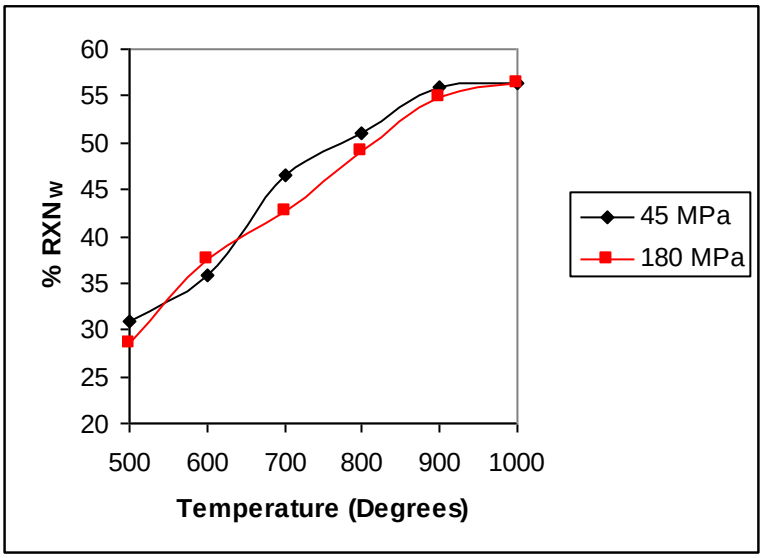

Figure 4.15 Effect of compaction pressure (45 and 180 MPa) on mass change for sample 454510 as a function of temperature.

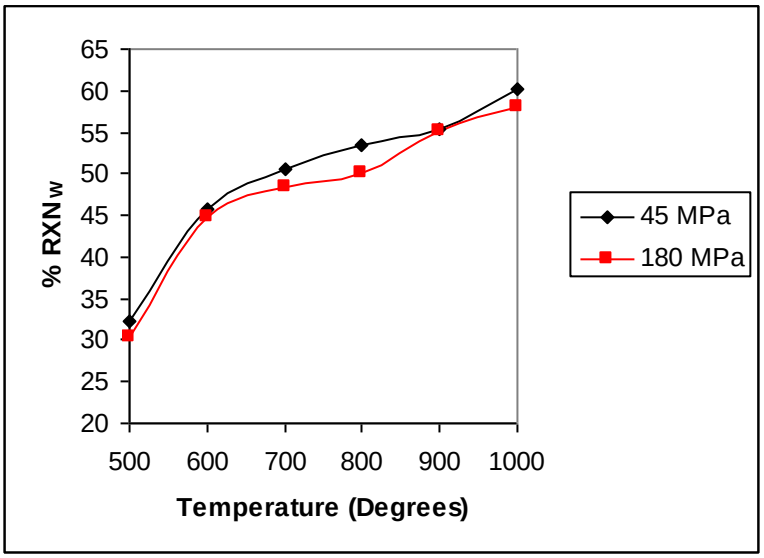

Figure 4.16 Effect of compaction pressure (45 and 180 MPa) on mass change for sample 505000 as a function of temperature.

From figures 4.13 to 4.16 there does not seem to be any correlation between compaction pressure and mass change.

However, table 4.2. in section 4.2 shows there is a relative decrease in total porosity and median pore diameter with increase in compaction

pressure. According to the Knudsen-Dushman [75] relationship, oxygen diffusion (C) of a cylindrical pore is related to the pore radius r by the relationship

$$C = C_b\left(1+\frac{3}{8}\frac{l}{r}\right)^{-1}$$

Where *r* is the median pore radius and l is the length of the cylindrical pore and C_b is the conductivity of a thin diaphragm.

The above relationship suggests that the pore size plays an important role in oxygen transport and as such one would expect higher oxygen flux and improved oxidation with decrease in compaction pressure. The fact that there is no significant increase in oxidation with reduction in compaction pressure might imply that in this case diffusion is not the rate limiting step in the oxidation process.

Further evidence to support this conclusion is provided by considering color homogeneity of the pellets. All pellets shows a homogenous color indicating that the same degree of reaction is occurring through out the pellet.

4.3.2 Amount of Al remaining after reaction as a measure of degree of reaction.

Use of mass change as a measure of degree of reaction assumes that oxidation of Al is the only reaction occurring during heat treatment of Al/Al_2O_3 and cBN compacts. However previous investigations [85, 86] have shown that at higher temperatures (above 800 ^oC) cBN gets oxidized according to the equation.

$$2BN+\frac{3}{2}O_2 \longrightarrow B_2O_3+N_2$$

The actual temperature of oxidation depends among other issues on crystallographic orientation, porosity and impurities. These unexpected reactions press some limitations on the use of mass change as a measure of degree of reaction in the Al-Al_2O_3-cBN system. This prompted the use of the actual amount of Al remaining after reaction expressed as a percentage of the amount present initially as a measure of degree of reaction. This degree of reaction is denoted by a subscript Al $\%RXN_{Al}$ to distinguish it from the previous degree of reaction ($\%RXNw$) in equation 4.3.3 which is obtained from mass change incurred as a result of aluminum oxidation.

Thus $$\%RXN_{Al} = \left[1 - \left(\frac{Al_f}{Al_i}\right)\right] * 100 \quad \text{.....(4.3.4)}$$

Where Al_f represents amount of Aluminum remaining in the pellet after reaction and Al_i represent amount of Al in the precursor powders before milling . Results of degree of reaction as a function of temperature and pressure for all sample compositions are presented in tables A.13 to A.16 in the appendix section of this thesis.

Phase analysis

Quantitative phase analysis for reacted samples was done for samples reacted at different temperatures. For all samples there is a gradual decrease in aluminum content and a corresponding increase in alumina with increase in reaction temperature. cBN remains relatively stable although at high temperatures there is significant decrease. For an example sample 502030 has a cBN content of 27.5 at 1000 ^oC.

A summary of phase composition for all material treated to various temperatures is given in appendix A.1 of this thesis.

Figures 4.17 to 4.19 are X- ray diffractograms which show how α-Al_2O_3 increased and Al and transitional Al_2O_3 decreased with increase in temperature for the various sample compositions.

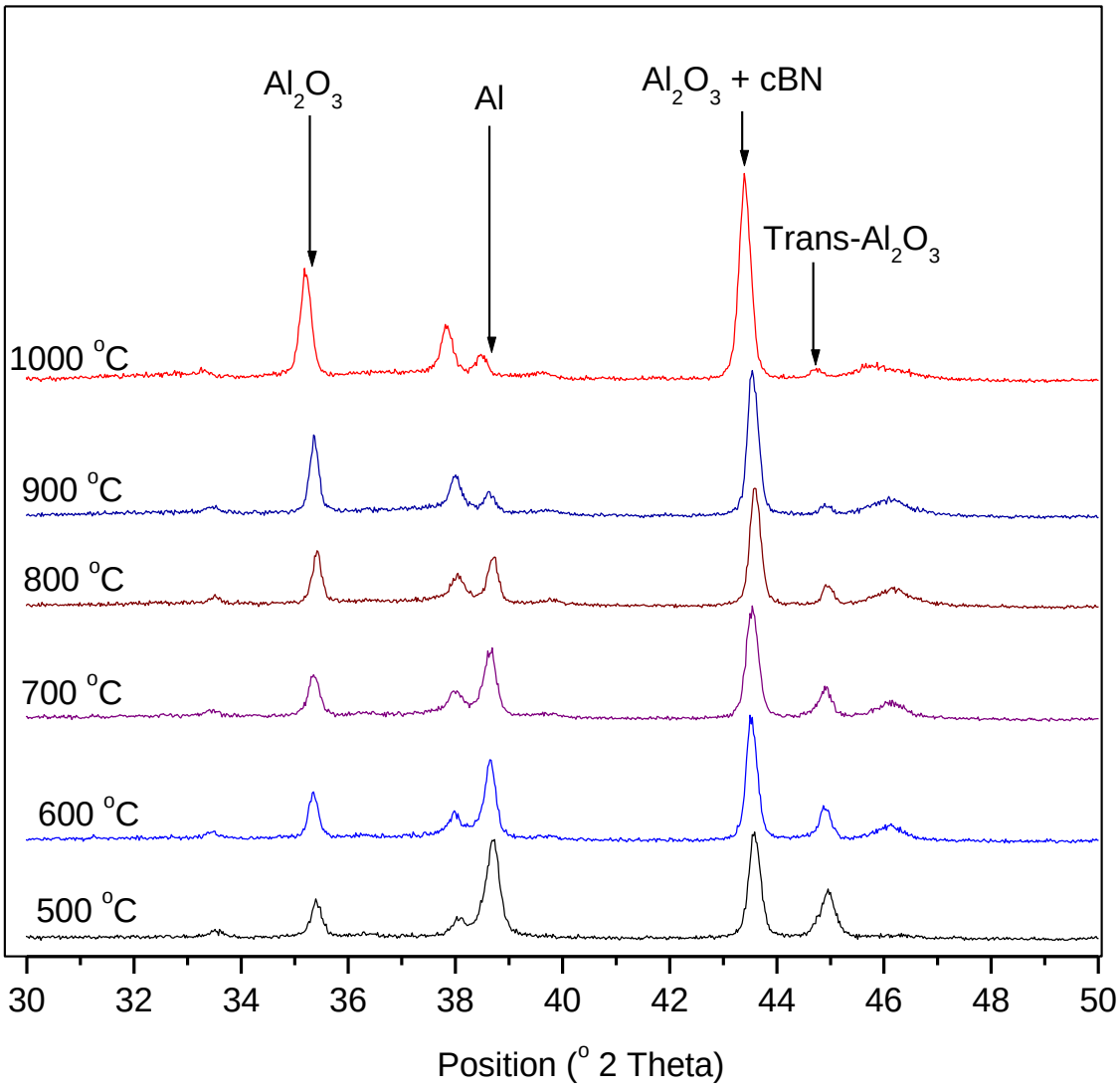

Figure 4.17 Phase evolution of sample 502030 as a function of temperature.

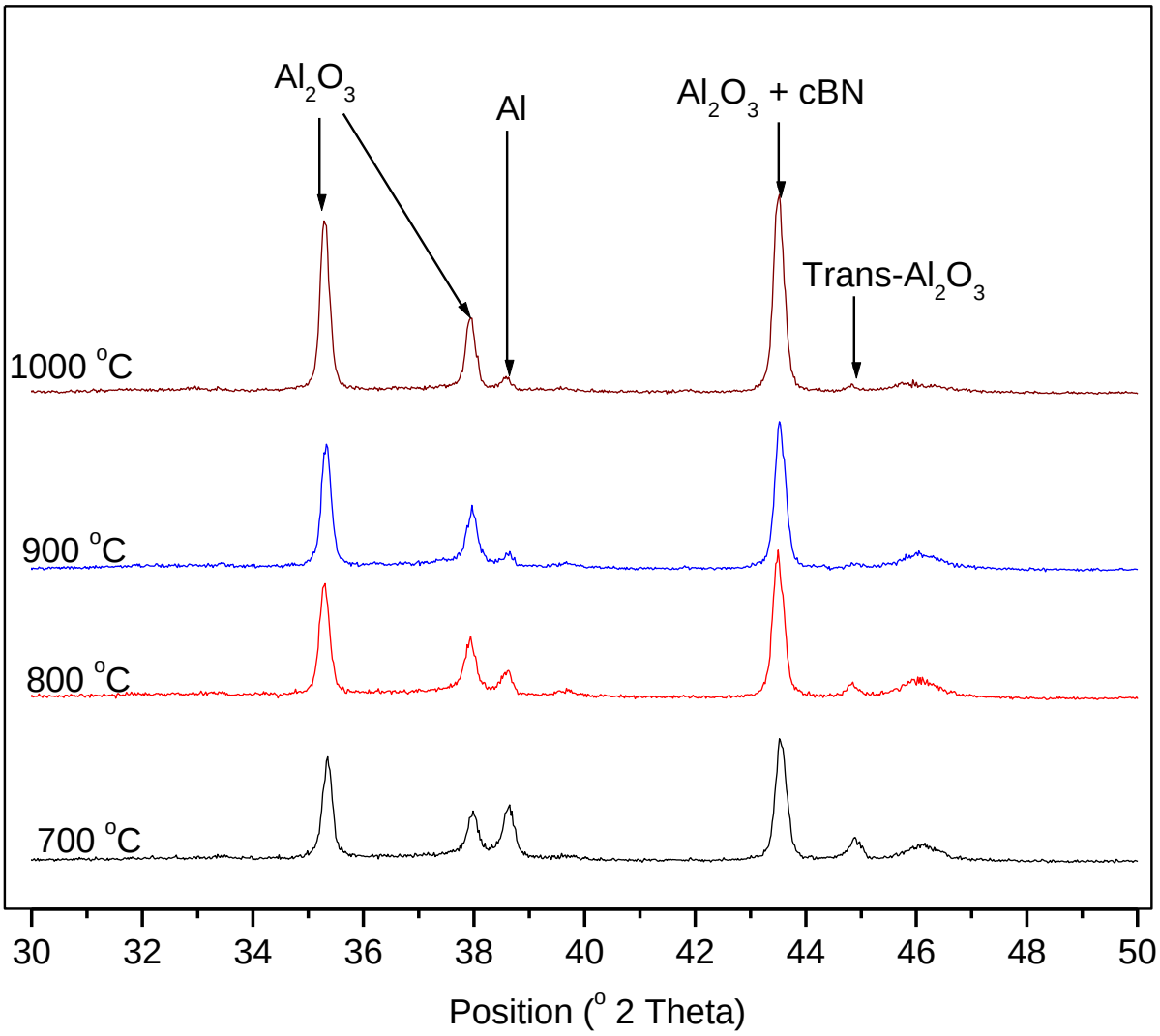

Figure 4.18 Phase evolution of sample 504010 as a function of temperature.

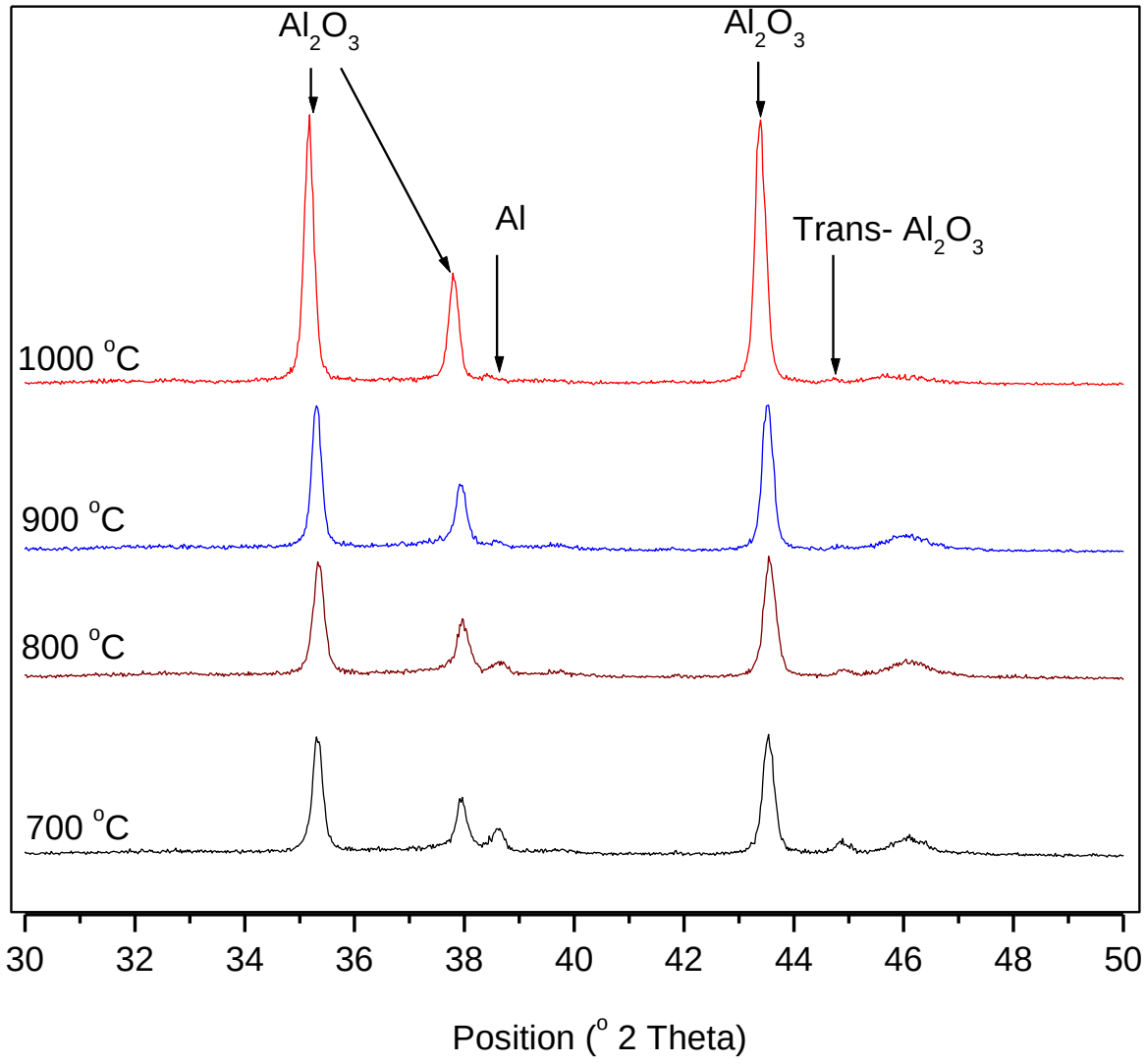

Figure 4.19 Phase evolution of sample 505000 as a function of temperature.

Degree of reaction as a function of time at 500 ^{o}C

Isothermal experiments were done for all samples at 500 ^{o}C and degrees of reaction as defined in equation 4.3.4 were evaluated after 0, 60, 120, 180 and 300 minutes and results are shown in figure 4.20.

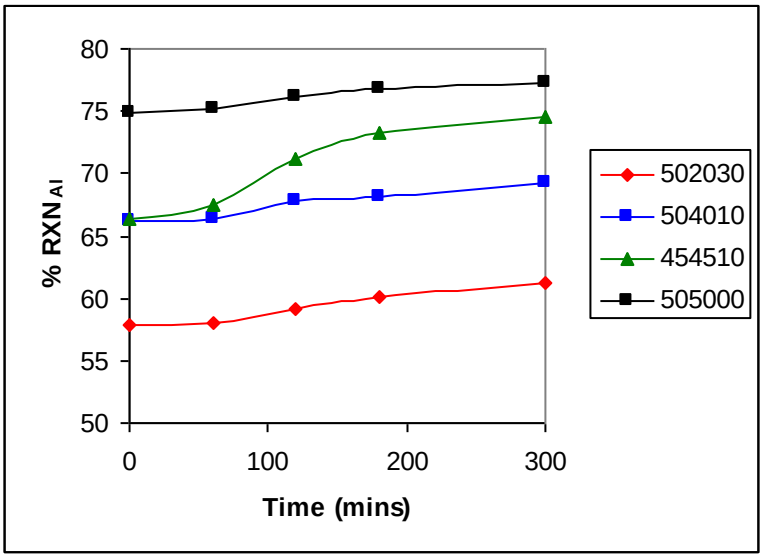

Figure 4.20 Degree of reaction as a function of time at 500 ^{o}C for samples compacted at 45 MPa.

Sample composition 505000 has the highest degree of reaction at 500 ^{o}C and sample 502030 has the lowest. In general there is an increase in degree of reaction for all sample compositions with increase in dwell time.

Degree of reaction as a function of temperature

Figures 4.21 and 4.22 show the degrees of reaction (as defined in equation 4.3.4) as a function of temperature for all samples at 45 MPa and 180 MPa respectively.

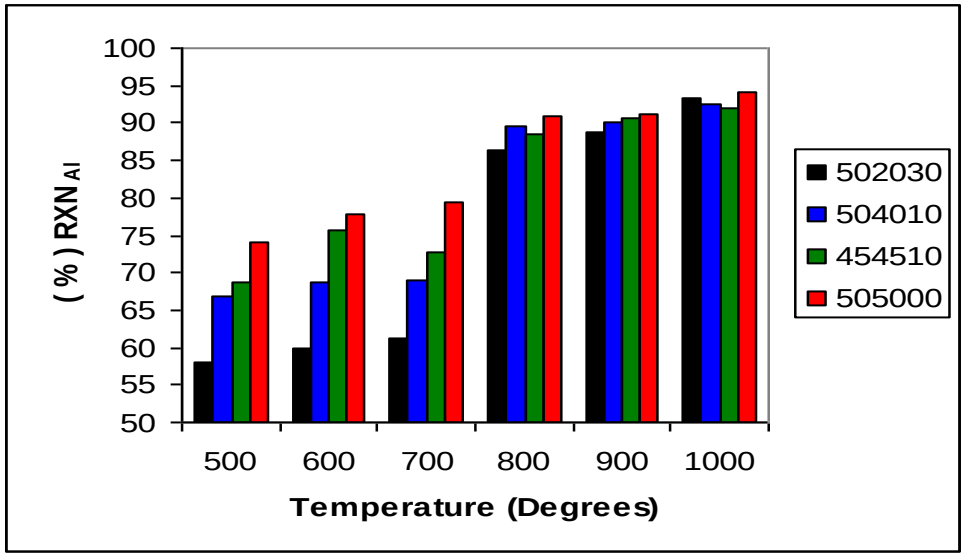

Figure 4.21 Degree of reaction as a function of Temperature for samples compacted at 45 MPa.

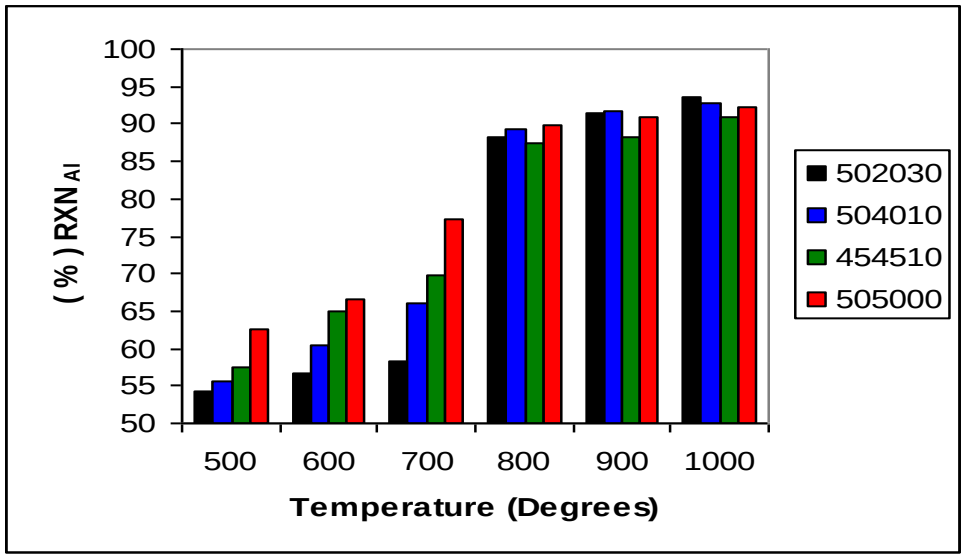

Figure 4.22 Degree of reaction as a function of Temperature for samples compacted at 180 MPa.

For all compositions degree of reaction is increasing with increase in temperature. The composition without BN (505000) shows the highest degree of reaction and composition with highest BN (502030) exhibits the lowest degree of reaction. Samples compositions with 10% BN are in between these two extremes.

Effect of pressure on Degree of reaction

The effect of compaction pressure on the degree of reaction was assessed by comparing samples of same compositions compacted at different pressures (45 and 180 MPa) and heat treated in the same manner. The results are shown in figures 4.23 to 4.26 below.

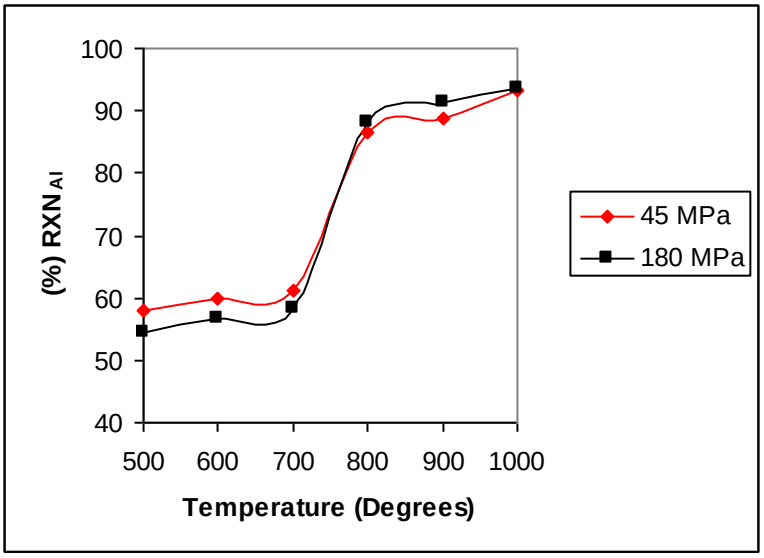

Figure 4.23 Comparing degree of reaction at 45MPa and 180 MPa for sample 502030.

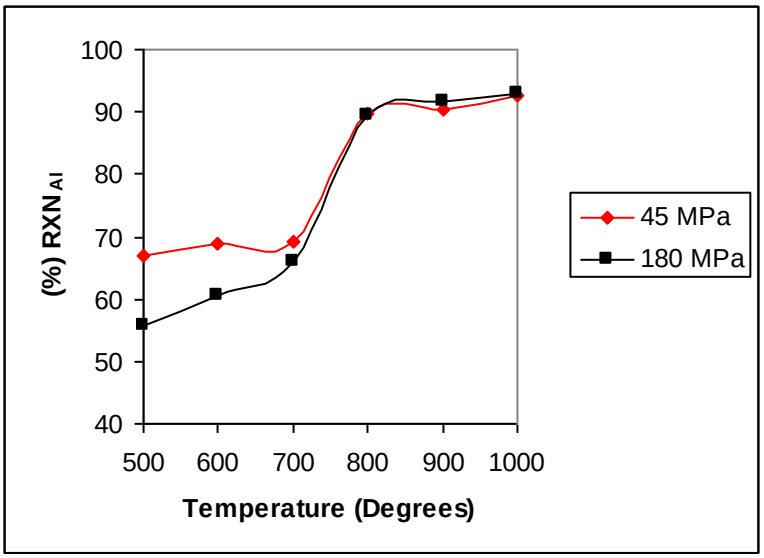

Figure 4.24 Comparing degree of reaction at 45MPa and 180 MPa for sample 504010.

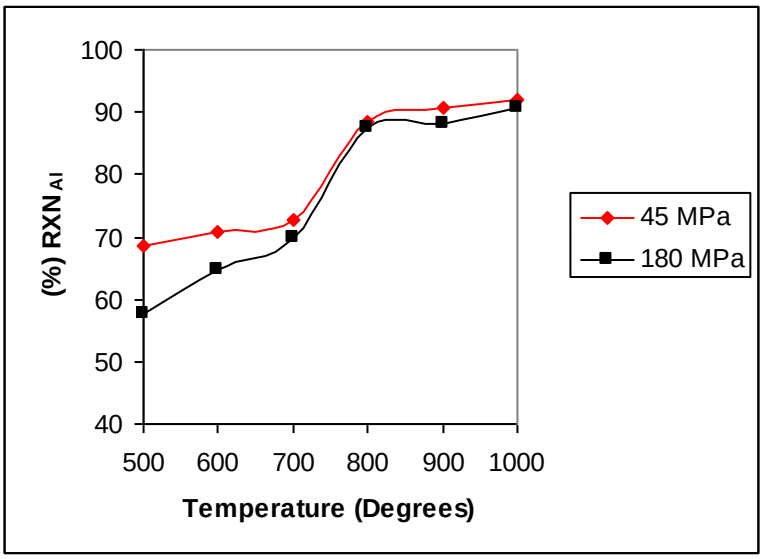

Figure 4.25 Comparing degree of reaction at 45MPa and 180 MPa for sample 454510.

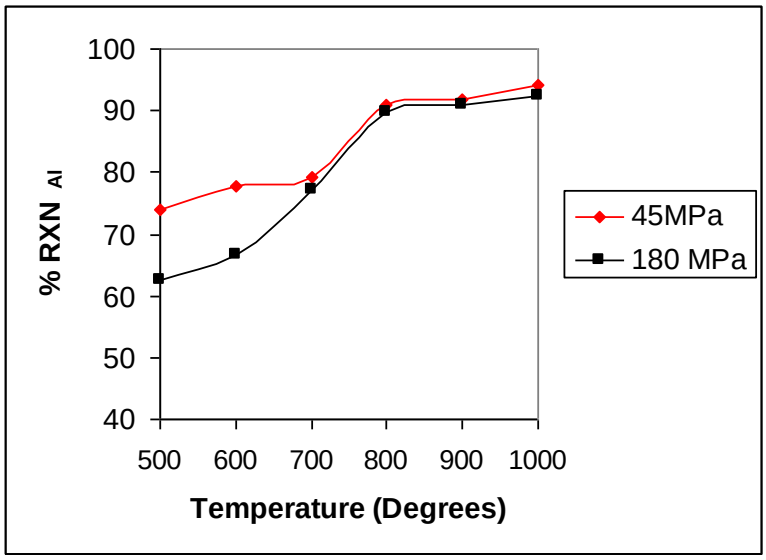

Figure 4.26 Comparing degree of reaction at 45MPa and 180 MPa for sample 505000.

From figures 4.23 to 4.26 it is evident that at lower temperatures (up to 700 ^{o}C) for all sample compositions there is a relatively higher degree of reaction for samples compacted at 45 MPa compared to their counterparts compacted at 180 MPa.

4.3.3 Concluding remarks.

This section compares the two methods used to assess degree of reaction in sections 4.3.1 and 4.3.2 that is equation 4.3.3 and 4.3.4 respectively.

Both degrees of reaction (by mass change and aluminum content) increase with increase in dwell time at 500 ^{o}C becoming constant after 3 to 4 hours for all sample compositions. This means that there is a limit to the amount of aluminum that can be oxidized in the solid state. This is because as more aluminum is oxidized an oxide layer develops

whose thickness increases with time making oxygen diffusion path longer hence reaction slows down before the metal melts.

Both mass change and degree of reaction increase with increase in temperature in the same manner with highest values being realized around 700- 800 ^{o}C. This sudden increase around 700 ^{o}C can be related to the melting of aluminum. When aluminum melts (melting point of aluminum is 660 ^{o}C), because of the poor wetting between aluminum and alumina the molten aluminum gets exposed as droplets resulting in instant oxidation hence a sudden increase in degree of reaction.

Sample without cBN (505000) has highest degree of reaction and sample with highest cBN (502030) has the lowest degree of reaction. This effect is highly pronounced at lower temperatures and can be ascribed to the formation of B_2O_3 glassy phase which protects the aluminum from oxidation resulting in retardation of reaction.

Rate limiting step.

In order to fully understand oxidation of aluminum in the reaction bonded aluminum oxide process it is necessary to identify which of the processes is rate limiting.

The oxidation of Al in RBAO process can be divided into two main steps which are

1. Diffusion of air through the Al/Al_2O_3 pellet
2. Reaction of air with Al metal to give Al_2O_3

One of these steps should be rate limiting and according to classical theory of gas/ solid reactions the slowest of the above processes would be the rate limiting process.

If air diffusion through the pellet is rate limiting then it means air will be consumed as soon as it reaches the Al surface. This would mean that oxidation will progress from the edges of the pellet towards the centre

similar to the shrinking core model. In this instance one would expect an oxide rich surface and a metal rich core.

If on the other hand reaction of air with the metal is the rate limiting process then one would expect the air to be in abundant and evenly distributed through out the pellet. In this case there is enough gas for reaction and so oxidation would take place evenly through out the pellet. In this case one would expect a uniform reaction through out.

In order to ascertain which of the above processes is rate limiting, elemental analysis (Oxygen and aluminum) was done along the width of a 505000 pellet of diameter 18mm and thickness 4mm reacted to 800 ^{o}C for zero minutes. This was done in order to establish if there was a compositional gradient across the pellet. From figure 4.27 it is clear that the aluminum distribution is constant through out the width of the pellet. This suggests that the rate of reaction is slow relative to rate of air duffusion through the pores.

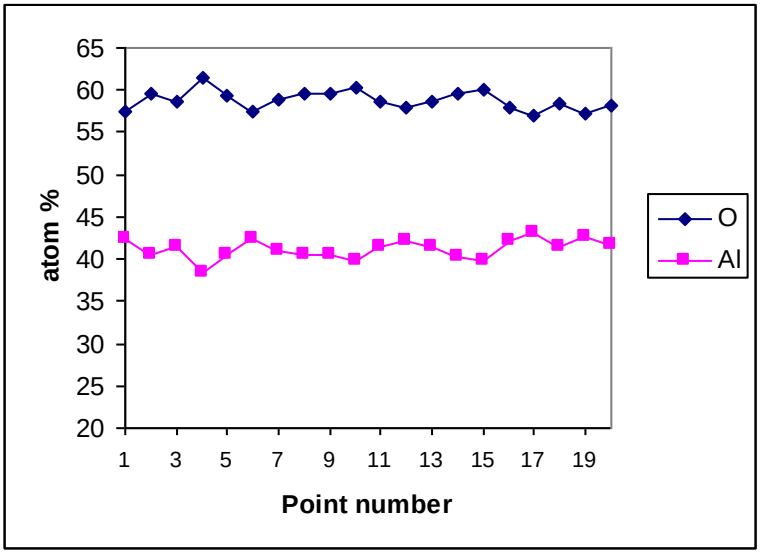

Figure 4.27 Elemental analysis along the width of a 505000 sample (180 MPa) reacted to 800 ^{o}C for zero minutes.

4.4 Interaction of Al_2O_3 and cBN

This section deals with the interactions occurring between cBN and alumina at high temperatures. X-ray analysis for samples reacted in air has revealed that samples containing cubic boron nitride (502030, 504010 and 454510) would form aluminum borate as a secondary phase if reacted to 1000 ^oC. Synthesis of aluminum borates is well documented in literature [108, 109] Jun Wang *et al* [108] have shown that Al_2O_3 reacts with B_2O_3 to yield $Al_4B_2O_9$ and $Al_{18}B_4O_{33}$ at 750 and 1050 ^oC respectively. The actual mechanism involved is not well known although it is suggested that Al_2O_3 grains absorb liquid B_2O_3 to yield $Al_4B_2O_9$. Existing literature also shows that oxidation of cBN starts at temperatures around 800 ^oC. Oxidation product is mainly B_2O_3(s) and Nitrogen gas. Thus studying the interaction between cBN and alumina at high temperatures reduces to investigating the B_2O_3-Al_2O_3 system.

Al_2O_3-B_2O_3 phase diagram

In order to fully understand the interactions occurring between Al_2O_3 and B_2O_3 it is necessary to study the relevant phase diagram first. For the purpose of this study a Al_2O_3-B_2O_3 phase diagram was calculated using FactSAGE 5.4.1 and is shown in figure 4.28 below.

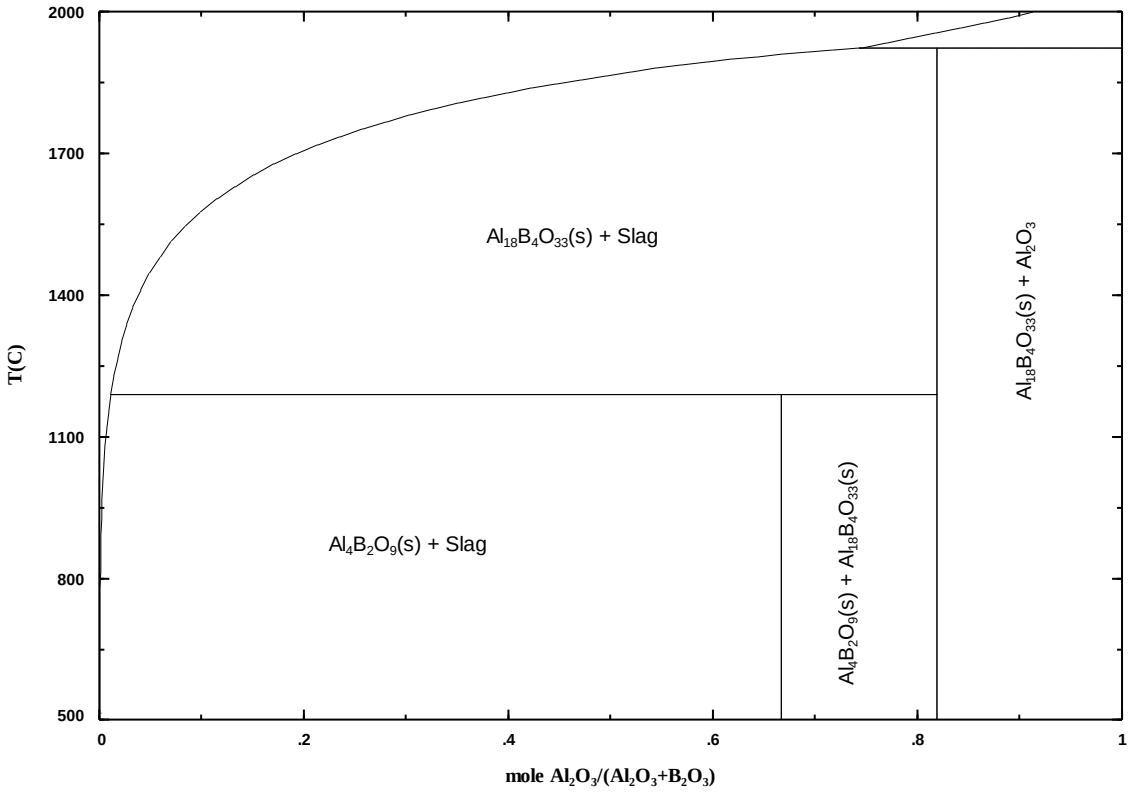

Figure 4.28 Phase diagram of Al_2O_3-B_2O_3

From the phase diagram it is clear that Al_2O_3 and B_2O_3 react to form $Al_4B_2O_9$ and/or $Al_{18}B_4O_{33}$ depending on the composition and temperature. If Al_2O_3 to B_2O_3 ratio is less than 67% the most favorable borate phase would be $Al_4B_2O_9$ which then transforms into $Al_{18}B_4O_{33}$ at temperatures above 1150 ^oC. If the Al_2O_3 to B_2O_3 ratio is between 67-82% both $Al_4B_2O_9$ and $Al_{18}B_4O_{33}$ can be formed at temperatures below 1150 ^oC and thereafter only $Al_{18}B_4O_{33}$ will be stable. At Al_2O_3: B_2O_3 ratio greater than 82% only $Al_{18}B_4O_{33}$ is formed. Thus with the

Al_2O_3:B_2O_3 compositions in this work the most likely borate phase to be formed is $Al_{18}B_4O_{33}$.

Formation of B_2O_3

Since formation of borate phases depends on the availability of Al_2O_3 and B_2O_3 it is necessary to investigate formation of B_2O_3. In this study formation of $B_2O_{3(s)}$ from oxidation of cubic boron nitride can be estimated indirectly by considering depletion of cBN during heat treatment in air. Phase analysis of samples reacted to 1000 ^oC shows that for samples containing cBN the amount of cBN remaining after reacting at 1000 ^oC is lower than the amount initially present before reaction. For example sample 502030 has 27.5% cBN by volume after being reacted to 1000 ^oC compared to 30% before reaction. This difference in cBN content can be accounted for by the reaction

$2BN + 3/2O_2 \rightarrow B_2O_3 + N_2$.

Reaction of B_2O_3 and Al_2O_3

The actual temperature at which B_2O_3 and Al_2O_3 react to form $Al_4B_2O_9$ and $Al_{18}B_4O_{33}$ is not well known. Wang et al [108] have reported that Al_2O_3 grains absorb liquid B_2O_3 to yield $Al_4B_2O_9$ and $Al_{18}B_4O_{33}$ at 750 and 1050 ^oC respectively. In this study evolution of borate phases was monitored by X-ray diffraction. Figure 4.29 shows diffractograms for sample 502030 reacted for various times at 1000 ^oC. From the diffractograms it is evident that B_2O_3 and Al_2O_3 interact at 1000 ^oC to give $Al_{18}B_4O_{33}$.

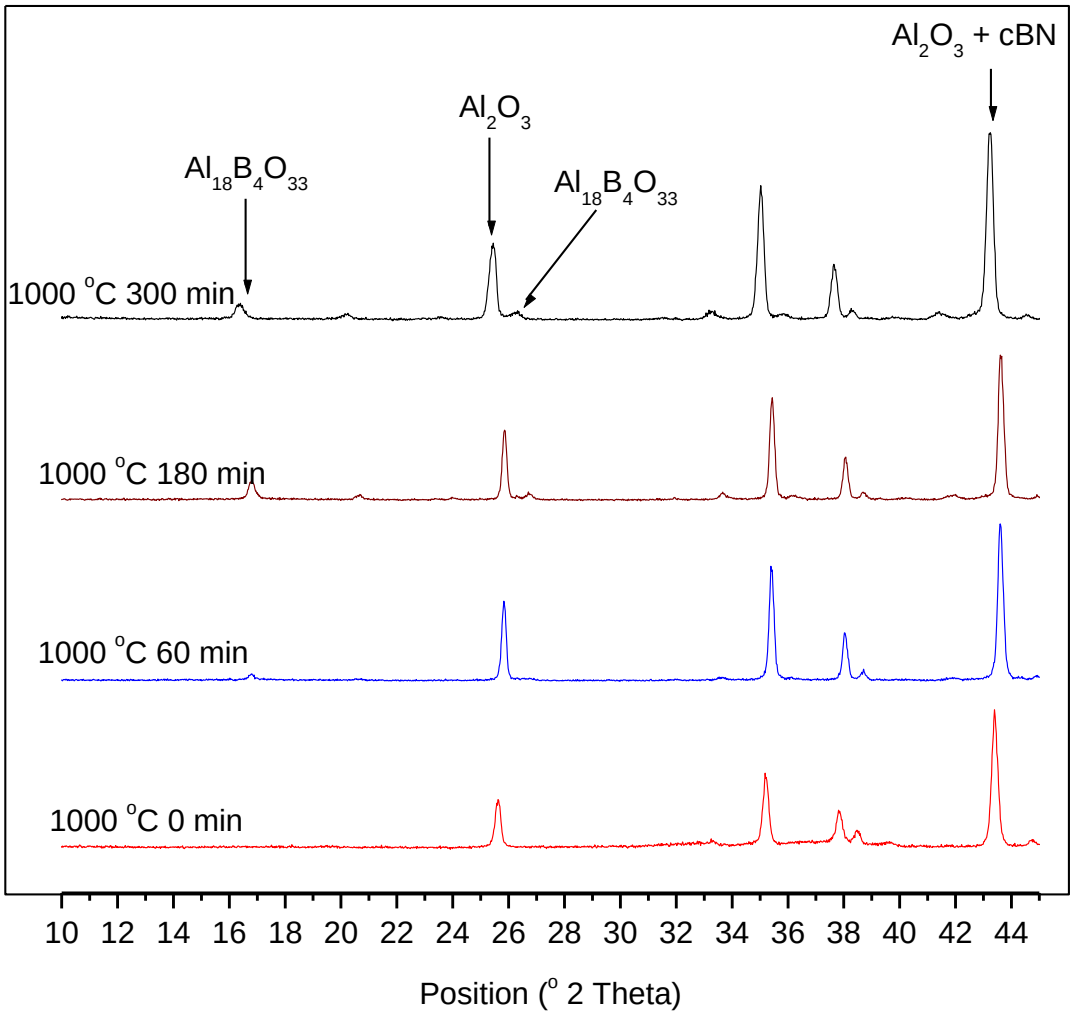

Figure 4.29 X-ray diffractograms for sample 502030 heat treated to 1000 °C for various times.

Thermodynamic considerations

Thermodynamic calculations were done using FactSAGE 5.4.1 to verify The formation of B_2O_3 from cBN and its subsequent interaction with Al_2O_3 to form $Al_{18}B_4O_{33}$. Gibbs free energies were calculated and used to justify feasibility of the reactions.

a. Formation of B_2O_3

$2BN + 1.5\ O_2 \rightarrow B_2O_3 + N_2$

ΔG's for the above reaction were -702.04KJ at 800 ^oC and -693.2KJ at 1000 ^oC. From these values it is clear that the above reaction is feasible at these temperatures.

b. Formation of $Al_{18}B_4O_{33}$

$9Al_2O_3 + B_2O_3 \rightarrow Al_{18}B4O_{33}$

ΔG's for the above reaction were -165.09KJ at 800 ^oC and -167.7KJ at 1000 ^oC. These values also indicate that interaction of Al_2O_3 and B_2O_3 at these temperatures to yield $Al_{18}B_4O_{33}$ is a feasible reaction.

4.5 Properties of reacted bodies

Reacted density

Densities for reaction bonded samples were determined geometrically by measuring the height, diameter and mass of the reacted pellets. From results sample with highest cBN has highest reacted density through out. This is expected since the higher the cBN the higher the green density hence the reacted density should inherently be higher also.

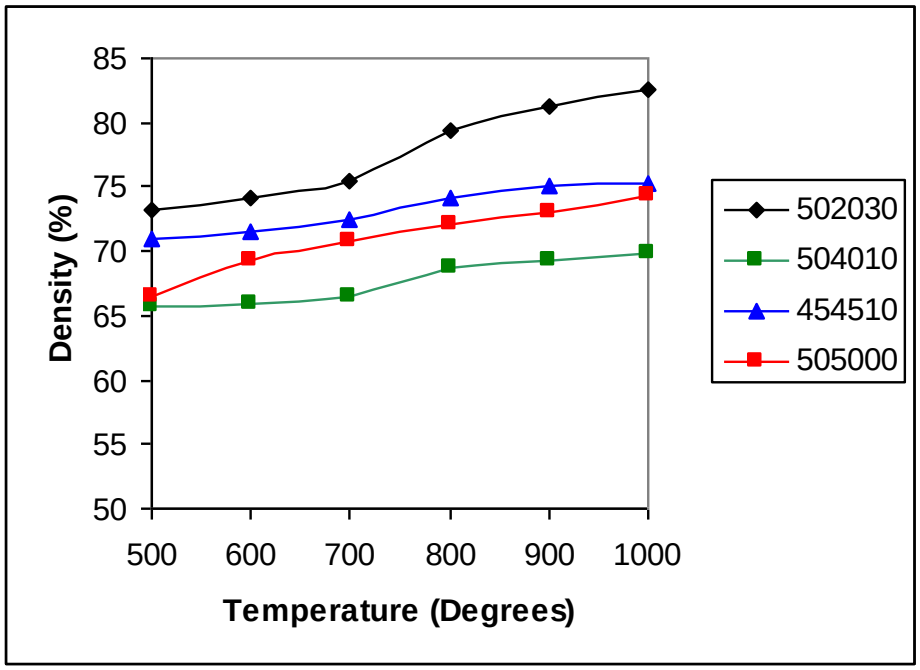

Figure 4.30 Reacted densities as a function of temperature for samples pressed at 180 MPa.

Microstructure

Microstructure of reacted bodies shows that after reaction materials consists of a homogenous mixture of mainly Al_2O_3 as shown in figure 4.31. At this stage it is difficult to distinguish Al from Al_2O_3. However under the optical microscope some fine metallic inclusions could be

seen evenly distributed within the Al_2O_3 matrix. For samples with cBN some large cBN grains could be seen evenly distributed within a Al_2O_3 matrix as shown in figure 4.32.

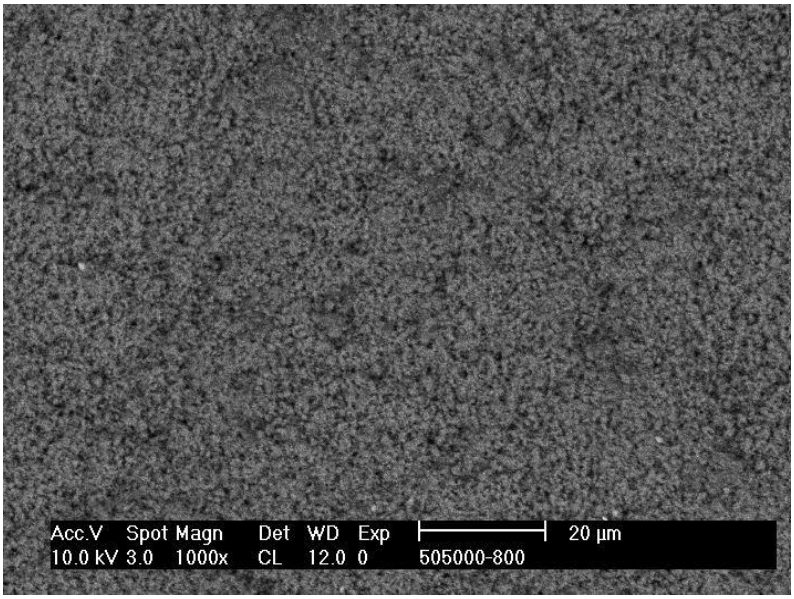

Figure 4.31 Fractured surface of sample 505000 compacted at 90 MPa and reacted to 800 ^{o}C in air.

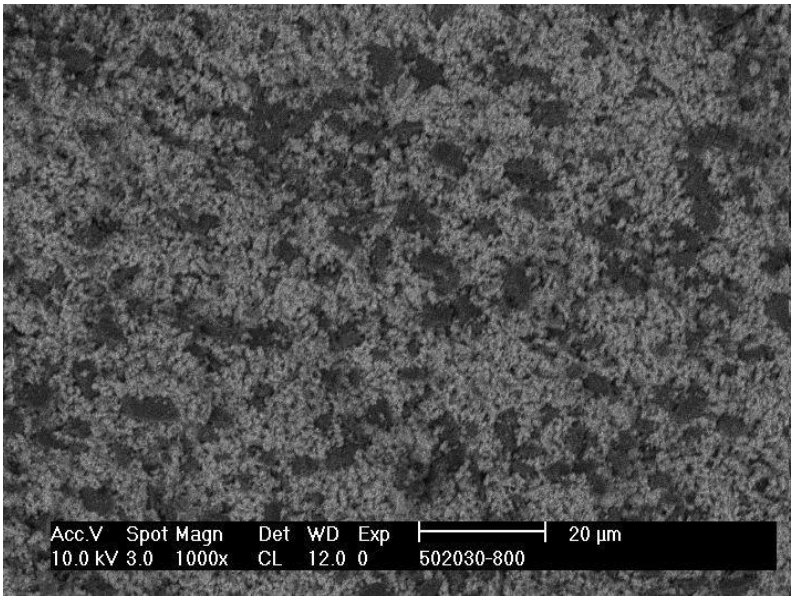

Figure 4.32 Fractured surface of sample 502030 compacted at 90 MPa and reacted to 800 ^{o}C in air.

4.6 Properties of sintered materials.

Introduction

In this section properties of sintered materials are discussed. For sintering experiments samples reacted to 800 ^{o}C and 1000 ^{o}C for zero minutes were used. The criteria used in choosing these samples was based on the following argument.

Ideally the heat treatment cycle in air was meant to convert all the aluminum into alumina. From table A.1 to A.4 in Appendix section of this thesis which shows aluminum content as a function of temperature it is clear that for all sample compositions aluminum content decreases with increase in temperature with samples heat treated to 1000 ^{o}C having the least amount of aluminum.

However it has also been shown that if samples are heat treated to 1000 ^{o}C there is a likelihood of some of the boron nitride being oxidized into B_2O_3 which will later interact with Al_2O_3 to form alumino borate phases. The amount of aluminum in samples heat treated to 800 ^{o}C is not very different from those which were reacted to 1000 ^{o}C.

Thus based on the above arguments it was decided to sinter both samples which have been heat treated to 800 ^{o}C and 1000 ^{o}C in air. All samples were sintered at 1300 ^{o}C for two hours using a hot pressing facility described in section 3.2 of this thesis. Initially Argon was used as the sintering gas to avoid oxidation of Boron nitride. For samples heat treated to 800 ^{o}C additional sintering experiments were also done under vacuum.

Thus sintered samples are going to be divided into three groups as follows

1. Samples heat treated to 1000 ^{o}C in air and sintered to 1300 ^{o}C in argon denoted with a superscript 1000 1300 Ar e.g 502030 $^{1000\ 1300Ar}$.

2. Samples heat treated to 800 ^{o}C in air and sintered to 1300 ^{o}C in argon denoted with a superscript 800 1300Ar e.g 502030 $^{800\ 1000Ar}$.

3. Samples heat treated to 800 ^{o}C in air and sintered to 1300 ^{o}C in vacuum denoted with a superscript 800 1300V e.g 502030 $^{800\ 1300V}$.

In each case the following properties were determined phase analysis (X ray diffraction), density(Archimedes method), microstructural features (SEM), hardness and fracture toughness.

Phase analysis

Phase composition of the hot pressed materials was done using x ray diffraction as explained in section 3.3.1 of this thesis and phase compositions are shown in table 4.3.

Table 4.3 Phase composition of sintered materials

	Composition % volume			
Sample	Al	Al_2O_3	BN	$Al_{18}B_4O_{33}$
502030 $^{1000\ 1300\ Ar}$	1.8	67.2	27.1	3.7
504010 $^{1000\ 1300\ Ar}$	1.3	86.2	9.3	3.0
454510 $^{1000\ 1300\ Ar}$	1.2	85.9	9.2	3.6
505000 $^{1000\ 1300\ Ar}$	1.2	98.7	0	0
502030 $^{800\ 1300\ Ar}$	2.2	70.5	27.3	0
504010 $^{800\ 1300\ Ar}$	1.7	88.8	9.4	0
454510 $^{800\ 1300\ Ar}$	1.4	89.1	9.4	0
505000 $^{800\ 1300\ Ar}$	1.5	98.4	0	0
502030 $^{800\ 1300\ v}$	2.3	70.3	27.3	0
504010 $^{800\ 1300\ v}$	1.9	88.2	9.8	0
454510 $^{800\ 1300\ v}$	2.4	87.7	9.7	0
505000 $^{800\ 1300\ v}$	1.3	98.6	0	0

Samples 502030, 504010 and 454510 had Al_2O_3 , cBN and some Al when initially heat treated to 800 ^oC followed by sintering to 1300 ^oC in either Argon or vacuum and sample 505000 had only Al_2O_3 and Al as the only crystalline phases after sintering to 1300 ^oC.

However samples 502030, 504010 and 454510 after heat treatment at 1000 ^oC followed by sintering at 1300 ^oC in Argon had $Al_{18}B_4O_{33}$ in addition to Al_2O_3 and cBN . This can be explained as follows .

On heating cBN to 1000 ^oC there is a likelihood that some cBN decomposes into armophous B_2O_3 which then reacts with Al_2O_3 at high temperatures to form crystalline $Al_{18}B_4O_{33}$. X ray diffractograms of samples heat treated under various conditions are shown in figures 4.33 to 4.35 .

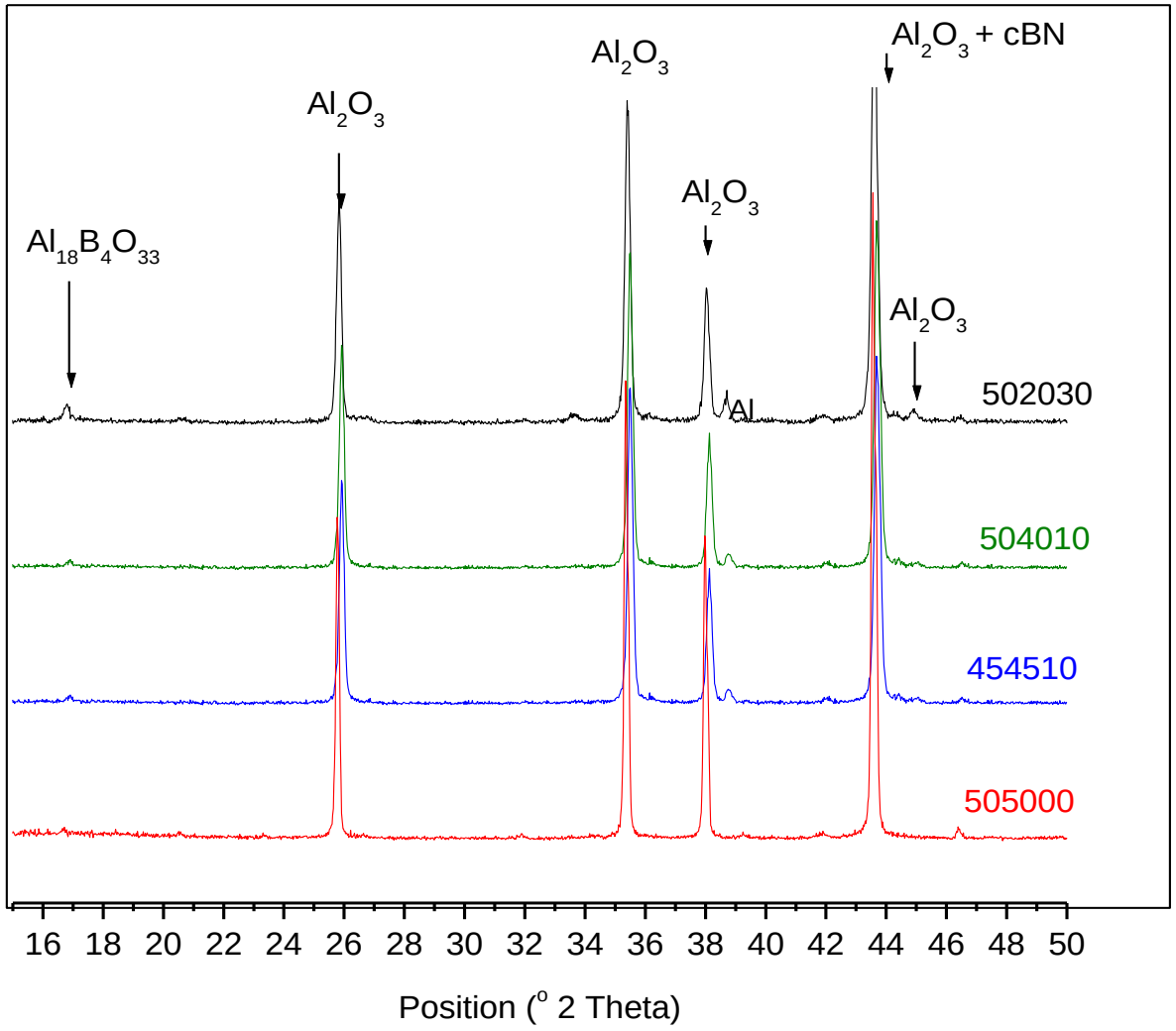

Figure 4.33 Phase compositions for materials heat treated to 1000 °C in air followed by sintering to 1300 °C in Argon.

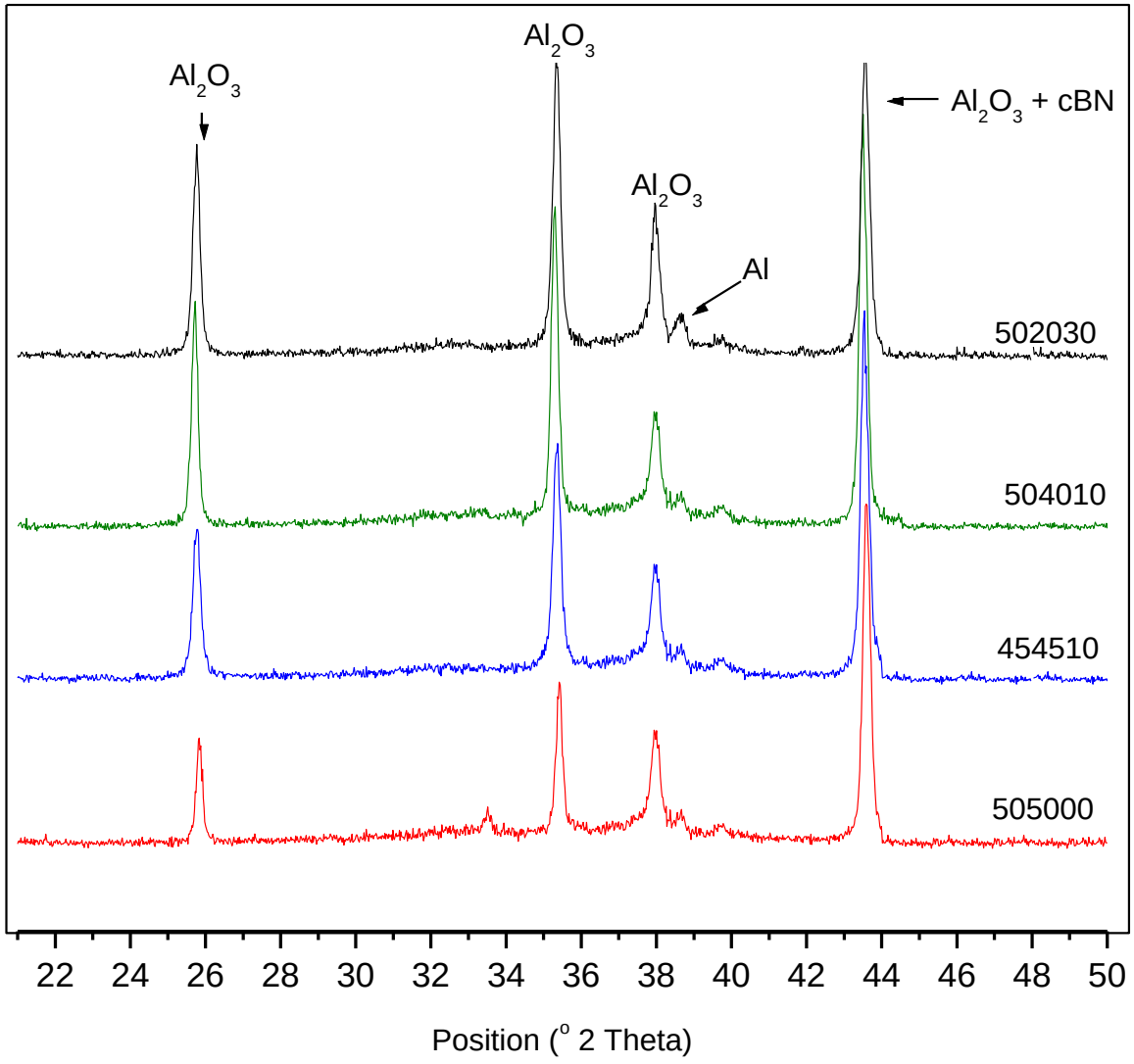

Figure 4.34 Phase compositions for materials heat treated to 800 °C in air followed by sintering to 1300 °C in Argon.

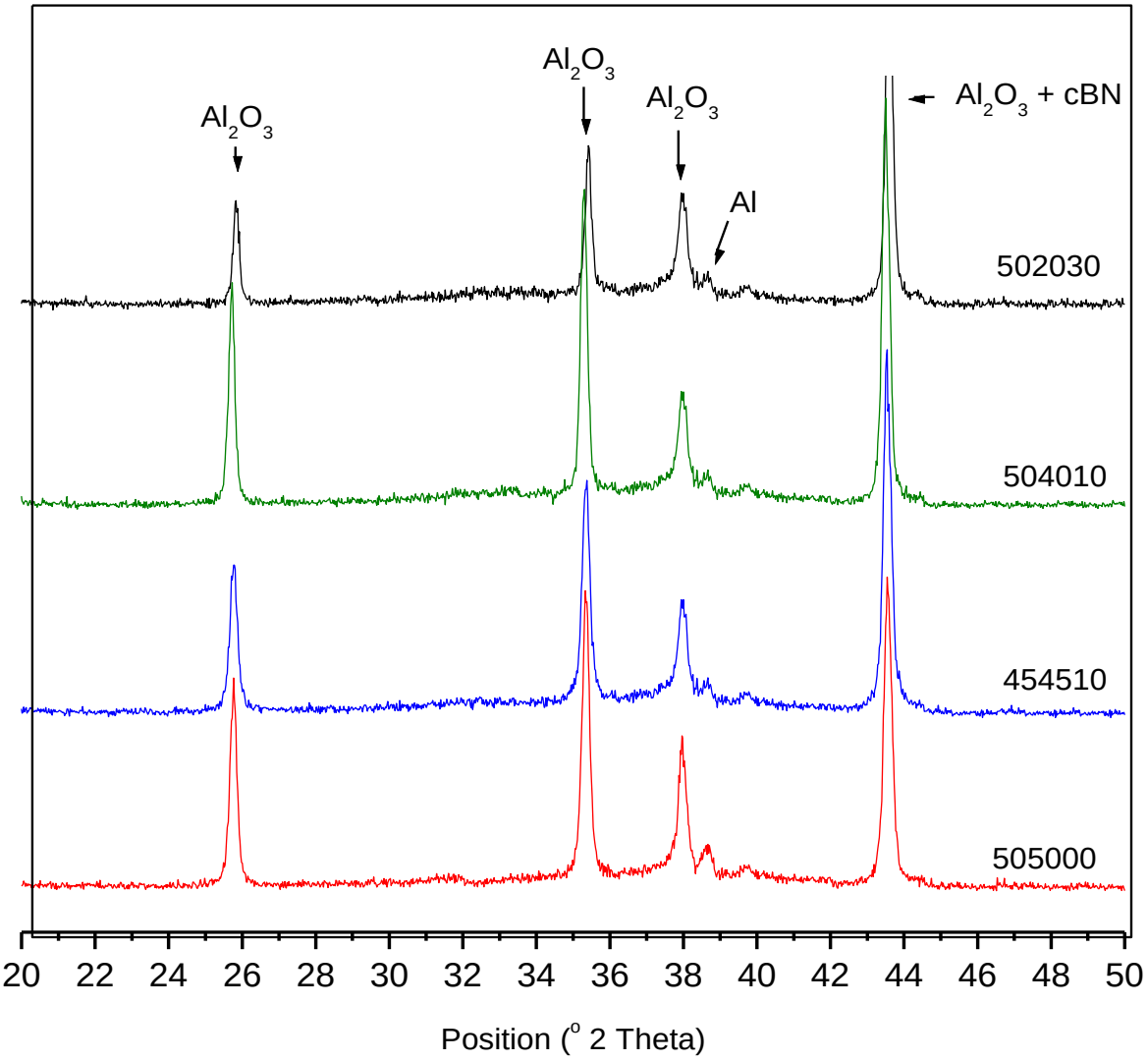

Figure 4.35 Phase compositions for materials heat treated to 800 °C in air followed by sintering to 1300 °C in Vacuum.

Sintered densities.

Densities of sintered materials were determined by means of the Archimedes method described in section 3.3.5 of this thesis. The theoretical densities were calculated using the rule of mixtures, using the following theoretical densities for the constituents phases Al 2.7, Al_2O_3 3.98, cBN 3.48 and $Al_{18}B_4O_{33}$ 2.68g/cm^3 . The volume proportions of the various phases were determined using the quantitative X ray diffraction method described in section 3.3.1 of this thesis. Densities of sintered samples are shown in table 4.4.

Table 4.4 Density of sintered materials.

Sample	Density g/cm^3	Density (%)
502030 $^{1000\ 1300\ Ar}$	3.55	94.12
504010 $^{1000\ 1300\ Ar}$	3.70	95.45
454510 $^{1000\ 1300\ Ar}$	3.69	95.33
505000 $^{1000\ 1300\ Ar}$	3.86	97.38
502030 $^{800\ 1300\ Ar}$	3.65	95.67
504010 $^{800\ 1300\ Ar}$	3.77	96.40
454510 $^{800\ 1300\ Ar}$	3.78	96.57
505000 $^{800\ 1300\ Ar}$	3.85	97.22
502030 $^{800\ 1300\ v}$	3.68	96.50
504010 $^{800\ 1300\ v}$	3.79	97.02
454510 $^{800\ 1300\ v}$	3.79	97.19
505000 $^{800\ 1300\ v}$	3.95	99.67

Effect of composition on sintered density

For samples heat treated under the same conditions density decreases with increase in cBN content. This can be explained by the hardness of cBN and its resistance to plastic deformation which results in it not participating in the sintering process. Figure 4.36 shows the effect of composition on density for samples sintered under different conditions.

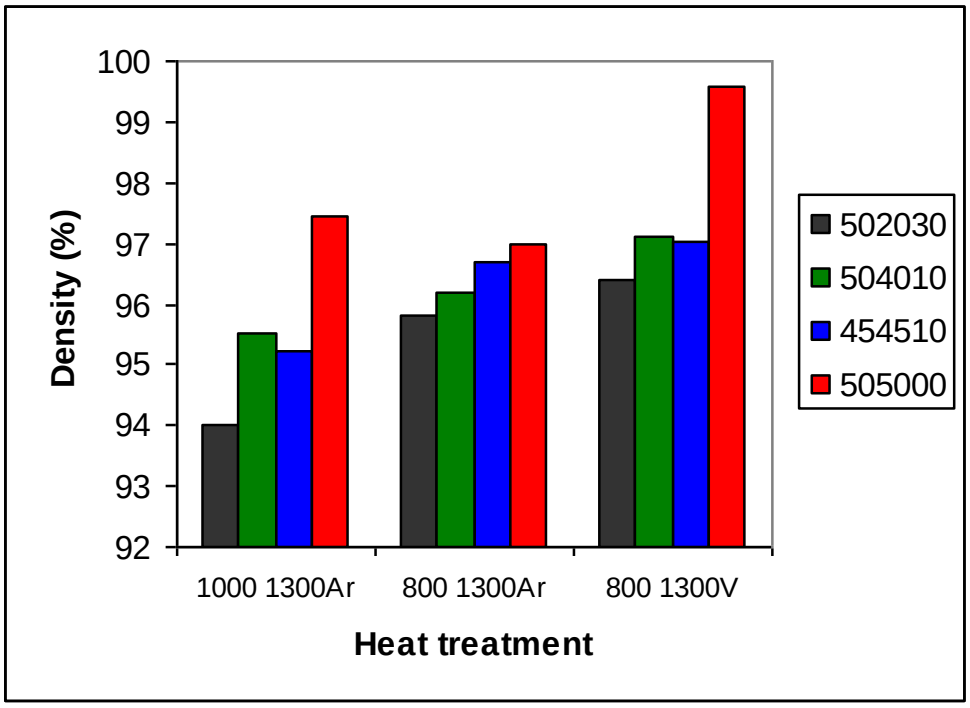

Figure 4.36 Effect of composition and heat treatment on density of sintered samples.

Effect of heat treatment on sintered density

For all materials density changes with heat treatment. Samples with cBN, exhibit a relatively lower degree of densification if initially heat treated to 1000 ^{o}C compared to when they are when initially heat treated to 800 ^{o}C.

This lowering of density when samples reacted at 1000 ^{o}C can be attributed to the presence of $Al_{18}B_4O_{33}$ which has a lower density (2.68g/cm3) compared to Al_2O_3 (3.98g/cm^3). This slight decrease in density is not realized in sample without cBN (505000).

Effect of sintering atmosphere on sintered density.

For all samples a major improvement in density is realized if samples are sintered under vacuum compared to Argon,. This is because towards the final stages of sintering some argon gas is trapped in the pores and closure of these pores depends on the ease with which the trapped Argon can diffuse into the surrounding matrix. A comparison of densities obtained by sintering in Argon versus sintering under vacuum is shown in figure 4.37. From figure 4.37 it can be seen that the density obtained by sintering under vacuum is more pronounced in the sample which does not have cBN (505000). This sample has the highest density of 99.67%

Microstructural analysis

a. Alumina matrix.

Sample 505000 when sintered at 1300 ^{o}C consists of a homogenous matrix with well defined grains in the submicron region. Figure 4.38 and 4.39 show micrograph of alumina matrices sintered in Argon and vacuum at 1300 ^{o}C followed by thermal etching at 1200 ^{o}C in air. Sintering in vacuum does not have any significant effect on microstructure although it results in improved densification.

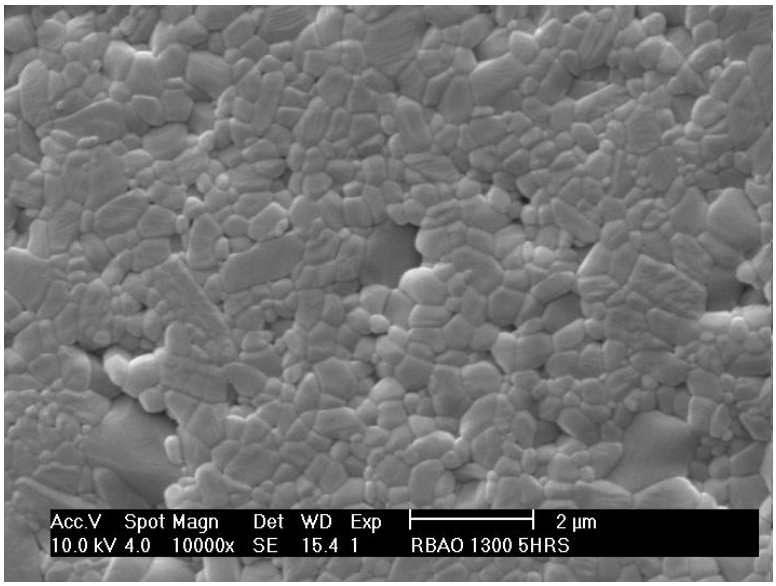

Figure 4.37 SEM image of sample 505000 reacted to 800 ^{o}C in air and sintered at 1300 ^{o}C in Argon.

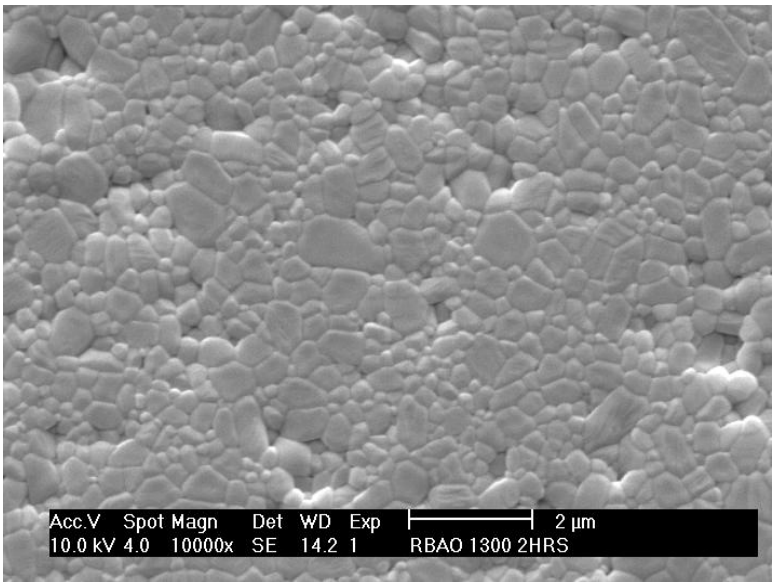

Figure 4.38 SEM image of sample 505000 reacted to 800 ^{o}C in air and sintered at 1300 ^{o}C under vacuum.

b. Samples with cBN

Samples with cBN (502030, 504010 and 4545100 consist of cBN particles (dark colour) evenly distributed within an alumina matrix (lighter colour) as shown in figures 4.40 and 4.41.

In figure 4.42 (higher magnification) shows that there is no reaction between cBN and surrounding alumina. This results in pores being formed on the alumina cBN interface and this could be one of the reasons why density decreases with increase in cBN.

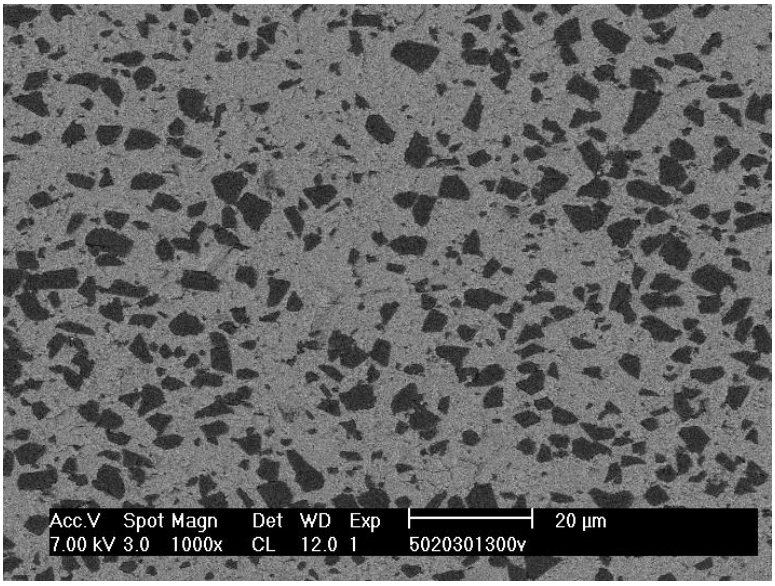

Figure 4.39 SEM image of sample 502030 reacted to 800 ^{o}C in air and sintered at 1300 ^{o}C in Argon.

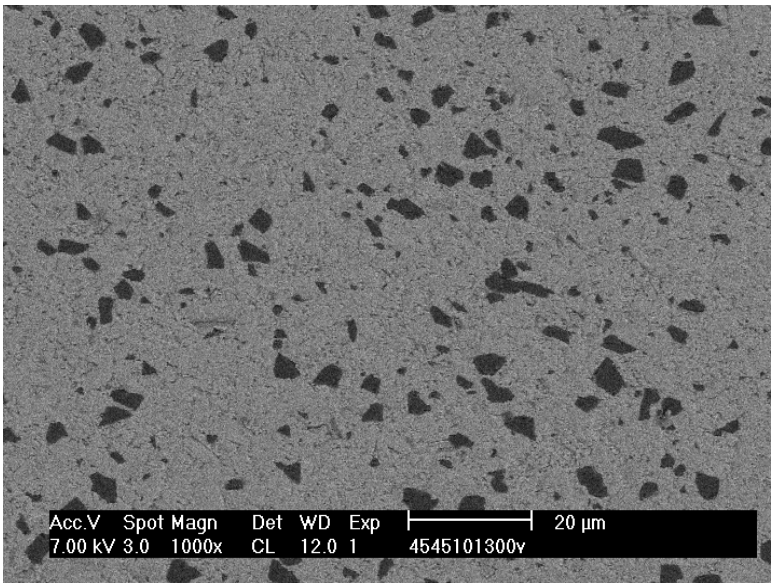

Figure 4.40 SEM image of sample 504010 reacted to 800 ^{o}C in air and sintered at 1300 ^{o}C in Argon.

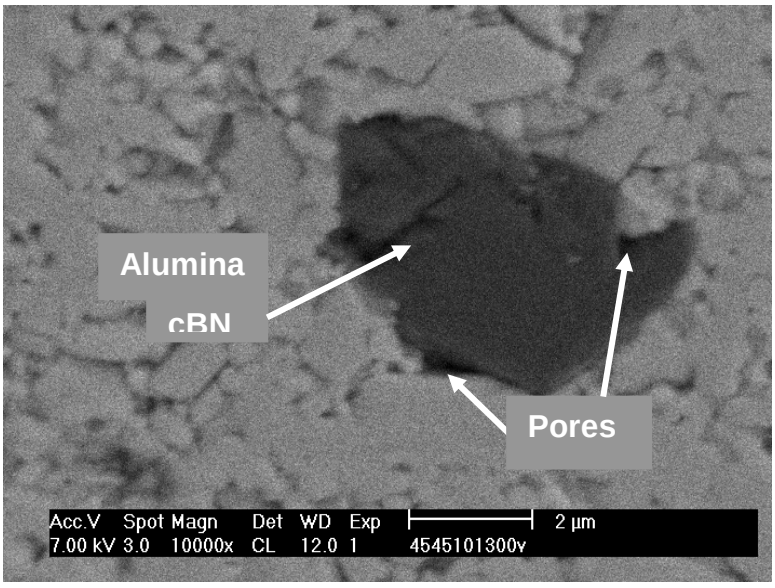

Figure 4.41 SEM image of sample 454510 reacted to 800 ^{o}C in air and sintered at 1300 ^{o}C in Argon.

Mechanical properties of sintered materials.

Hardness and fracture toughness of the sintered materials were determined using the indentation method as described in section 3.3.6 of this thesis. Figure 4.43 is a typical indentation on a polished section of one of the materials.

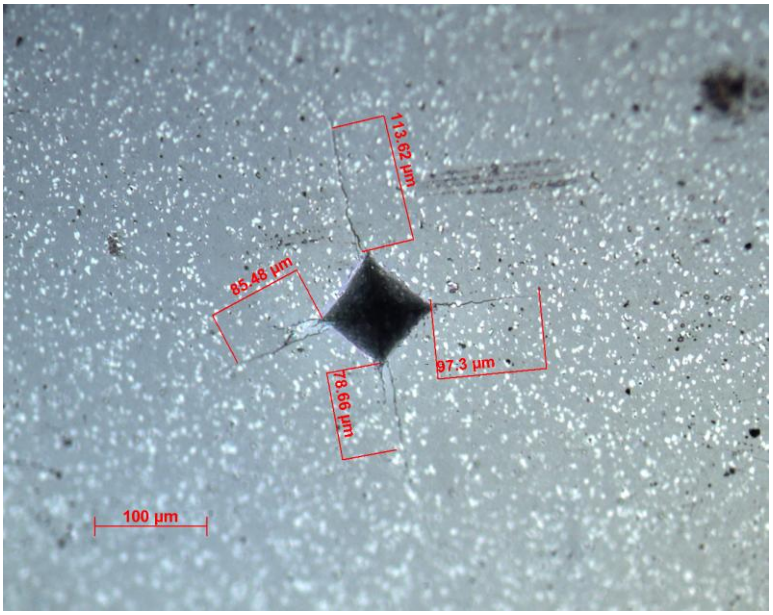

Figure 4.42 A typical indent produced on a 504010 sample using a 10 kg load for 10 seconds.

Table 4.5 Hardness and fracture toughness values for samples heat treated under various conditions

Sample	H_{v10} (GPa)	K_{IC} (MPa $m^{1/2}$)
502030 $^{1000\ 1300\ Ar}$	22.2 ±1.2	3.9±0.5
504010 $^{1000\ 1300\ Ar}$	19.9±1.7	3.5±0.7
454510 $^{1000\ 1300\ Ar}$	20.1±1.1	3.3±0.8
505000 $^{1000\ 1300\ Ar}$	18.5±2.2	NA
502030 $^{800\ 1300\ Ar}$	24.5±1.6	3.9±0.8
504010 $^{800\ 1300\ Ar}$	21.8±0.9	3.3±0.9
454510 $^{800\ 1300\ Ar}$	20.7±0.8	2.8±1.0
505000 $^{800\ 1300\ Ar}$	18.5±1.1	2.0±0.9
502030 $^{800\ 1300\ v}$	24.6±0.9	3.9±1.2
504010 $^{800\ 1300\ v}$	22.1±1.1	3.2±1.1
454510 $^{800\ 1300\ v}$	21.8±0.8	3.2±1.0
505000 $^{800\ 1300\ v}$	20.2±1.2	2.8±0.7

Effect of composition on hardness

For all sample compositions hardness is seen to increase with increase in cBN content. This is expected since boron nitride has a higher hardness compared to alumina and hence by the rule of mixtures the resultant hardness of a composite should increase with increase in volume fraction of the harder phase. For an example for samples heat treated at 1000 ^{o}C in air followed by sintering at 1300 ^{o}C in Argon hardness increases from 18.58 GPa for material without cBN (505000) to 22.24 GPa for sample with 30 % volume cBN (502030). Figure 4.44 shows the effect of cBN content on hardness for samples heat treated under various conditions.

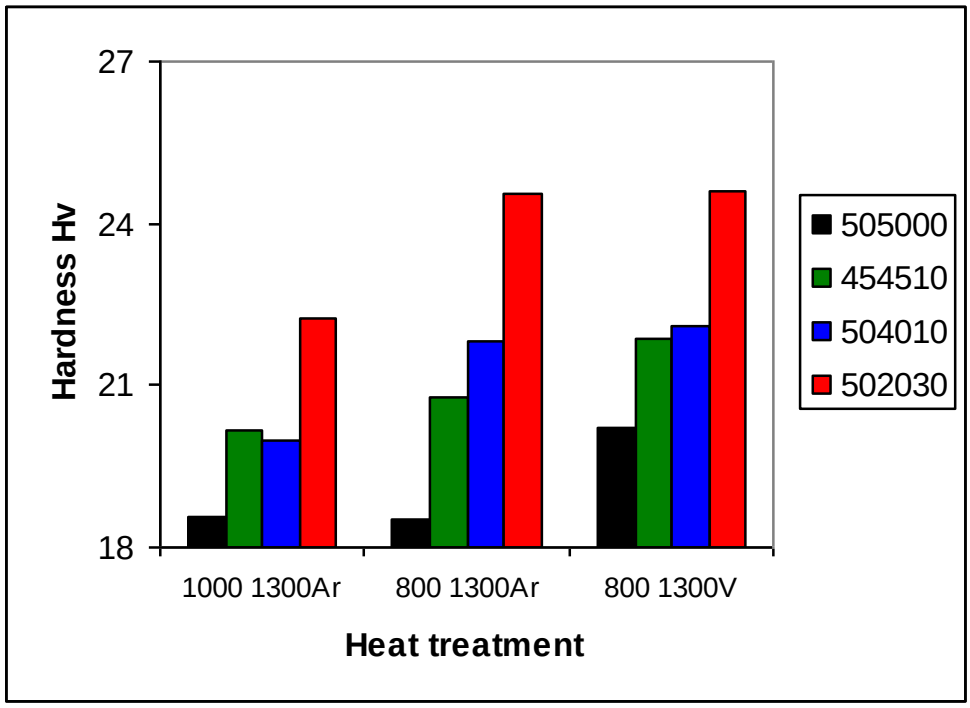

Figure 4.43 Effect of composition on hardness for samples heat treated under various conditions.

Effect of heat treatment on hardness

Hardness is also dependent on heat treatment . Samples heat treated in air at 1000 ^{o}C followed by sintering at 1300 ^{o}C in Argon have slightly lower hardness values compared to same materials which have been heat treated at 800 ^{o}C in air followed by sintering at 1300 ^{o}C in argon. For an example sample 502030 has a hardness of 24.5 GPa when heat treated at 800 ^{o}C followed by sintering to 1300 ^{o}C compared to 22.2 GPa when initially heat treated to 1000 ^{o}C followed by sintering to 1300 ^{o}C. This compromise in hardness for samples heat treated at 1000 ^{o}C can be attributed to the presence of $Al_{14}B_4O_{33}$ phase.

Hardness values for samples heat treated in air at 800 ^{o}C followed by sintering at 1300 ^{o}C in vacuum are higher than hardness of same

materials heat treated in air at 800 ^{o}C followed by sintering at 1300 ^{o}C in Argon. Improvement of hardness for samples sintered under vacuum compared to their counterparts sintered in argon can be ascribed to increased densities achieved by vacuum sintering. Figure 4.45 shows the effect of various heat treatments and composition on hardness.

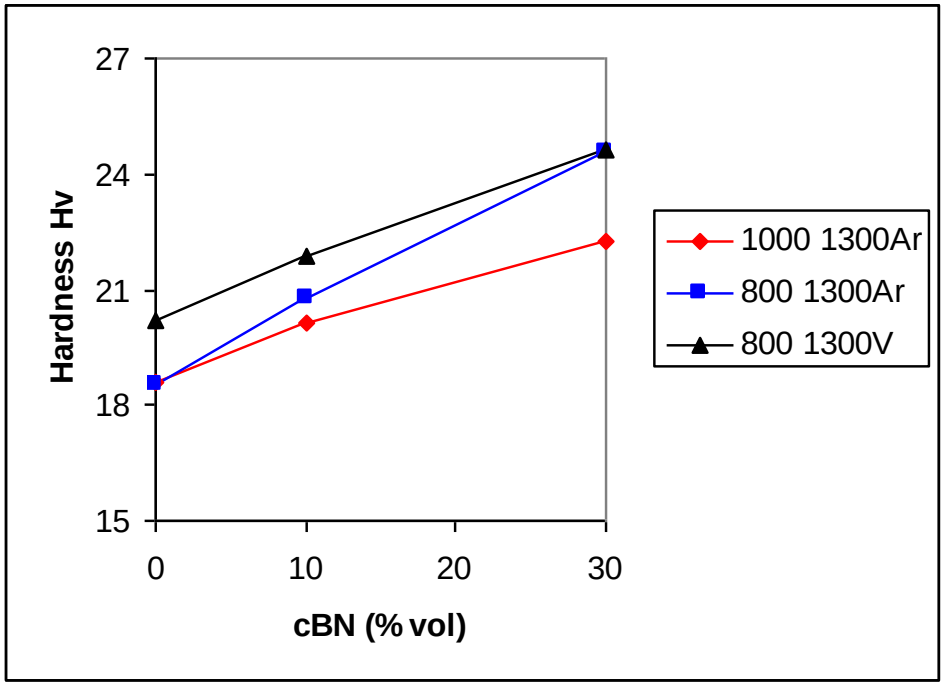

Figure 4.44 Comparison of hardness values for samples heat treated under various conditions.

Effect of composition on fracture toughness.

Presence of cBN in an alumina matrix has resulted in improved fracture toughness values. For an example for sample reacted at 800 ^{o}C in air followed by sintering to 1300 ^{o}C in Argon fracture toughness has increased from 2.0 MPa $m^{1/2}$ for sample without cBN to 3.9 MPa $m^{1/2}$ for sample with 30 % volume cBN. Figure 4.46 shows the effect of cBN content on fracture toughness for samples heat treated at 800 ^{o}C followed by sintering at 1300 ^{o}C in Argon. This enhancement of fracture

toughness can be attributed to crack deflection by cBN particles as shown in figure 4.47. As the cBN content increases it means the propagating crack will follow a more tortuous path resulting in even higher fracture toughness values.

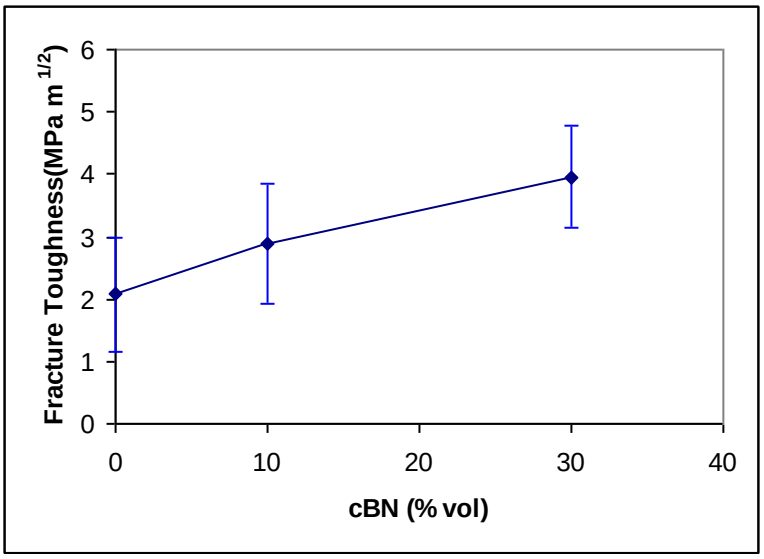

Figure 4.45 Effect of cBN content on fracture toughness for samples heat treated at 800 ^{o}C in air followed by sintering at 1300 ^{o}C in Argon.

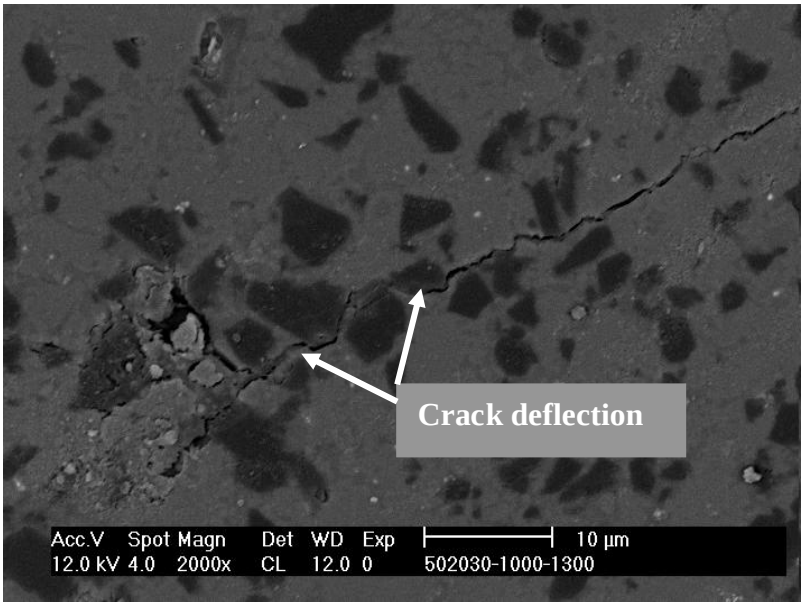

Figure 4.46 Crack deflection around cBN particles in sample 502030 sintered at 1300 ^{o}C in Argon.

Effect of heat treatment on fracture toughness

Considering same materials sintered under different conditions there does not seem to be any correlation between fracture toughness and heat treatment. For an example sample 502030 when heat treated to 800 ^{o}C in air followed by sintering at 1300 ^{o}C in Argon has a fracture toughness of 3.96 MPa $m^{1/2}$ (highest recorded for all samples) which goes down to 3.90 MPa $m^{1/2}$ when the sintering is done in vacuum. Thus unlike density and hardness which increase on changing atmosphere from Argon to vacuum , fracture toughness does not improve with change of sintering atmosphere.

Chapter 5

Conclusions and recommendations

5.1 Summary

This work has demonstrated that incorporating cubic boron nitride in a reaction bonded aluminum oxide matrix results in composite materials with improved hardness and fracture toughness compared to pure aluminum oxide.

Reaction bonded aluminum oxide matrix.

Reaction bonded aluminum oxide (RBAO) was used instead of conventionally sintering alumina. This required pre heat treating the composites in an oxidizing atmosphere to facilitate oxidation of aluminum into alumina without oxidizing cubic boron nitride into B_2O_3.

This required a thorough understanding of the oxidation kinetics of aluminum. In particular the effects of the following factors on the oxidation of aluminum in RBAO were investigated,

1. Compaction pressure
2. Temperature
3. Chemical composition

The effects of each factor on the oxidation of aluminum are summarized below.

Compaction pressure.

Compacts were made at different pressures 45, 90 and 180 MPa. It was observed that degrees of reaction (conversion of Al into Al_2O_3) did not vary much with change in compaction pressure.

Temperature.

For all sample compositions degree of reaction increased with increase in temperature with maximum oxidation taking place in the range 600 – 800 degrees.

Chemical composition.

Comparing materials with different cubic boron nitride loading revealed that presence of cubic boron nitride inhibits oxidation of aluminum. This can be attributed to the possibility of BN forming a thin film of B_2O_3 in the vicinity of Al which then hinders diffusion of air resulting in lower degrees of oxidation.

The oxidation investigations showed that heat treating samples containing cubic boron nitride to higher temperatures (1000 ^oC) results in the formation of B_2O_3 which then reacts with Al_2O_3 to form $Al_{18}B_4O_{33}$. Thus to avoid formation of B_2O_3 and $Al_{18}B_4O_{33}$ it was decided that the optimum temperature for oxidizing aluminum in reaction bonded aluminum oxide process (RBAO) is 800 ^oC.

Sintered samples

Samples reacted to 800 ^oC and 1000 ^oC in air were sintered to 1300 ^oC in vacuum and Argon for further densification.

It was observed that density decreased with increase in cubic boron nitride. This could be related to the hardness of cubic boron nitride and its resistance to plastic deformation.

For all samples there was an appreciable improvement in densification if sintering was done under vacuum compared to Argon.

For all samples, introduction of cubic boron nitride resulted in appreciable improvement in hardness and fracture toughness. Both

hardness and fracture toughness increased with increase in cubic boron nitride loading.

Thus this investigation demonstrated that introducing cubic boron nitride (up to 30% by volume) in a reaction bonded aluminum oxide matrix results in a composite material which has enhanced properties compared to pure alumina. This composite has hardness and fracture toughness values of 24.6 GPa and 3.9 MPa $m^{1/2}$ respectively making it possible candidate for wear applications.

5.2 Future work

Sample 502030 when sintered for 2 hours at 1300 ^{o}C under vacuum had the best mechanical properties (hardness and fracture toughness values of 24.6 GPa and 3.9 MPa $m^{1/2}$ respectively) and a density of 96.50%. Mechanical properties can further be enhanced by increasing cubic boron nitride content to say 40%. This however, is most likely to further reduce the density. Density can be improved by increasing sintering temperature say to 1350 ^{o}C and sintering time to 5 hours.

In order to fully understand the effect of cubic boron nitride on the properties of alumina it might also be worth doing a detailed microstructural characterization of the cBN/alumina interface region. In particular high resolution electron microscopy (HREM) imaging can provide considerable detail of the interface structure which can then be used to explain enhancement in fracture toughness and hardness.

Appendix

Table A.1. Composition by volume of sample 502030 as a function of temperature and pressure.

PRESSURE MPa	TEMP ^{o}C	TIME MINS	% Composition Volume			
			Al	Al_2O_3	cBN	AlBO
45	500	0	21.27	48.80	29.93	0.00
45	600	0	19.87	50.20	29.93	0.00
45	700	0	19.00	51.09	29.91	0.00
45	800	0	6.77	63.36	29.87	0.00
45	900	0	5.52	65.62	28.86	0.00
45	1000	0	3.20	69.26	27.55	0.00
45	1000	60	1.43	66.08	26.55	5.94
45	1000	180	1.34	59.56	26.24	12.85
45	1000	300	1.10	60.67	25.70	12.53
180	500	0	22.50	47.55	29.95	0.00
180	600	0	21.29	48.80	29.90	0.00
180	700	0	20.20	49.59	30.21	0.00
180	800	0	5.80	64.33	29.87	0.00
180	900	0	4.20	66.94	28.86	0.00
180	1000	0	3.16	67.39	29.44	0.00
180	1000	60	3.07	61.70	29.70	5.52
180	1000	180	2.76	58.57	28.55	10.12
180	1000	300	2.61	61.71	25.07	10.61

Table A.2 Composition by volume of sample 504010 as a function of temperature and pressure.

PRESSURE MPa	TEMP ^{o}C	TIME MINS	% Composition Volume			
			Al	Al_2O_3	cBN	AlBO
45	500	0	17.08	72.99	9.93	0.00
45	600	0	15.97	74.35	9.68	0.00
45	700	0	15.42	74.61	9.98	0.00
45	800	0	5.19	84.90	9.90	0.00
45	900	0	4.90	85.22	9.88	0.00
45	1000	0	3.75	86.37	9.87	0.00
45	1000	60	4.32	85.92	9.76	0.00
45	1000	180	1.76	82.66	9.69	5.89
45	1000	300	1.63	82.46	9.39	6.51
180	500	0	21.57	68.43	10.00	0.00
180	600	0	19.30	70.70	10.00	0.00
180	700	0	16.42	73.60	9.98	0.00
180	800	0	5.32	84.78	9.90	0.00
180	900	0	4.21	85.91	9.88	0.00
180	1000	0	3.60	86.54	9.86	0.00
180	1000	60	2.03	88.32	9.65	0.00
180	1000	180	1.31	83.22	9.32	6.16
180	1000	300	1.23	82.26	9.04	7.47

Table A.3 Composition by volume of sample 454510 as a function of temperature and pressure.

PRESSURE MPa	TEMP ^{o}C	TIME MINS	% Composition Volume			
			Al	Al_2O_3	cBN	AlBO
45	500	0	13.21	76.80	10.00	0.00
45	600	0	12.50	77.50	10.00	0.00
45	700	0	12.01	78.01	9.97	0.00
45	800	0	5.15	85.02	9.83	0.00
45	900	0	4.15	86.04	9.81	0.00
45	1000	0	3.50	86.72	9.78	0.00
45	1000	60	2.70	87.67	9.63	0.00
45	1000	180	1.14	85.22	9.49	4.14
45	1000	300	1.12	82.94	9.37	6.57
180	500	0	18.50	71.51	10.00	0.00
180	600	0	15.30	74.70	10.00	0.00
180	700	0	13.02	77.01	9.97	0.00
180	800	0	5.51	84.67	9.83	0.00
180	900	0	5.20	85.00	9.81	0.00
180	1000	0	4.05	86.60	9.35	0.00
180	1000	60	2.18	88.51	9.30	0.00
180	1000	180	1.38	82.97	9.11	6.55
180	1000	300	1.36	82.46	8.91	7.28

Table A.4 Composition by volume of sample 505000 as a function of temperature and pressure.

PRESSURE MPa	TEMP ^{o}C	TIME MINS	% Composition Volume			
			Al	Al_2O_3	cBN	AlBO
45	500	0	17.20	82.80	0.00	0.00
45	600	0	13.31	86.69	0.00	0.00
45	700	0	10.11	89.89	0.00	0.00
45	800	0	4.50	95.50	0.00	0.00
45	900	0	4.03	95.97	0.00	0.00
45	1000	0	2.92	97.08	0.00	0.00
45	1000	60	0.00	100.00	0.00	0.00
45	1000	180	0.00	100.00	0.00	0.00
45	1000	300	0.00	100.00	0.00	0.00
180	500	0	18.25	81.75	0.00	0.00
180	600	0	16.30	83.70	0.00	0.00
180	700	0	11.12	88.88	0.00	0.00
180	800	0	5.05	94.95	0.00	0.00
180	900	0	4.50	95.50	0.00	0.00
180	1000	0	3.48	96.52	0.00	0.00
180	1000	60	1.74	98.26	0.00	0.00
180	1000	180	1.26	98.74	0.00	0.00
180	1000	300	1.19	98.81	0.00	0.00

Table A.5 Composition by mass of sample 502030 as a function of temperature and pressure.

PRESSURE MPa	TEMP ^{o}C	TIME MINS	% Composition Mass			
			Al	Al_2O_3	cBN	AlBO
45	500	0	16.14	54.59	29.27	0.00
45	600	0	15.00	55.87	29.13	0.00
45	700	0	14.30	56.68	29.02	0.00
45	800	0	4.88	67.35	27.76	0.00
45	900	0	3.96	69.37	26.68	0.00
45	1000	0	2.27	72.51	25.22	0.00
45	1000	60	1.03	70.10	24.63	4.24
45	1000	180	0.99	64.68	24.92	9.40
45	1000	300	0.81	65.71	24.34	9.14
180	500	0	17.15	53.43	29.42	0.00
180	600	0	16.16	54.59	29.25	0.00
180	700	0	15.28	55.28	29.45	0.00
180	800	0	4.17	68.16	27.67	0.00
180	900	0	3.00	70.45	26.56	0.00
180	1000	0	2.25	70.73	27.02	0.00
180	1000	60	2.23	66.01	27.78	3.98
180	1000	180	2.03	63.51	27.07	7.39
180	1000	300	1.91	66.69	23.69	7.72

Table A.6 Composition by mass of sample 504010 as a function of temperature and pressure.

PRESSURE MPa	TEMP ^{o}C	TIME MINS	% Composition Mass			
			Al	Al_2O_3	cBN	AlBO
45	500	0	12.42	78.26	9.31	0.00
45	600	0	11.57	79.39	9.04	0.00
45	700	0	11.15	79.54	9.30	0.00
45	800	0	3.63	87.45	8.92	0.00
45	900	0	3.42	87.69	8.89	0.00
45	1000	0	2.61	88.55	8.85	0.00
45	1000	60	3.01	88.23	8.76	0.00
45	1000	180	1.24	85.84	8.80	4.12
45	1000	300	1.15	85.74	8.54	4.56
180	500	0	15.94	74.54	9.52	0.00
180	600	0	14.15	76.40	9.45	0.00
180	700	0	11.92	78.75	9.34	0.00
180	800	0	3.72	87.36	8.92	0.00
180	900	0	2.93	88.20	8.87	0.00
180	1000	0	2.50	88.66	8.83	0.00
180	1000	60	1.40	90.00	8.60	0.00
180	1000	180	0.92	86.32	8.45	4.30
180	1000	300	0.87	85.66	8.23	5.24

Table A.7 Composition by mass of sample 454510 as a function of temperature and pressure.

PRESSURE MPa	TEMP ^{o}C	TIME MINS	% Composition Mass			
			Al	Al_2O_3	cBN	AlBO
45	500	0	9.48	81.27	9.25	0.00
45	600	0	8.95	81.82	9.23	0.00
45	700	0	8.59	82.22	9.19	0.00
45	800	0	3.60	87.54	8.85	0.00
45	900	0	2.89	88.31	8.80	0.00
45	1000	0	2.43	88.81	8.76	0.00
45	1000	60	1.87	89.53	8.60	0.00
45	1000	180	0.80	87.78	8.55	2.87
45	1000	300	0.79	86.11	8.51	4.59
180	500	0	13.52	77.05	9.42	0.00
180	600	0	11.06	79.62	9.32	0.00
180	700	0	9.34	81.44	9.22	0.00
180	800	0	3.85	87.28	8.86	0.00
180	900	0	3.63	87.53	8.83	0.00
180	1000	0	2.82	88.79	8.38	0.00
180	1000	60	1.51	90.20	8.29	0.00
180	1000	180	0.97	86.17	8.27	4.58
180	1000	300	0.96	85.84	8.11	5.10

Table A.8 Composition by mass of sample 505000 as a function of temperature and pressure.

PRESSURE MPa	TEMP ^{o}C	TIME MINS	% Composition Mass			
			Al	Al_2O_3	cBN	AlBO
45	500	0	12.35	87.65	0.00	0.00
45	600	0	9.43	90.57	0.00	0.00
45	700	0	7.09	92.91	0.00	0.00
45	800	0	3.10	96.90	0.00	0.00
45	900	0	2.77	97.23	0.00	0.00
45	1000	0	2.00	98.00	0.00	0.00
45	1000	60	0.00	100.00	0.00	0.00
45	1000	180	0.00	100.00	0.00	0.00
45	1000	300	0.00	100.00	0.00	0.00
180	500	0	13.15	86.85	0.00	0.00
180	600	0	11.67	88.33	0.00	0.00
180	700	0	7.82	92.18	0.00	0.00
180	800	0	3.48	96.52	0.00	0.00
180	900	0	3.10	96.90	0.00	0.00
180	1000	0	2.39	97.61	0.00	0.00
180	1000	60	1.19	98.81	0.00	0.00
180	1000	180	0.86	99.14	0.00	0.00
180	1000	300	0.81	99.19	0.00	0.00

Table A.9 Mass change as a function of temperature and pressure for sample 502030.

PRESSURE MPa	TEMP ^{o}C	TIME MINS	W_1 Grams	W_2 Grams	dW_{Th}	$\left(\frac{W_2 - W_1}{dW_{Th}}\right)*100$
45	500	0	0.9741	1.0706	37.24	26.60
45	600	0	0.9744	1.1001	37.24	34.64
45	700	0	0.9825	1.1488	37.24	45.40
45	800	0	0.9645	1.1366	37.24	47.91
45	900	0	1.031	1.2495	37.24	56.91
45	1000	0	0.9918	1.2299	37.24	64.47
45	1000	60	0.8871	1.1906	37.24	91.87
45	1000	180	0.7344	0.9870	37.24	92.36
45	1000	300	0.5875	0.7899	37.24	92.51
180	500	0	1.0113	1.1388	37.24	33.85
180	600	0	0.9711	1.1000	37.24	35.64
180	700	0	0.9925	1.1503	37.24	42.69
180	800	0	0.9745	1.1402	37.24	45.69
180	900	0	1.061	1.2795	37.24	55.30
180	1000	0	1.0099	1.2390	37.24	60.92
180	1000	60	0.8933	1.1900	37.24	89.19
180	1000	180	0.8026	1.0750	37.24	91.14
180	1000	300	0.8664	1.1600	37.24	91.00

Table A.10 Mass change as a function of temperature and pressure for sample 504010.

PRESSURE MPa	TEMP ^{o}C	TIME MINS	W_1 Grams	W_2 Grams	dW_{Th}	$\left(\frac{W_2 - W_1}{dW_{Th}}\right)*100$
45	500	0	0.8512	0.9326	36.11	26.48
45	600	0	0.8535	0.9433	36.11	29.14
45	700	0	0.8826	1.0050	36.11	38.41
45	800	0	0.8454	0.9908	36.11	47.63
45	900	0	0.8705	1.0207	36.11	47.78
45	1000	0	0.8722	1.0230	36.11	47.88
45	1000	60	0.9002	1.1710	36.11	83.31
45	1000	180	0.768	1.0010	36.11	84.02
45	1000	300	0.776	1.0290	36.11	90.29
180	500	0	0.8835	0.9685	36.11	29.68
180	600	0	0.873	0.9579	36.11	26.97
180	700	0	0.8826	0.9953	36.11	35.50
180	800	0	0.8454	0.9803	36.11	44.37
180	900	0	0.8705	1.0205	36.11	47.72
180	1000	0	0.8722	1.0220	36.11	47.56
180	1000	60	1.008	1.2900	36.11	77.47
180	1000	180	0.6367	0.8253	36.11	82.03
180	1000	300	0.7618	0.9875	36.11	82.05

Table A.11 Mass change as a function of temperature and pressure for sample 454510.

PRESSURE MPa	TEMP ^{o}C	TIME MINS	W_1 Grams	W_2 Grams	dW_{Th}	$\left(\frac{W_2 - W_1}{dW_{Th}}\right)*100$
45	500	0	0.9337	1.0258	31.88	30.94
45	600	0	0.9253	1.0308	31.88	35.76
45	700	0	0.9248	1.0620	31.88	46.54
45	800	0	0.9256	1.0762	31.88	51.04
45	900	0	0.9363	1.1033	31.88	55.95
45	1000	0	0.9719	1.1463	31.88	56.29
45	1000	60	1.0082	1.2606	31.88	78.53
45	1000	180	0.926	1.1625	31.88	80.11
45	1000	300	0.8994	1.1340	31.88	81.82
180	500	0	0.95	1.049	31.88	32.66
180	600	0	0.9326	1.0439	31.88	37.53
180	700	0	0.9248	1.05	31.88	42.64
180	800	0	0.9256	1.0850	31.88	54.02
180	900	0	0.9363	1.1030	31.88	55.85
180	1000	0	0.9719	1.1463	31.88	56.29
180	1000	60	0.3599	0.4475	31.88	76.35
180	1000	180	0.8532	1.0672	31.88	78.68
180	1000	300	1.0116	1.2655	31.88	78.73

Table A.12 Mass change as a function of temperature and pressure for sample 505000.

PRESSURE MPa	TEMP ^{o}C	TIME MINS	W_1 Grams	W_2 Grams	dW_{Th}	$\left(\frac{W_2 - W_1}{dW_{Th}}\right)*100$
45	500	0	0.6901	0.7695	35.57	32.35
45	600	0	0.6909	0.8031	35.57	45.66
45	700	0	0.6639	0.7831	35.57	50.48
45	800	0	0.6479	0.7708	35.57	53.33
45	900	0	0.6904	0.8264	35.57	55.38
45	1000	0	0.688	0.8355	35.57	60.29
45	1000	60	0.6935	0.9136	35.57	89.23
45	1000	180	0.7348	0.9746	35.57	91.75
45	1000	300	0.7283	0.9653	35.57	91.49
180	500	0	0.6793	0.7648	35.57	35.38
180	600	0	0.6899	0.8000	35.57	44.87
180	700	0	0.6639	0.7781	35.57	48.35
180	800	0	0.6479	0.7636	35.57	50.20
180	900	0	0.6904	0.8260	35.57	55.22
180	1000	0	0.5323	0.6933	35.57	85.03
180	1000	60	0.5327	0.6934	35.57	84.81
180	1000	180	0.7113	0.9365	35.57	89.01
180	1000	300	0.7432	0.9845	35.57	91.28

Table A.13 Degree of reaction as a function of temperature and pressure for sample 502030.

PRESSURE MPa	TEMP ^{o}C	TIME MINS	Al *Initial (g)*	Al *final (g)*	$\left[1-\left(\frac{Al_{final}}{Al_{initial}}\right)\right]*100$
45	500	0	0.412	0.17	58.08
45	600	0	0.412	0.17	59.98
45	700	0	0.416	0.16	61.12
45	800	0	0.408	0.06	86.41
45	900	0	0.436	0.05	88.66
45	1000	0	0.420	0.03	93.34
45	1000	60	0.375	0.01	96.72
45	1000	180	0.311	0.01	96.85
45	1000	300	0.249	0.01	97.42
180	500	0	0.428	0.20	54.37
180	600	0	0.411	0.18	56.73
180	700	0	0.420	0.18	58.16
180	800	0	0.412	0.05	88.11
180	900	0	0.449	0.04	91.46
180	1000	0	0.427	0.03	93.48
180	1000	60	0.378	0.03	92.98
180	1000	180	0.340	0.02	93.57
180	1000	300	0.367	0.02	93.97

Table A.14 Degree of reaction as a function of temperature and pressure for sample 504010.

PRESSURE MPa	TEMP ^{o}C	TIME MINS	Al *Initial (g)*	Al *final (g)*	$\left[1-\left(\frac{Al_{final}}{Al_{initial}}\right)\right]*100$
45	500	0	0.349	0.12	66.82
45	600	0	0.350	0.11	68.83
45	700	0	0.362	0.11	69.05
45	800	0	0.347	0.04	89.62
45	900	0	0.357	0.03	90.22
45	1000	0	0.358	0.03	92.55
45	1000	60	0.369	0.04	93.46
45	1000	180	0.315	0.01	96.07
45	1000	300	0.318	0.01	96.27
180	500	0	0.363	0.16	55.59
180	600	0	0.358	0.14	60.54
180	700	0	0.362	0.12	65.97
180	800	0	0.347	0.04	89.38
180	900	0	0.357	0.03	91.62
180	1000	0	0.358	0.03	92.85
180	1000	60	0.414	0.02	95.62
180	1000	180	0.261	0.01	97.09
180	1000	300	0.313	0.01	97.24

Table A.15 Degree of reaction as a function of temperature and pressure for sample 454510.

PRESSURE MPa	TEMP ^{o}C	TIME MINS	Al *Initial (g)*	Al *final (g)*	$\left[1-\left(\frac{Al_{final}}{Al_{initial}}\right)\right]*100$
45	500	0	0.383	0.10	74.63
45	600	0	0.380	0.09	75.69
45	700	0	0.335	0.09	72.76
45	800	0	0.335	0.04	88.43
45	900	0	0.339	0.03	90.60
45	1000	0	0.352	0.03	92.08
45	1000	60	0.365	0.02	93.54
45	1000	180	0.335	0.01	97.24
45	1000	300	0.326	0.01	97.24
180	500	0	0.344	0.15	57.59
180	600	0	0.338	0.12	64.84
180	700	0	0.335	0.10	69.89
180	800	0	0.335	0.04	87.53
180	900	0	0.339	0.04	88.19
180	1000	0	0.352	0.03	90.81
180	1000	60	0.130	0.01	94.80
180	1000	180	0.309	0.01	96.65
180	1000	300	0.367	0.01	96.69

Table A.16 Degree of reaction as a function of temperature and pressure for sample 505000.

PRESSURE MPa	TEMP ^{o}C	TIME MINS	Al *Initial (g)*	Al *final (g)*	$\left[1-\left(\frac{Al_{final}}{Al_{initial}}\right)\right]*100$
45	500	0	0.250	0.10	74.90
45	600	0	0.250	0.08	69.76
45	700	0	0.268	0.06	79.31
45	800	0	0.262	0.02	90.88
45	900	0	0.279	0.02	91.80
45	1000	0	0.278	0.02	94.08
45	1000	60	0.280	0.00	100.00
45	1000	180	0.297	0.00	100.00
45	1000	300	0.294	0.00	100.00
180	500	0	0.275	0.10	62.55
180	600	0	0.279	0.09	66.52
180	700	0	0.268	0.06	77.20
180	800	0	0.262	0.03	89.77
180	900	0	0.279	0.03	90.83
180	1000	0	0.215	0.02	92.31
180	1000	60	0.215	0.01	96.16
180	1000	180	0.288	0.01	97.20
180	1000	300	0.300	0.01	97.34

References

1. A. Krell. Handbook of Ceramic Hard Materials, Edited by R. Riedel, Willey-VCH. 2000.

2. O. Zywitzki, F Fietzke, K. Goedecke, S. Schiller, V. Alfredson, T. Hilding, B. Ljungberg, M. Sjostrand, PVD Al_2O_3 coated cutting tool, Patent US2003027015.

3. V. Alfredson, T. Hilding, M. Sjoestrand, B.Ljundberg, PVD Al_2O_3 coated cutting tool, Patent EP1253215.

4. P. Littecke S. Soederberg, Al_2O_3 coated cutting tool, Patent US6382951.

5. J. Shiraishi, S. Kukino and T. Nakai, Cutting tool of Al_2O_3-coated cubic boron nitride-based sintered material, Patent EP1120387.

6. J.G. Baldoni and S.T.Buljan, Ceramics for machining, Ceramic Bulletin, (1988) 67, 381-387.

7. R. Morales, A. Bravo, A. J. Melendo M. D. Rodrighuez, High temperature stress relaxation in Ti and Cu doped reaction bonded Al_2O_3, Journal of European Ceramic Society 22, 2002, 2641-2645.

8. R. Davidge, R.J. Brook R.I. Todd C. Walker and C. Borsa. Fabrication, characterization and properties of alumina nanocomposites, Edited by F.R Sale 249-264.

9. K.Nihara. New design concept of structural ceramics, Ceramic nanocomposites, The centenial memorial Issue of the Ceramic Society of Japan 99 , 1991, 974-982.

10. R. Morrel. Handbook of properties of Technical Ceramics. Part 1. An introduction for the Engineer and Designer Elsevier Academic press, 1985 4.

11. S. Somiya, F. Aldinger. N. Claussen, R.Spriggs, K. Uchino, K. Koumoto, M. Kaneno Handbook of Advanced ceramics. Volume II 2003, Elsevier Academic press, 334.

12. R. Riedel. Handbook of ceramic hard materials, Weinheim New York 1986.

13. F.Franklin Y. Wang Treatise on Material Science and Technology Volume 9. Academic Press 1976, 261.

14 . K. K. Chawla. Ceramic matrix composites. Chapman and Hall 1993, 213.

15. D. Hasselman and R. M Fulrath, Proposed fracture theory of a dispersion-strengthened glass matrix, Journal of American Ceramic Society 49, 1966 68-72.

16. K. T Farber and A.G. Evans, Crack deflection processes—II. Experiment, Acta Metallurgica 31 1983, 577-584.

17. C. Wei and P.F Becher ,Improvement s in mechanical properties in SiC by the addtion of TiC particles, Journal of American Ceramic Society 67, 1984, 571-574.

18. A. G. Evans and K. T. Farber, Toughening of Ceramics by Circumferential Microcracking **,** Journal of American Ceramic Society 64 1981, 394-398.

19. D. L. Porter and A. H. Heuer, Mechanisms of Toughening Partially Stabilized Zirconia (PSZ), Journal of American Ceramic Society 60 1977, 183-184 .

20 A. G. Evans, The mechanical performance of fiber-reinforced ceramic matrix composites, Materials Science and Engineering A107 1989, 227-239.

21. Z. Misirli, A. Uguz and T. Baykara, Effect of additives on the microstructure and mechanical properties of commercial alumina ceramics, Material Characterisation 33 ,1994 329-341 .

22 . A. Krell. Improved hardness and hierarchic influences on wear in submicron sintered alumina, Material Science and Engineering A209 1996, 156-163.

23 . A Muchtar and L. C. Lim, Indentation fracture toughness of high purity submicron alumina, Acta Metallurgica 46, 1998 1683-1698.

24. R.S. Mishra and A.K. Mukherjee, Processing of high hardness-high toughness alumina matrix nanocomposites , Material Science and Engineering A301, 2001 97-101.

25. W. H.Gitzen, Alumina as a Ceramic Material, American Ceramic Society 1970.

26. W. Lee and W.M. Rainforth , Ceramic microstructures, Chapman and Hall, London 1994.

27. Germany Industry standard 60672.

28. N. Louet, H. Reveron and G. Fantozzi ,Sintering behaviour and microstructural evolution of ultrapure α-alumina containing low amounts of SiO_2, Journal of the European Ceramic Society 28, 2007 205-215.

29. E. Volceanov, A. Volceanov and S. Stoleriu , Assessment on mechanical properties controlling of alumina ceramics for harsh service conditions, Journal of the European Ceramic Society 27, 2007 759-762.

30. V.Y. Kodash, J.R. Groza, K.C. Cho, B.R. Klotz and R.J. Dowding , Field-assisted sintering of nanopowders, Materials Science and Engineering, 385 2004 367-371 .

31. A. Shui, L. Zeng and K. Uematsu ,Relationship between sintering shrinkage anisotropy and particle orientation for alumina powder compacts, Scripta Materialia 55 ,2006 831-834.

32. W.D Kingery and H.K Bowen and D.R Uhimann, Introduction to Ceramics, New York: John Willey & Sons,1975.

33. Y. Zhou, Effects of heating rate and particle size on pulse electric current sintering of alumina, Scripta Materialia 48 2003, 1631-1636.

34. N. J. Shaw and A. H. Heuer. On particle coarsening during sintering, Acta Metallurgic 31, 1983 55-59.

35. W.A Gray,The packing of solid particles,Chapman and Hall, London, 1968.

36. F.F Lange, Powder Processing Science and Technology for Increased Reliability,Journal Of American Ceramic Society 72 1989 3-15.

37. M. F. Yan, R. M. Cannon, H. K. Bowen and U. Chowdhry, Effect of grain size distribution on sintered density, Material science and engineering 60 1983, 275-81.

38. T.Shou Yeh and M.D.Sacks, Effect of Particle Size Distribution on the Sintering of Alumina, Journal of the American Ceramic Society 71 1988, C-484-87.

39 R. L Coble and J. E Burke, Sintering in Ceramics, Progress in Ceramic Science Vol 3. Macmillan New York, 1963.

40. L. Changxia, Z.Jianhua, S. Junlong and Z. Xihua, Pressureless sintering of large-scale fine structural alumina matrix ceramic guideway materials, Materials Science and Engineering 444, 2007 58-63.

41. O. Guillon, S. Krauß and J. Rödel, Influence of thickness on the constrained sintering of alumina films, Journal of the European Ceramic Society 27 2007, 2623-2627.

42. S.J. Bennison and M. P Harmer, Grain-Growth Kinetics for Alumina in the Absence of a Liquid Phase, Journal of American ceramic Society C68 1985, C22-C24.

43 . R. L Coble. Sintering Alumina, Effect of Atmospheres, Journal of American Ceramic Society 45 1962, 123-27.

44. J. Li, Y. Pan, F. Qiu, L. Huang and J. Guo ,Alumina ceramics fabricated from bimodal alumina with additives, Materials Science and Engineering 5 2006, 611-619.

45. S.J Benison and M. P Harmer, Swelling of Hot-Pressed Al_2O_3 Journal of American Ceramic Society 68 1985, 591- 97.

46. A. Mocellin and W. D Kingery. Microstructural Changes During Heat Treatment of Sintered Al_2O_3, Journal of American Ceramic Society 56 1973, 309-14.

47 . C. Carry and A. Mocellin. Structural superplasticity in single phase crystalline ceramics. Ceramics International 13 1987, 89-98.

48. A. Mark Thompson and Martin P. Harmer, Influence of Atmosphere on the Final-Stage Sintering Kinetics of Ultra-High-Purity Alumina, Journal of American Ceramic Society 76 1993, 2248-56.

49. A. Shui, L. Zeng and K. Uematsu, Relationship between sintering shrinkage anisotropy and particle orientation for alumina powder compacts, Scripta Materialia 55 2006, 831-834.

50. R. K. Bordia, R. Zuo, O. Guillon, S.M. Salamone and J. Rödel Anisotropic constitutive laws for sintering bodies, Acta Materialia 54 2006, 111-118.

51. H. Z. Wang, L. Gao, L. H. Gui and J. K. Guo. Preparation and properties of intragranular Al_2O_3-SiC nanocomposites, Nanostructured Materials 10 1998, 947-953.

52 . C. Nivot, F. Valdivieso and P. Goeuriot ,Nitrogen pressure effects on non-isothermal alumina sintering, Journal of the European Ceramic Society 26 2006, 9-15.

53. R. Edwards Cutting Tools, The Institute of Materials 1993 .

54 .K.F. Cai , D.S. McLachlan, N. Axen, R. Manyatsa, Preparation, microstructures and properties of Al_2O_3 –TiC composites, Ceramics International 28 2002, 217-222.

55 . X.Q.You, T.Z. Si, N.Liu, P.P Ren, Y.D. Xu, J.P Feng, Effect of grain size on thermal shock resistance of Al_2O_3–TiC ceramics, Ceramics International 31 2005, 33-38.

56. C. Huang, J. Wang and C. Huang ,Sintering behavior and microwave dielectric properties of nano alpha-alumina, Materials Letters 59 2005, 3746-3749.

57 . B.L Karihaloo. Contribution of $t \rightarrow m$ Phase Transformation to the Toughening of ZTA, Journal of American Ceramic Society 74, 1991 1703-1706.

58. P.F. Becher, K.B. Alexander, W. Warmick, Influence of ZrO_2 Grain Size and Content on the Transformation Response in the $Al_2O_3ZrO_2$ (12 mol% CeO_2) System , Journal of American Ceramic Society 76 1993 657-663.

59. S. Hori, M. Yoshimura, S. Somiya, Strength-Toughness Relations in Sintered and Isostatically Hot-Pressed ZrO_2-Toughened Al_2O_3, Journal of American Ceramic Society 69 1986, 169-172.

60. D. Casellas, M. M. Nagl, L. Llanes and M. Anglada. Fracture toughness of alumina and ZTA ceramics: microstructural coarsening effects, Journal of Materials Processing Technology 143 2003, 148-152.

61 . L. Wang, J.Lin Shi and Zi-Le Hua, The influence of addition of WC particles on mechanical properties of alumina–matrix composite, Material letters 50 2000, 179-182.

62. W. Acchar, A. E. Martinelli, F. A. Vieira and C. A. A. Cairo, Sintering behaviour of alumina–tungsten carbide composites, Material Science and Engineering 284 2000, 84-87.

63. W. Acchar and J. L. Fonseca. Sintering behavior of alumina reinforced with (Ti, W)carbides, Material Science and engineering 371A 2004, 382-387.

64. Y. Mok Ko, W. T.Kwon, Y.-Wook Kim. Development of Al_2O_3–SiC composite tool for machining application, Ceramics International 30 2004, 2081-2086.

65. N. Claussen, S. Wu & D. Holz, Reaction bonding of aluminum oxide (RBAO) composites, Processing,reaction mechanisms and properties, Journal of European Ceramic Society 14 1994, 97-109.

66. N. Claussen, T. Le and S. Wu. Low shrinkage reaction bonding in alumina, Journal of European Ceramic society 5 1989, 29-35.

67. D. Holz, S. Wu, S.Scheppokat and N. Claussen. Effect of Processing Parameters on Phase and Microstructure Evolution in RBAO Ceramics, Journal of American Ceramic Society 77 1994, 2509-2517.

68 .E. Suvaci and G. L. Messing Processing, Kinetics of template growth in alumina during the process of templated grain growth (TGG), Acta Materialia 49 2001, 2075-2081.

69 . F. Essl, J.Bruhn, R.Janssen, N. Claussen, Wet milling of Al-containing powder mixtures as precursor materials for reaction bonding of alumina (RBAO) and reaction sintering of alumina–aluminide alloys (3A), Materials Chemistry and Physics 61 1999 69-77.

70. E. Suvaci and G. L. Messing, Seeding of the Reaction-Bonded Aluminum Oxide Process , Journal of American Ceramic Society 3 2001, 657-659.

71. M. Kumagai and G. L Messing, Controlled Transformation and Sintering of a Boehmite Sol-Gel by α-Alumina Seeding, Journal of American Ceramic Society 9 1985, 500-505.

72. M. Kumagai and G. L. Messing. J. Am. Ceram. Enhanced Densification of Boehrmite Sol-Gels by α-Alumina Seeding , Journal of American Ceramic Society 11 1984, C230-231.

73 . N. Claussen, S. Wu & D. Holz.Reaction bonding of aluminum oxide (RBAO) composites, Processing,reaction mechanisms and properties, Journal of European Ceramic Society 14 1994, 97-109.

74. Il-Soo Kim, Sang-Jin Lee, Effects of alumina type and attritor ball size on the processing of RBAO – ZrO_2 ceramics, Materials letters 48 2001, 247-251.

75. S. Wu, Dietmar, and N. Claussen, Mechanisms and Kinetics of Reaction-Bonded Aluminum Oxide Ceramics, Journal of American Ceramic Society 76 1993 970-80.

76. K. Nona and C. Liddell, Shrinking core models in hydrometallurgy: What students are not being told about the pseudo-steady approximation, Hydrometallurgy 79 2005, 62-68.

77. S. Homma and S. Matsumoto, Gas–solid reaction model for a shrinking spherical particle with unreacted shrinking core, Chemical Engineering Science 60 2005 , 4971-4980.

78. J. Szekely J. W. Evans and H.Y.Sohn, Gas Solid Reactions Academic Press 1976, 108-173.

79. O. Levenspiel. Chemical reaction Engineering. John Wiley and Sons 1972, 357-376.

80. P.Shaun. Gaus, H. M. Chan, M. P. Harmer and S.Hugo. Caram. Microscopic modeling of the reaction bonding of aluminum oxide. Journal of the European Ceramic Society 17 1997, 971-975.

81. D.E Garcia. , R.Jansen., and N.Claussen, In Third Euro-Ceramics, Vol 3, Engineering Ceramics, ed P. duran & J.F. Fernandez. Faenza editrice Iberica, S.L 1993, 719-724

82 . S. Scheppokat, N. Claussen and R. Hannink,RBAO composites containing TiN and TiN/TiC, Journal of the European Ceramic Society 16 1996, 919-27.

83. G. Will and P.G. Perkins, Is there a new form of boron nitride with extreme hardness? , Diamond and Related Materials 10 2001, 2010-2017.

84. G. Demazeau , High pressure diamond and cubic boron nitride synthesis , Diamond and related materials 4 1995, 284-287.

85. T. E. Mosuang and J. E. Lowther .Relative stability of cubic and different hexagonal forms of boron nitride, Journal of Physics and Chemistry of Solids 63 2002, 363-368.

86 . T. Nakano , H. Ikawa and O. Fukunaga. Synthesis of cubic boron nitride using Li_3BN_2, $Sr_3B_2N_4$ and $Ca_3B_2N_4$ as solvent-catalysts, Diamond and related Materials 3 1993, 75-82.

87 . S.K. Singhal, J. Von der Gonna, G. Nover, H.J. Meurer and B.P. Singh, Synthesis of cubic boron nitride at reduced pressures in the presence of $Co[(NH_3)_6]Cl_3$ and NH_4F, Diamond and Related Materials 14 2005, 1389-1394.

88. X. C. Wang, X. P. Jia, T. C. Zhang, G. Z. Ren, H. J. Liu, C. Y. Zang, P. W. Zhu, H. A. Ma and G. T. Zou cBN ,Synthesis in the system of hBN–Mg and bonded water, Diamond and Related Materials 12 2003, 57-60.

89. V. L. Solozhenko, V. V. Chernyshev, G. V. Fetisov, V. B. Rybakov and I. A. Petrusha ,Structure analysis of the cubic boron nitride crystals, Journal of Physics and Chemistry of Solids 51 1990, 1011-1012.

90. S.K.Singhal and J.K Park. Synthesis of cubic boron nitride from amorphous boron nitride containing oxide impurity using Mg-Al alloy catalyst solvent, Journal of Crystal Growth 260 2004, 217-222.

91. O. Fukunaga, T. Miyake and N. Ohashi ,Formation of diamond and graphite at high pressure using glassy carbon source, Diamond and Related Materials 14 2005, 160-166.

92. V. A. Fomichev and M. A. Rumsh, Investigation of X-ray spectra of hexagonal and cubic boron nitride, Journal of Physics and Chemistry of Solids 29 1968, 1015-1024.

93. F. P. Bundy .Ultra-high pressure apparatus. Physics Reports 34 1988 ,133-176.

94. V.L Solozhenko, Thermodynamics of dense boron nitride modifications and a new phase P,T diagram for BN, Thermochimica Acta 218 1993, 221-227.

95. G. Will , G. Nover and J. von der Gonna, New Experimental Results on the Phase Diagram of Boron Nitride, Journal of Solid State Chemistry 154 2000, 280-285.

96. H. Lorenz and I. Orgzall, Influence of the initial crystallinity on the high pressure–high temperature phase transition in boron nitride, Acta Materialia 52 2004, 1909-1916.

97 . H. Sachdev , R. Haubner, H. Noth and B. Lux, Investigation of the c-BN/h-BN phase transformation at normal pressure, Diamond and Related Materials 6 1997, 286-292.

98 V. A. Lavrenko and A. F. Alexeev, High-temperature oxidation of boron nitride, Ceramics International 12 1986, 25-31.

99. N. Jacobson and S. Farmer. High-Temperature Oxidation of Boron Nitride: I, Monolithic Boron Nitride, Journal of American Ceramic Society 82 1999, 393-398.

100. PCBN cutting tools, Element Six.

101. E. Benko. J. Morgiel and T. Czeppe, BN sintered with Al: Microstructure and hardness, Ceramic international 23 1997, 89-91.

102. T. Ohash, K. Yamamoto, Y. Hamada T. Tanase, Some properties and cutting performance of polycrystalline cubic boron nitride with no additives, International Journal of Refractory Metals and Hard Materials 16 1998, 403-407.

103. R. Bodkin. PhD Thesis University of the Witwatersrand, Johannesburg 2004.

104. T.K Harris E.J Brookes and C.J Taylor, The effect of temperature on the hardness of polycrystalline cubic boron nitride cutting tool materials, International Journal of Refractory Metals and Hard Materials 22 2004, 105-110.

105. Element Six catalogue on PCBN cutting tool materials.

106. E. Benko, J. Skrzypek B. Krolicka A. Wyczesany T. Barr. cBN–TiN, cBN–TiC composites: chemical equilibria, microstructure and hardness mechanical investigations, Diamond and related Materials 8 1999, 1838-1846.

107. M. Wakatsuki. K.Ichinose,T. Aoki, Synthesis of Polycrystalline cBN Material Research Bulletin 7 1972, 999 -1003.

108. F. P. Bundy,The preparation of synthetic diamonds , Carbon 10 1972, 335-340.

109. J. Wang, J.Sha, Q. Yang Y. Wang, Synthesis of aluminium borate nanowires by sol–gel method. Material Research Bulletin 40 2005, 1551-1557.

109. Y. Li and R.P.H. Chang, Synthesis and characterization of aluminum borate ($Al_{18}B_4O_{33}$, $Al_4B_2O_9$) nanowires and nanotubes, Materials Chemistry and Physics 97 2006, 23-30.